

REF

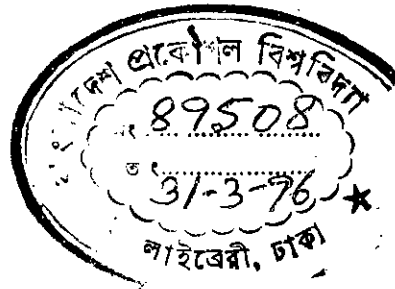
623.80414

1996

ASI

**PERFORMANCE STUDY OF OPTICAL  
TRANSMISSION SYSTEM WITH FORWARD  
ERROR CORRECTION CODING**

A Thesis submitted to the Electrical and Electronic Engineering Department  
of BUET, Dhaka, in partial fulfilment of the requirements  
for the degree of  
**Master of Science in Engineering**  
(Electrical and Electronic)



**MD. ASIFUR RAHMAN**



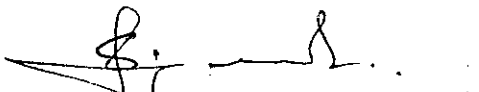
January 1996

**DEDICATED TO ALL WHO INSPIRED ME**

## DECLARATION

This work has been done by me and it has not been submitted elsewhere for the award of any degree or diploma.

Countersigned

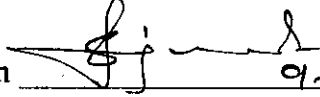
  
\_\_\_\_\_  
( Dr. Satya Prasad Majumder )  
Supervisor

  
\_\_\_\_\_  
( Md. Asifur Rahman )


The thesis titled " PERFORMANCE STUDY OF OPTICAL TRANSMISSION SYSTEM WITH FORWARD ERROR CORRECTION CODING " submitted by Md. Asifur Rahman, Roll No. 921369F, Session 1990-'91-'92 to the Electrical and Electronic Engineering Department of BUET has been accepted as satisfactory for partial fulfillment of the requirements for the degree of Master of Science in Engineering ( Electrical and Electronic ).

### Board of Examiners

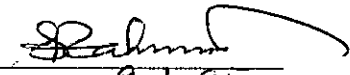
1. Dr. Satya Prasad Majumder  
Associate Professor  
Department of EEE  
BUET, Dhaka-1000

Chairman  9-1-91  
( Supervisor )

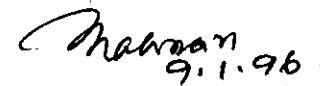
2. Dr. A.B.M. Siddique Hossain  
Professor and Head of the  
Department of EEE  
BUET, Dhaka-1000

Member  9-1-96  
( Ex-officio )

3. Dr. Saifur Rahman  
Assistant Professor  
Department of EEE  
BUET, Dhaka-1000

Member  9.1.95

4. Md. Mujibur Rahman  
Divisional Engineer  
Gulshan Exchange  
BTTB, Dhaka

Member  9.1.96.  
( External )

## **CONTENTS**

<b>ACKNOWLEDGMENTS</b>		vii
<b>ABSTRACT</b>		viii
<b>LIST OF FIGURES</b>		ix
<b>LIST OF PRINCIPAL SYMBOLS</b>		xiii
<b>LIST OF ABBREVIATIONS</b>		xv
<b>CHAPTER-1</b>	<b>INTRODUCTION</b>	1
1.1	Prologue	2
1.2	Importance of Coding in Optical Communication systems and their benefits	2
1.3	Forward Error Correction -- A brief review	3
1.4	Advantages of FSK system and previous work on FSK direct detection system without codes	4
1.5	Objectives of this thesis	8
1.6	Organization of the thesis	9
<b>CHAPTER-2</b>	<b>OPTICAL DIRECT DETECTION FSK WITH AND WITHOUT CODING</b>	10
2.1	Prologue	11
2.2	A model receiver description	12
	2.2.1 Discriminator Operation	12
2.3	Theoretical analysis for optical FSK with direct detection	14
2.4	Theoretical analysis for coded optical FSK	22
	2.4.1 Coding topologies	22
	2.4.2 FSK with Convolution coding	28
	2.4.3 FSK with Reed-Solomon's coding	30
2.5	Results and discussion	31
<b>CHAPTER-3</b>	<b>OPTICALLY PREAMPLIFIED FSK WITH AND WITHOUT CODING</b>	76

3.1	Prologue	77
3.2	Preamplifier basics	77
3.3	The combined receiver model	78
3.4	Theoretical analysis of preamplified FSK	78
3.5	Coded FSK with optical preamplifier	81
3.6	Results and discussion	81
3.7	Conclusions and suggestions for future work	107

<b>REFERENCES</b>	<b>109</b>
-------------------	------------

## **ACKNOWLEDGMENTS**

I would like to express my sincerest indebtedness and profound gratitude to my honourable supervisor Dr. Satya Prasad Majumder, Associate Professor of the Department of Electrical and Electronic Engineering, BUET, for his consistent but friendly supervision and encouragement throughout the entire completion of this work. The time constraint that almost made this thesis more than a challenge was practically conquered by his exceptional and nontraditional guidance. I owe him this total work.

I convey my deepest regards also to Dr. A.B.M. Siddique Hossain, Head of the Department of Electrical and Electronic Engineering, BUET, for his inspiration and support concerning the administrative part.

I would like to mention the tireless effort contributed by my wife for typing and helping me all the way up to the end. The constant support and encouragement from my brother and parents without which, this work would have never be completed.

## ABSTRACT

Direct detection has become recent attraction for the optical communication designers. The obvious reasons are low cost, simplicity and a lot more which is yet to be evaluated. However, the direct detection technique has the limitation in data rate for application in power limited free-space optical channels due to relatively low optical power output of semiconductor laser diode. The work undertaken here is confined to direct detection scheme which though have a few shortcomings possess a significant immunity to noise interference compared to the heterodyne detection concept. This is because the direct detection technique does not use the phase information. Our attempt is to explore this particular phenomena and judge the overall performance.

A theoretical analysis for direct detection optical frequency shift keying (FSK) transmission system is provided employing forward error correction (FEC) coding to combat the effect of phase noise of transmitting laser due to non-zero linewidth. Two types of coding viz. Convolutional coding (CC) and Reed-Solomon's (RS) coding are considered with hard decision Viterbi decoding to investigate their relative effectiveness in overcoming the degrading effect of laser phase noise.

The performance results at a bit rate of 2.5 Gb/s are also evaluated for different receiver and system parameters. The penalty suffered by the coded and uncoded systems at a bit error rate (BER) of  $10^{-9}$  are determined in the presence/absence of laser phase noise. The improvements in the receiver sensitivity due to coding i.e. the coding gains are also evaluated at  $BER = 10^{-9}$  for rate 1/2 CC with constraint length  $K = 4, 7$  and  $(15, 9)$ ,  $(15, 7)$  RS coding techniques. Further the reductions in the power penalty for the coded system over uncoded system are also determined for a specified bit error rate. The current effort proves beneficial to the context of relaxing laser specification and cost optimization.



## LIST OF FIGURES

1.1	Direct detection and Heterodyne detection	5
2.1	Block diagram of a FSK direct detection receiver employing MZI with decoder	13
2.2	Basic configuration of a MZI for WDM/FDM multiplexer/demultiplexer	15
2.3	MZI as an optical frequency discriminator	17
2.4	Aux channel for ARQ	23
2.5	Convolutional encoder with $M = 3$ , $k = 1$ and $n = 2$	24
2.6	Coded communication channel	25
2.7	Plots of bit error probability $P_b$ vs transmitted signal power $P_s(\text{dB}_m)$ for uncoded and rate 1/2 convolutionally coded ( $K = 4, 7$ ) FSK with modulation index $h = 0.5$ and laser linewidth $\Delta\nu T = 0.000$	32
2.8	Same as Fig. 2.7 with $\Delta\nu T = 0.005$	33
2.9	Same as Fig. 2.7 with $\Delta\nu T = 0.008$	34
2.10	Same as Fig. 2.7 with $\Delta\nu T = 0.010$	35
2.11	Same as Fig. 2.7 with $\Delta\nu T = 0.030$	36
2.12	Plots of bit error probability $P_b$ vs transmitted signal power $P_s(\text{dB}_m)$ for uncoded and rate 1/2 convolutionally coded ( $K = 4, 7$ ) FSK with modulation index $h = 1.0$ and laser linewidth $\Delta\nu T = 0.000$	38
2.13	Same as Fig. 2.12 with $\Delta\nu T = 0.011$	39
2.14	Same as Fig. 2.12 with $\Delta\nu T = 0.014$	40
2.15	Same as Fig. 2.12 with $\Delta\nu T = 0.020$	41
2.16	Same as Fig. 2.12 with $\Delta\nu T = 0.030$	42
2.17	Plots of bit error probability $P_b$ vs transmitted signal power $P_s(\text{dB}_m)$ for uncoded and rate 1/2 convolutionally coded ( $K = 4, 7$ ) FSK with modulation index $h = 2.0$ and laser linewidth $\Delta\nu T = 0.000$	43
2.18	Same as Fig. 2.17 with $\Delta\nu T = 0.017$	44
2.19	Same as Fig. 2.17 with $\Delta\nu T = 0.032$	45
2.20	Same as Fig. 2.17 with $\Delta\nu T = 0.048$	46
2.21	Plots of bit error probability $P_b$ vs transmitted signal power $P_s(\text{dB}_m)$ for uncoded and Reed-Solomon's coded FSK with modulation index $h = 0.5$ and laser linewidth $\Delta\nu T = 0.000$	47

2.22	Same as Fig. 2.21 with $\Delta\nu T = 0.005$	48
2.23	Same as Fig. 2.21 with $\Delta\nu T = 0.008$	49
2.24	Same as Fig. 2.21 with $\Delta\nu T = 0.010$	50
2.25	Same as Fig. 2.21 with $\Delta\nu T = 0.030$	51
2.26	Plots of bit error probability $P_b$ vs transmitted signal power $P_s(\text{dB}_m)$ for uncoded and Reed-Solomon's coded FSK with modulation index $h = 1.0$ and laser linewidth $\Delta\nu T = 0.000$	53
2.27	Same as Fig. 2.26 with $\Delta\nu T = 0.011$	54
2.28	Same as Fig. 2.26 with $\Delta\nu T = 0.014$	55
2.29	Same as Fig. 2.26 with $\Delta\nu T = 0.020$	56
2.30	Same as Fig. 2.26 with $\Delta\nu T = 0.030$	57
2.31	Plots of bit error probability $P_b$ vs transmitted signal power $P_s(\text{dB}_m)$ for uncoded and Reed-Solomon's coded FSK with modulation index $h = 2.0$ and laser linewidth $\Delta\nu T = 0.000$	58
2.32	Same as Fig. 2.31 with $\Delta\nu T = 0.017$	59
2.33	Same as Fig. 2.31 with $\Delta\nu T = 0.032$	60
2.34	Same as Fig. 2.31 with $\Delta\nu T = 0.048$	61
2.35	Plots of power penalty due to laser phase noise at $P_b = 10^{-9}$ as a function of the modulation index $h$ with $\Delta\nu T = 0.005$ and $\Delta\nu T = 0.010$	62
2.36	Plots of power penalty due to laser phase noise at $P_b = 10^{-9}$ for rate 1/2 convolutionally coded $K = 4$ FSK with direct detection as a function of the modulation index $h$ with $\Delta\nu T = 0.005$ and $\Delta\nu T = 0.010$	63
2.37	Same as Fig. 2.36 with $K = 7$	64
2.38	Plots of power penalty vs modulation index $h$ (15,9) RS coded FSK at $P_b = 10^{-9}$ for $\Delta\nu T = 0.005$ and $\Delta\nu T = 0.010$	65
2.39	Same as Fig. 2.38 with (15,7) RS coded	66
2.40	Plots of power penalty due to phase noise at $P_b = 10^{-9}$ for uncoded and rate 1/2 convolutionally coded FSK as a function of normalized laser linewidth $\Delta\nu T$ for modulation index $h = 0.5$	67
2.41	Same as Fig. 2.40 with $h = 1.0$	68
2.42	Same as Fig. 2.40 with $h = 2.0$	69
2.43	Plots of power penalty due to phase noise at $P_b = 10^{-9}$ for uncoded and RS coded FSK as a function of normalized laser linewidth $\Delta\nu T$ for modulation index $h = 0.5$	70
2.44	Same as Fig. 2.43 with $h = 1.0$	71

2.45	Same as Fig. 2.43 with $h = 2.0$	72
2.46	Plots of coding gain at $P_b = 10^{-9}$ vs normalized laser linewidth $\Delta\nu T$ for rate 1/2 convolutionally coded FSK with constraint length $K = 4$ and $K = 7$ for $h = 0.5$ , $h = 1.0$ and $h = 2.0$	73
2.47	Plots of coding gain at $P_b = 10^{-9}$ vs normalized laser linewidth $\Delta\nu T$ for RS (15,9) and (15,7) coded FSK for $h = 0.5$ , $h = 1.0$ and $h = 2.0$	74
3.1	Block diagram of a FSK direct detection receiver employing MZI with preamplifier and decoder	79
3.2	Plots of bit error probability $P_b$ vs transmitted signal power $P_s(\text{dB}_m)$ for uncoded and rate 1/2 convolutionally coded ( $K = 4, 7$ ) optically preamplified FSK ( $G = 30\text{dB}$ ) with modulation index $h = 1.0$ and laser linewidth $\Delta\nu T = 0.000$	83
3.3	Same as Fig. 3.2 with $\Delta\nu T = 0.008$	84
3.4	Same as Fig. 3.2 with $\Delta\nu T = 0.014$	85
3.5	Same as Fig. 3.2 with $\Delta\nu T = 0.019$	86
3.6	Plots of bit error probability $P_b$ vs transmitted signal power $P_s(\text{dB}_m)$ for uncoded and rate 1/2 convolutionally coded ( $K = 4, 7$ ) optically preamplified FSK ( $G = 40\text{dB}$ ) with modulation index $h = 1.0$ and laser linewidth $\Delta\nu T = 0.000$	87
3.7	Same as Fig. 3.6 with $\Delta\nu T = 0.008$	88
3.8	Same as Fig. 3.6 with $\Delta\nu T = 0.014$	89
3.9	Same as Fig. 3.6 with $\Delta\nu T = 0.019$	90
3.10	Plots of bit error probability $P_b$ vs transmitted signal power $P_s(\text{dB}_m)$ for uncoded and Reed-Solomon's coded optically preamplified FSK ( $G = 30\text{dB}$ ) with modulation index $h = 1.0$ and laser linewidth $\Delta\nu T = 0.000$	91
3.11	Same as Fig. 3.10 with $\Delta\nu T = 0.008$	92
3.12	Same as Fig. 3.10 with $\Delta\nu T = 0.014$	93
3.13	Same as Fig. 3.10 with $\Delta\nu T = 0.019$	94
3.14	Plots of bit error probability $P_b$ vs transmitted signal power $P_s(\text{dB}_m)$ for uncoded and Reed-Solomon's coded optically preamplified FSK ( $G = 40\text{dB}$ ) with modulation index $h = 1.0$ and laser linewidth $\Delta\nu T = 0.000$	95
3.15	Same as Fig. 3.14 with $\Delta\nu T = 0.008$	96
3.16	Same as Fig. 3.14 with $\Delta\nu T = 0.014$	97
3.17	Same as Fig. 3.14 with $\Delta\nu T = 0.019$	98

3.18	Plots of coding gain at $P_b = 10^{-9}$ vs normalized laser linewidth $\Delta\nu T$ for rate 1/2 convolutionally coded optically preamplified FSK ( $G = 30\text{dB}$ ) with constraint length $K = 4$ and $K = 7$ for $h = 1.0$	99
3.19	Same as Fig. 3.18 with $G = 40\text{dB}$	100
3.20	Plots of coding gain at $P_b = 10^{-9}$ vs normalized laser linewidth $\Delta\nu T$ , Reed-Solomon's (15,9) and (15,7) coded optically preamplified FSK ( $G = 30\text{dB}$ ) for $h = 1.0$	101
3.21	Same as Fig. 3.20 with $G = 40\text{dB}$	102
3.22	Plots of power penalty due to phase noise at $P_b = 10^{-9}$ for uncoded and rate 1/2 convolutionally coded optically preamplified FSK ( $G = 30\text{dB}$ ) as a function of normalized laser linewidth $\Delta\nu T$ for modulation index $h = 1.0$	103
3.23	Same as Fig. 3.22 with $G = 40\text{dB}$	104
3.24	Plots of power penalty due to phase noise at $P_b = 10^{-9}$ for uncoded and Reed-Solomon's coded optically preamplified FSK ( $G = 30\text{dB}$ ) as a function of normalized laser linewidth $\Delta\nu T$ for modulation index $h = 1.0$	105
3.25	Same as Fig. 3.24 with $G = 40\text{dB}$	106

## LIST OF PRINCIPAL SYMBOLS

$n(t)$	Additive noise due to amplifier spontaneous emission ( ASE )
$P_b$	Bit error rate
$T$	Bit period
$R_b$	Bit rate
$k$	Block length
$K_B$	Boltzmann's constant
CG	Coding Gain
$\tau$	Delay occurred due to path difference
$\delta(f)$	Delta function in frequency
$\delta(t)$	Delta function in time
$B_e$	Effective bandwidth of baseband filter in receiver
$N_{\text{excess}}$	Excess noise power
$M(f)$	FM response of laser
$\Delta f$	Frequency deviation of FSK signal
$\delta_\nu$	Frequency separation
$\eta_{in}$	Input coupling efficiency of optical amplifier
$\mathcal{F}^{-1}$	Inverse Fourier transform
$m(t)$	Inverse Fourier transform of $M(f)$
$\mu(t)$	Laser instantaneous frequency fluctuation
$\beta T$	Linewidth to bit ratio
$R_L$	Load resistance
$d_{\text{min}}$	Minimum free hamming distance
$I(t)$	Modulating signal
$h$	Modulation index
$B_o$	Noise equivalent bandwidth (NEB) of optical amplifier
$F_e$	Noise figure of receiver
$\Delta\nu T$	Normalized linewidth of laser
M	Order of M-ary pulse position modulation
$\eta_{out}$	Output coupling efficiency of optical amplifier
$\Delta L$	Path difference of MZI
$\phi_s$	Phase due to FSK signal
$\phi_n$	Phase due to laser phase noise
$N_{s-sp}$	Power due to signal-spontaneous beat noise
G	Preamplifier Gain
$\eta$	Quantum efficiency of photodetector
$P_s$	Received signal power
$P_{in}$	Receiver power input

$T_r$	Receiver temperature in Kelvin
$R_d$	Responsivity of the photodetector
$N_{shot}$	Shot noise power
$T_r$	Temperature of receiver
$N_{th}$	Thermal noise power
$n$	Total encoded block length
$\sigma_x^2$	Variance of phase noise

## LIST OF ABBREVIATIONS

APD	Avalanche photodetector
ASE	Amplifier's spontaneous emission
ASK	Amplitude shift keying
AWGN	Additive white gaussian noise
BEC	Binary erasure channel
BER	Bit error rate
BPPM	Binary PPM
BSC	Binary symmetric channel
BW	Bandwidth
CPFSK	Continuous phase FSK
CPSK	Continuous phase FSK
dB <sub>m</sub>	decibel relative to 1 mw
DFA	Doped fibre amplifier
DFB	Distributed feedback
DFT	Discrete Fourier Transform
DMC	Discrete memoryless channel
EDFA	Erbium doped fibre amplifier
erfc	Complementary error function
FPI	Fabry Perot Interferometer
FSK	Frequency shift keying
FSK-DD	FSK with direct detection
IF	Intermediate frequency
IFT	Inverse Fourier Transform
IM/DD	Intensity modulation and direct detection
ISI	Inter-symbol interference
LD	Laser diode
LW	linewidth
MZI	Mach-Zehnder interferometer
NEB	Noise equivalent bandwidth
NRZ	Non-return to zero
NRZ-FSK	FSK with NRZ data
OFD	Optical frequency discriminator
OFDM	Optical frequency division multiplexing
OOK	ON-off keying
PDF	Probability density function
PN	Phase noise
PPM	Pulse position modulation
TDMA	Time division multiple access

<b>FDM</b>	<b>Frequency division multiplexing</b>
<b>PSD</b>	<b>Power spectral density</b>
<b>PSK</b>	<b>Phase shift keying</b>
<b>SNR</b>	<b>Signal to noise ratio</b>
<b>SLA</b>	<b>Semiconductor laser amplifier</b>
<b>WDM</b>	<b>Wavelength division multiplexing</b>



# **CHAPTER 1**

## **INTRODUCTION**

Table of contents :

- 1.1 Prologue
- 1.2 Importance of Coding in Optical Communication systems and their benefits
- 1.3 Forward Error Correction -- A brief review
- 1.4 Advantages of FSK system and previous work on FSK direct detection system without codes
- 1.5 Objectives of this thesis
- 1.6 Organization of the thesis



## 1.1 Prologue :

Since the introduction of Optical Fibre in Communication systems in 1960, the vast bandwidth of this spectacular media has always provoked the interests of all. The quest of the maximum beneficial method to harness the underutilized free band-space has brought about numerous techniques & proposals. A few of these has only been analyzed thoroughly to reach for a final goal. Many of these attempts have given new insights to explore even further deeper. The significant progress accomplished in the last few years in the development of high speed fibre optics has helped to move multigigabit-per-second systems close to commercial reality. The trend of these studies is essentially enriching the domain of this media for all futuristic Communication systems.

## 1.2 Importance of Coding in Optical Communication systems and their benefits :

Today many long haul optical communication systems has been established, most of these employ monomode optical fibres. These fibres usually have bandwidths that are orders of magnitude greater than the bandwidth of information being transmitted over them. Therefore the excess bandwidth can be harnessed to increase the receiver sensitivity. Various nonlinear effects like additive white gaussian noise, optical amplifier spontaneous emission etc. impose embargo in the maximum achievable data transmission rate and receiver sensitivity. Coding data prior to transmission and subsequent decoding while at receiving enables us to reduce the aforesaid difficulties to a significant extent. The role of forward error correction coding in relaxing laser specifications, increasing receiver sensitivity and increasing packing efficiency of FDMA networks has attracted much research interests in the last decades[1-9]. In particular coding offers the following advantages[1-3] :

1. Compared to the uncoded case, the signal to noise ratio per information bit ( $E_b/N_o$ )

required with coding is reduced by the coding gain (actually more because for the coded signal, the linewidth to bit ratio  $\beta T$  is reduced due to the increase of the channel rate).

2. For a specified signal power, the coding gain can be used to relax the laser linewidth specifications.
3. For substantial phase noise (linewidth to bit ratio  $\beta T$  of the order of one), a significantly wider bandwidth is needed for the receiver front-end IF filter than would be used in the case of zero phase noise. The motivation for this is to accommodate the frequency-broadened signal that is caused by considerable phase noise. The wider bandwidth implies a higher IF and hence greater vulnerability to  $f^2$ -type thermal noise in the receiver. Coding by permitting a narrower IF filter, thus reduces the vulnerability of the receiver to the  $f^2$ -type noise.

### 1.3 Forward Error Correction Coding -- A brief review :

Error correction coding is commonly used in digital communications to improve the average probability of bit error. The two common features of all error-correction codes are structured redundancy and noise averaging. Structured redundancy is a method of inserting extra or redundant symbols into the information message. Noise averaging is obtained by making the redundant symbols to depend on a span of several information symbols. The uniqueness of structured redundancy makes it possible to tolerate some fraction of the symbols in a block of several information symbols being in error without destroying the uniqueness of the information message it conveys, thereby causing a block error. Also noise averaging indicates that the error rate decreases with increasing block length.

Coding schemes are often divided into two broad classes :

- Linear Block Codes
- Convolution Codes (or more generally , tree codes).

With block coding, the information data, which is usually binary symbols or bits (but many have been encoded in any alphabet of  $q > 2$  symbols), is segmented into block of  $k$ -bits of information each, where  $k$  is called the *block length*. Each information block can represent any one of  $M = 2^k$  distinct messages ( $M = q^k$  if  $q > 2$ ). The encoder then transforms each information block into a larger block of  $n$  bits ( $n > k$ ) by adding  $n - k$  redundant bits in a unique way. Each block of  $n$  bits from the encoder constitutes a *code word* contained in the set of  $M = 2^k$  possible code words. The code words are then fed to the modulator which generates a set of finite time duration waveforms for transmission over the channel. A block encoder is a *memoryless* device because each  $n$ -bit code word depends only on a specific  $k$ -bit information block and on no others. But it does not mean that the encoder does not contain memory elements. The ratio of information bits to total bits in a code word is called the *code rate*  $R$ . It is seen that

$$R = k/n$$

The correction capability of the code  $t$  is directly proportional to the amount of redundancy and can be bounded by the useful relation [10-13],

$$t \leq (n - k) / 2$$

If  $R_b$  is the information bit rate at input of the encoder, the coded bit rate  $R_c$  at the output of the encoder is

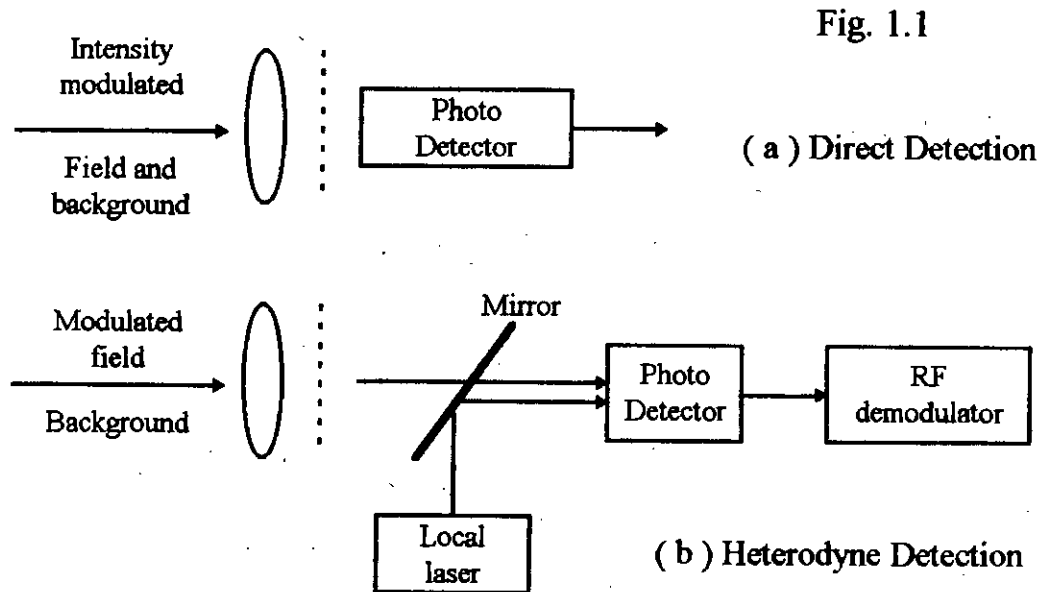
$$R_c = R_b/R = nR_b/k$$

Practical values for information block length  $k$  range from 3 to several hundreds and for  $R$  from 1/4 to 7/8.

#### **1.4 Advantages of FSK system and previous work on FSK direct detection system without codes :**

In a lightwave communication system, two important detection strategies are normally employed, viz. direct detection and coherent detection. In a direct detection reception, the intensity of the received optical field is directly converted to a current by a photodetector while in coherent detection, the received optical field is combined with

the light output from a local oscillator laser and the mixed optical field is converted to an intermediate frequency (IF) signal by heterodyning or directly to a baseband by homodyning.



Direct detection has become recent attraction for the optical communication designers. The obvious reasons are low cost, simplicity and a lot more which is yet to be evaluated. However, the direct detection technique has the limitation in data rate for application in power limited free-space optical channels due to relatively low optical power output of semiconductor laser diode. The work undertaken here is confined to direct detection scheme which though have a few shortcomings possess a significant immunity to noise interference compared to the heterodyne detection concept. This is because the direct detection technique does not use the phase information. Our attempt is to explore this particular phenomena and judge the overall performance which should reflect the actual improvement if there is any.

The nonzero linewidth of laser causes a BER floor and performance enhancement cannot be achieved beyond the BER floor by increasing the signal strength alone. Though the receiver performance can be improved by increasing the modulation index, but there lies a definite limit upto which this technique might help. Coding data prior to transmission has been a proven alternative to overcome this problem. Different coding schemes with different modulation formats has evoked innumerable combination to try for the designers. Direct detection optical communication systems

are very promising for future deep space applications, inter-satellite links and terrestrial line of sight communications. The current effort proves beneficial to the context of relaxing laser specification and cost optimization.

There are two categories of FSK system. One consists of FSK coherent detection systems and the other of FSK noncoherent detection system. Coherent detection means either IF synchronous detection or delay modulation. Noncoherent detection means envelope detection with appropriate filter. Coherent detection can achieve higher receiver sensitivity, though it requires high spectral purity for light sources. The CPFSK heterodyne delay demodulation system belongs to this category. Some high performance systems have been developed under this scheme by using external cavity LDs [14] or a distributed feedback (DFB) LD and a monolithic external cavity LD pair [15].

The FSK heterodyne dual filter and single filter detection systems are examples of noncoherent detection systems. In these systems, the phase information from the signal is not used. Therefore, a relatively large LD spectral spread can be tolerated and conventional DFB LDs becomes applicable. This is important for achieving a simple and stable system. Some experiments have been conducted using DFB LDs with single filter detection. However the dual detection system is particularly attractive because it offers a 3 dB higher receiver sensitivity than the single filter detection system. A 34 Mbit/s , 301 km transmission experiment with FSK dual filter detection has already reported [16].

The direct detection lightwave systems used in terrestrial communication are well matured. However there are adequate scope for further investigations in space borne direct detection lightwave systems. One important area which demand close examination is the study of the relative advantage of the various error correcting codes when combined with a modulation scheme used for optical pulse transmission. The use of error control coding is almost indispensable in space channel in order to ensure high energy efficiency and to reduce the required average power.

Although significant progress has been achieved during the last decade on coherent lightwave systems and many experimental and field trials of coherent systems have

been reported from various parts of the globe, the very nature of the constantly evolving technology places itself to more new and challenging problems that need to be addressed more widely and seriously in order to arrive at stable and acceptable system solution for practical adoption. A few of these problems has been the subject of closed examination carried out over a period of last four years.

McElice [4] investigated the use of Reed-Solomon's codes to increase the transmission efficiency of the system. Massey [5] studied the application of interleaved binary convolution codes and showed that the improvement was comparable with that of RS codes. However, all these works were concerned with erasure channel with quantum-noise limited operation. Gagliardi and Yuen [6] analyzed the system performance when false-alarm error as well as quantum noise error were considered.

Convolutional coding for the optical channel has also been investigated by Chan [7] in which he has reported the theoretical maximum coding gains. Forestieri, Gangopadhyay and Prati [8] analyzed the performance of several strategies for combining practical convolutional codes and PPM schemes in a direct detection optical channel and reported the practically achievable coding gains in the presence of background radiation for both photon counting and Avalanche Photodetector (APD) optical receivers. The performance of interleaved  $2^L$ -ary PPM with  $\delta$ -max soft-demodulation is superior to other M-ary strategies. However, in the presence of background noise, short-constraint-length CC on L separate channels in an interleaved  $2^L$ -ary PPM performed somewhat worse relative to RS coding on the full channel.

Recently, Atkin and Fung [9] investigated the performance of RS coded optical PPM system using direct and coherent detection and compared the performance of both uncoded and coded coherent PPM system with those for direct detection. It was found that the coded heterodyne PPM system has a 15.38 dB improvement over coded direct detection system. The receiver employed was a matched filter receiver and used threshold detection. In 1990 L. J. Cimini, JR. and G.J. Foschini have demonstrated the advantages of using forward error correction in an OOK optical communication system [2] to mitigate the effects of laser phase noise and AWGN. R. Schweikert and A. J. Vinck showed in a paper

that concatenated coding can be advantageously used in communication links with high data rates. This was achieved via multiplexing a set of regular Viterbi decoders [17]. The outer soft-decision SPC decoding, applied to correct decoding errors resulting from the inner decoding requires only a small amount of additional hardware, not likely to limit the decoding speed.

Y.T. Koh and F. Davidson studied the [performance of two concatenated coding systems using a  $K = 3, r = 1 / 2$  Convolutional code (inner code) and a (15, 9) or (15, 7) Reed-Solomon's code was (outer code) measured over a 5.76 km long atmospheric direct detection [1] optical communication channel. Inner code interleaving of  $100 \mu\text{s}$  combined with outer code interleaving of 240 bits (60 RS symbols) was found to be sufficient to obtain a decoded BER of less than  $10^{-6}$  under conditions of moderate channel turbulence ( $\sigma_{m\lambda}^2 = 0.6$ ) and an average of 6-10 detected photons per channel bit.

## 1.5 Objectives of this thesis :

The objective of the present research work is to investigate the efficacy of the forward error correction coding in improving the performance of optical direct detection FSK and ASK transmission systems in the presence of laser phase noise and optical amplifier's spontaneous emission noise. Further attempts will be made to determine the optimum system and receiver parameters for the design of coded optical FSK and ASK systems.

A detailed theoretical analysis is to be carried out to evaluate the bit error rate performance of optical FSK systems with direct detection receivers, employing two forward error correction coding techniques viz. convolutional coding and Reed-Solomon coding. The analysis is to be extended to include optical preamplifier in the receiver front end and to determine the effects of laser phase noise, amplifier's spontaneous emission noise and gain saturation of optical amplifier etc. on the system performance.

An analytical expression for the pair-wise error probability is to be developed to obtain the upper bounds on the bit error probability for the coded systems. Following



this analytical formulation, the performance results for the coded systems will be evaluated at a bit rate of 1 Gb/sec. The improvements in system performance over the uncoded system will also be determined at a specified bit error rate.

## **1.6 Organization of the thesis :**

In chapter 1 we have attempted to discuss the preliminary topics relevant to our subject and the importance of coding in optical communication system. A brief review of different coding schemes are also given.

In chapter 2 detailed theoretical analysis of error probability is discussed. We also provide the analytical expressions for bit error rate for optical receiver with Mach-Zehnder interferometer (MZI) as an optical frequency discriminator (OFD) considering the effects of laser phase noise and receiver noise.

In chapter 3 the popular erbium doped fibre amplifier (EDFA) is discussed which is used to improve the receiver sensitivity. The analysis takes further into account the effects of laser phase noise and amplifier spontaneous emission (ASE).

# **CHAPTER 2**

## **OPTICAL DIRECT DETECTION FSK WITH AND WITHOUT CODING**

Table of contents :

- 2.1 Prologue
- 2.2 A model receiver description
  - 2.2.1 Discriminator Operation
- 2.3 Theoretical analysis for optical FSK with direct detection
- 2.4 Theoretical analysis for coded optical FSK.
  - 2.4.1 Coding topologies
  - 2.4.2 FSK with Convolution coding
  - 2.4.3 FSK with Reed-Solomon's coding
- 2.5 Results and discussion.

## 2.1 Prologue :

Among the high promising modulation scheme now-a-days the frequency shift keying (FSK) is applied both in direct detection and coherent detection. This due to fact that it has a compact spectrum and it can take the advantage of the direct frequency modulation characteristics of distributed feedback (DFB) laser. However a significant degradation is noticed due to laser phase noise in heterodyne optical FSK system. Detailed theoretical analysis shows that coherent systems though have in general a gain of 10 - 20 dB more in comparison to their direct detection counterpart, yet the whole system is a lot more complex and expensive, not to mention about their high susceptibility to phase noise and amplifier spontaneous emission. Because of the requirement of the narrow bandwidth (LW) laser at both transmitter and receiver for the coherent case and additional circuits for the polarization matching between the received optical field and locally generated optical field, the phase of the transmitting laser has to be tracked at the receiver. The other problem with the coherent system is that the total effective LW is the sum of the transmitting and local oscillator (LO) lasers. Thus a higher modulation index may be required to attain a particular bit error rate (BER). The obvious penalty is the increased transmission bandwidth. For a coherent heterodyne system, the intermediate frequency (IF) is around 4 - 6 times the bit rate. So for a multi-gigabit system the receiver photodiode must have a very high bandwidth. Also a large amount of equalization is required at the receiver and existence of large  $f^2$  noise at high bit rate increases the receiver thermal noise. Hence in spite of the improved sensitivity the recent trend is to try the possibilities of the direct detection system.

The so called laser phase noise affects direct detection much less because direct detection does not utilize any phase information. Recently a direct detection FSK receiver which utilizes a Mach-Zehnder Interferometer as an optical discriminator is reported [18]. However, performance degradation of this type of receiver due to laser phase noise is determined but only for the uncoded case. Our attempt here is to introduce the combination of different coding and evaluate the results.

The following topics gradually explains the discriminator and related analytical expressions extending towards the coded analysis.

## **2.2 A model receiver description :**

The essentials of the proposed receiver is presented in fig. 2.1. The MZI acts only as an optical filter and differentially detects the 'mark' and 'space' of received FSK signal which are then directly fed to a pair of photodetectors. The difference of the two photocurrents are applied to the amplifier which is followed by an equalizer. The equalizer is required to equalize the pulse shape distortion caused by the photodetector capacitance and due to the input resistance and capacitance of the amplifier. The reshaped pulses after passing through the baseband filter is detected at the decision circuit by comparing it with a threshold of zero value.

One other type of discriminator is worthy of reference here, namely the Fabry-Perot etalon Interferometer; a small comparison in connection to direct detection would reveal some relevant aspects[19].

1. Mach-Zehnder Interferometer and the Fabry-Perot etalon Interferometer both can act as tunable filter (for multichannel application) and optical discriminator.
2. The OFDs (MZI/FPI) are built with passive components which are less costly compared to heterodyne system.
3. MZI provides easy tunability in multichannel system compared to heterodyne system which requires LDs with wide tuning range and narrow LW.
4. Receiver design is simple and less costly due to the absence of the sophisticated wideband IF circuits.

### **2.2.1 Discriminator operation :**

It is a common property of the interference filters to transmit a narrow band of wavelengths and blocking all wavelengths outside the band. In our receiver MZI is employed which is integrated with a silica based waveguide. It is a very promising device in wavelength division multiplexing (WDM) and frequency division

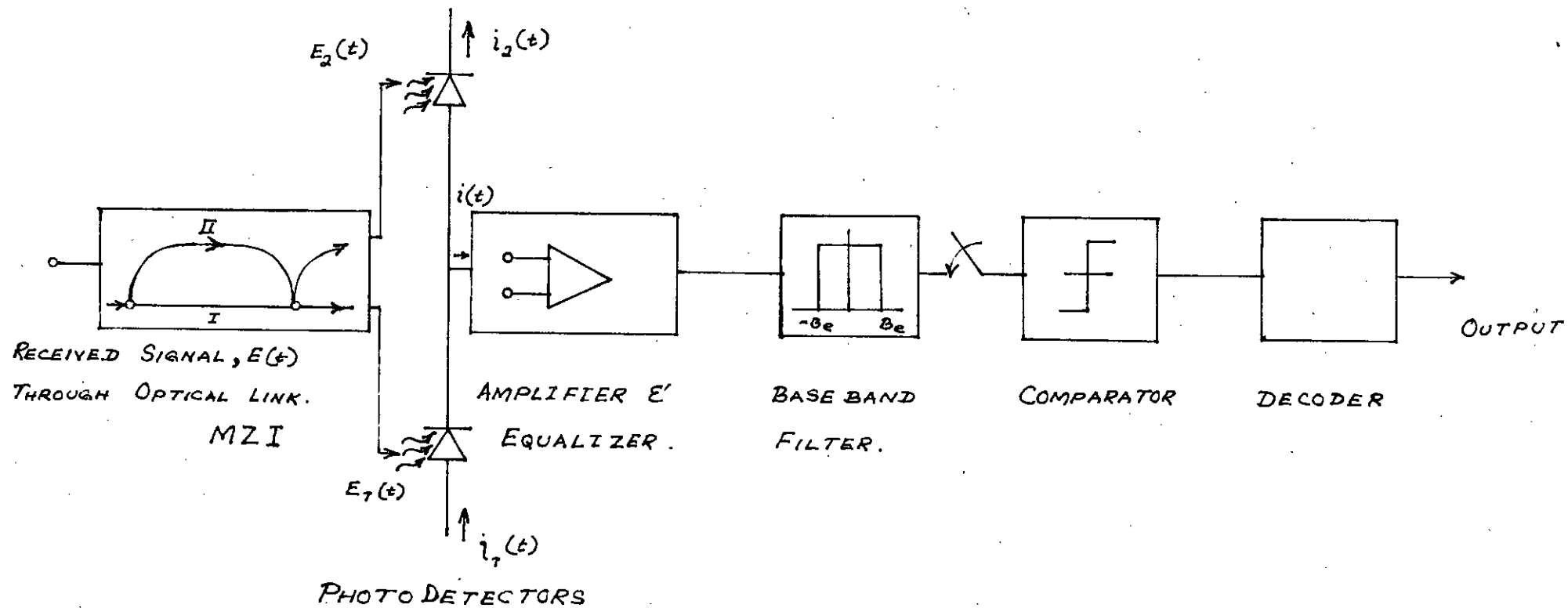


Fig. 2.1 Block diagram of a FSK direct detection receiver employing MZI with decoder

multiplexing (FDM) systems. Because of their high frequency selectivity without mechanical actuator (which is an essential for an FPI), MZI is 3 dB more power efficient compared to FPI. MZIs can be series cascaded to achieve increased transmission capacity[18-19].

Fig 2.2 shows the basic configurations of an MZI. It has two input ports, two output ports two 3 dB couplers and two waveguide arms with length difference  $\Delta L$ . The configuration in Fig. 2.2 (b) and 2.2 (c) are suitable for MZI with large  $\Delta L$  and small  $\Delta L$ , respectively. A thin film heater is placed in one of the arms. It acts as a phase shifter because the light path length of the heated waveguide arm changes due to the change of refractive index. The phase shifter is used for precise frequency tuning. Frequency spacing from the peak to bottom transmittance of the OFD is set equal to the peak to peak frequency deviation  $2\Delta f$  of the FSK signal. Consequently the 'mark' and the 'space' appear at the two output ports of the OFD. These outputs are differentially detected by the photodetectors with balanced configuration.

### 2.3 Theoretical analysis for optical FSK with direct detection :

If  $E(t)$  represents the signal input to the MZI Fig. 2.2 then the signals received at the output ports can be expressed as [19]

$$|E_2(t)| = |E(t)| \sin \left[ \frac{k(l_2 - l_1)}{2} \right] \quad (2.3.1)$$

and

$$|E_1(t)| = |E(t)| \cos \left[ \frac{k(l_2 - l_1)}{2} \right] \quad (2.3.2)$$

where,  $l_1$  and  $l_2$  are the lengths of two arms of MZI and  $k$  is the wave number which can be expressed as

$$k = \frac{w}{v} = \frac{2\pi}{\lambda} = \frac{2\pi f \eta_{eff}}{c} \quad (2.3.3)$$

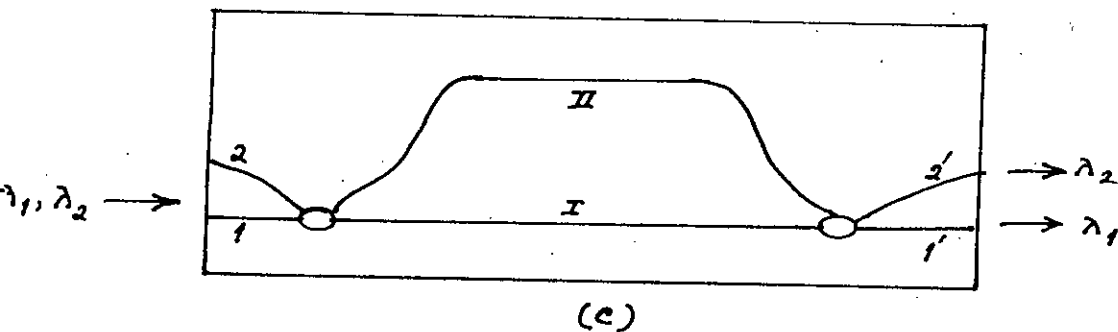
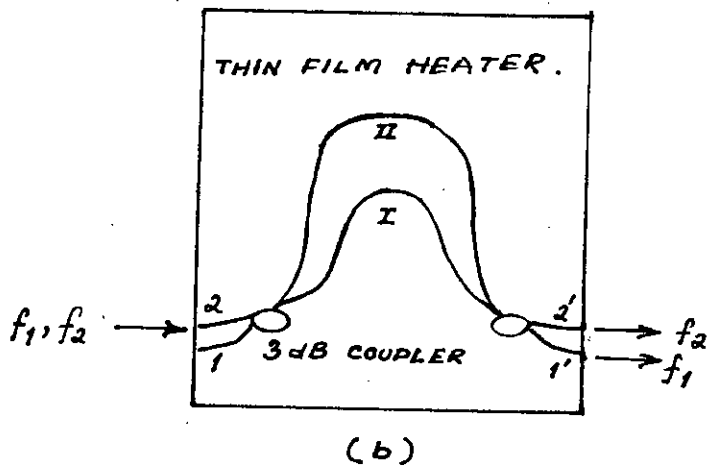
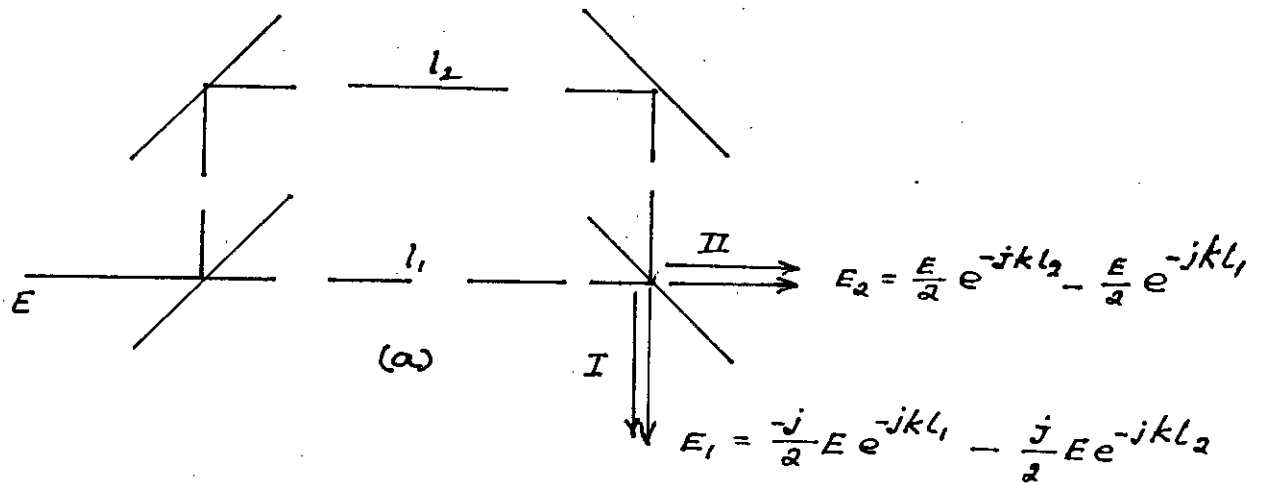


Fig. 2.2 Basic configuration of a Mach-Zehnder Interferometer for WDM/FDM multiplexer/demultiplexer. a) An MZI, b) An MZI with large  $\Delta L$  or narrow wavelength spacing and c) An MZI with small  $\Delta L$  or wide wavelength spacing.

$\eta_{eff}$ ,  $f$  and  $c$  are the effective refractive index of the waveguide, frequency of optical input signal and velocity of light in vacuum, respectively.

The transmittance of arm II of MZI

$$T_{II}(f) = \frac{|E_2(t)|^2}{|E(t)|^2} = \sin^2 \left[ \frac{k(l_2 - l_1)}{2} \right] = \sin^2 \theta \quad (2.3.4)$$

and that of arm I of MZI is

$$T_I(f) = \frac{|E_1(t)|^2}{|E(t)|^2} = \cos^2 \left[ \frac{k(l_2 - l_1)}{2} \right] = \cos^2 \theta \quad (2.3.5)$$

where,  $\theta$  is the phase factor related to the arm path difference  $\Delta L = l_2 - l_1$  and can be expressed as

$$\theta = \frac{k\Delta L}{2} = \frac{\pi f \eta_{eff} \Delta L}{c} \quad (2.3.6)$$

Normally  $\Delta L$  is chosen as

$$\Delta L = \frac{c}{4 \eta_{eff} \Delta f} \quad (2.3.7)$$

Therefore,

$$\theta = \frac{\pi f}{4 \Delta f} \quad (2.3.8)$$

Then we get

$$T_{II}(f) = \sin^2 \left( \frac{\pi f}{4 \Delta f} \right) \quad (2.3.9)$$

and

$$T_I(f) = \cos^2 \left( \frac{\pi f}{4 \Delta f} \right) \quad (2.3.10)$$

The two outputs of the MZI are therefore anti-symmetric and are shown in Fig. 2.3.

For an MZI used as an OFD,  $\Delta f$  is so chosen that [19]



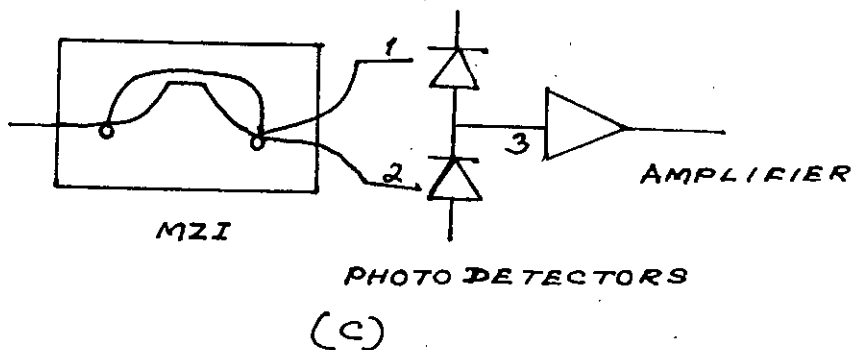
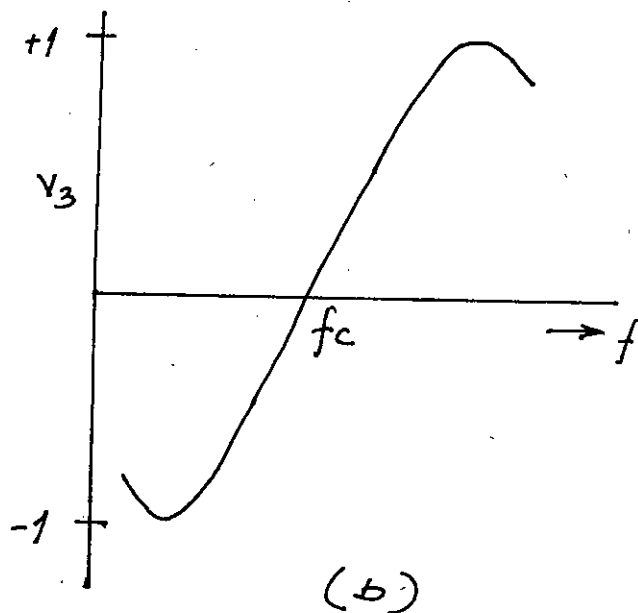
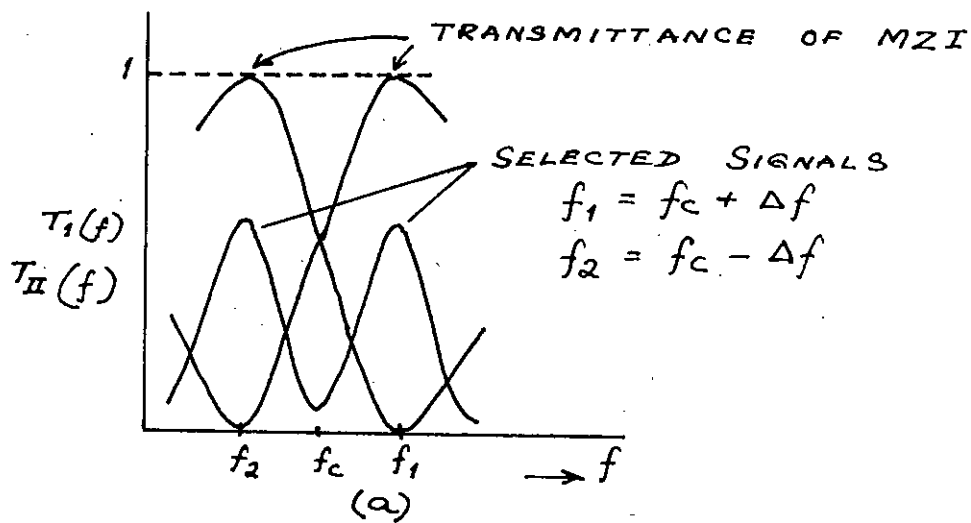


Fig. 2.3 MZI as an optical frequency discriminator a) Transmittance characteristic of MZI, b) Differential output of the balanced receiver and c) The balanced receiver with MZI.

$$\Delta f = \frac{f_c}{2n+1} \quad (2.3.11)$$

where,  $f_c$  is the carrier frequency of the FSK signal and  $n$  is an integer. The 'mark' and 'space' of FSK signals are represented by  $f_1$  and  $f_2$ , respectively where  $f_1 = f_c + \Delta f$  and  $f_2 = f_c - \Delta f$ .

Therefore, when 'mark' ( $f_1$ ) is transmitted

$$T_I = 1 \text{ and } T_H = 0 \quad (2.3.12)$$

Similarly, for transmission of 'space'

$$T_I = 0 \text{ and } T_H = 1 \quad (2.3.13)$$

Thus, two different signals  $f_1$  and  $f_2$ , can be extracted from the two output ports of MZI.

In our study the MZI is used only as an OFD due to the single channel mode of the operation. However full benefits of MZI can be exploited in a multichannel operation for a WDM/FDM system utilizing the periodicity of the transmittance versus frequency characteristics of an MZI[19].

The received optical signal at the input to MZI can be expressed as

$$E(t) = \sqrt{2P_s} \cos[2\pi f_c t + \phi_s(t) + \phi_n(t)] \quad (2.3.14)$$

where,  $P_s$  is the average optical power,  $f_c$  is the optical carrier frequency, and  $\phi_s(t)$  and  $\phi_n(t)$  are the signal and instantaneous phase noise of the transmitting laser, respectively.

The signal phase  $\phi_s(t)$  can be expressed as

$$\phi_s(t) = 2\pi \int_0^t I(\tau) * m(\tau) d\tau \quad (2.3.15)$$

where,  $I(t)$  is the modulating signal,  $*$  denotes convolution and  $m(t)$  denotes the inverse Fourier transform (IFT) of the FM response characteristic  $M(f)$  of transmitting DFB laser.

The phase due to laser instantaneous frequency noise can be expressed as[18]

$$\phi_n(t) = 2\pi \int_0^t \mu(t_1) dt_1 \quad (2.3.16)$$

where,  $\mu(t)$  represents the laser instantaneous frequency fluctuation which is Gaussian distributed with zero mean and having a white power spectral density of magnitude  $\Delta\nu/2\pi$ . If the transmitting laser has an ideal FM response characteristic, then  $M(f)$  is flat over all frequencies of the modulating signal and  $m(t)$  is a Dirac Delta function.

The normalization of  $M(f)$  is done in such a way that the magnitude of  $m(t)$  represents the desired peak deviation. We define the modulation index  $h$ , as the ratio of peak-to-peak frequency deviation to bit rate  $1/T$ , i.e.,  $h = 2\Delta f T$ . For a given modulation index  $h$ , the normalized  $m(t)$  will be a delta function having magnitude  $\Delta f$ . Thus  $m(t) = \mathfrak{F}^{-1}[M(f)] = \Delta f \cdot \delta(t)$ , where  $\mathfrak{F}^{-1}$  denotes the inverse Fourier transform. In case of random NRZ data

$$I(t) = \sum_{k=-\infty}^{\infty} a_k p(t - kT)$$

where,  $a_k = \pm 1$ , represents the  $k$ -th information bit and  $p(t)$  is the elementary rectangular pulse of unit amplitude and duration  $T$  seconds. For NRZ format the signal phase therefore can be expressed as

$$\phi_s(t) = 2\pi\Delta f \int_0^t \sum_k a_k p(t_1 - kT) dt_1 \quad (2.3.17)$$

The optical fields at the output of two branches of MZI can be expressed as

$$E_2(t) = \frac{1}{2} [E(t - \tau_b) - E(t - \tau_a)] \quad (2.3.18)$$

and

$$E_1(t) = \frac{-j}{2} [E(t - \tau_a) - E(t - \tau_b)] \quad (2.3.19)$$

where,  $\tau_a = \frac{\eta l_1}{c}$  and  $\tau_b = \frac{\eta l_2}{c}$ .

Let us define the time delay due to path difference in MZI as

$$\tau = \tau_b - \tau_a = \frac{\eta(l_2 - l_1)}{c} \quad (2.3.20)$$

Without any loss of generality we can take  $\tau_a = 0$ , then  $\tau_a = \tau$ . Using (2.3.13), (2.3.16) and (2.3.17), the output current of upper photodetector is given by,

$$\begin{aligned} i_2(t) &= R_d |E_2(t)|^2 \\ &= \frac{R_d P_o}{2} \left[ 1 - \cos \left\{ 2\pi f_c \tau + 2\pi\Delta f \int_{t-\tau}^t \sum_k a_k p(t_1 - kT) dt_1 + \Delta\phi_n(t, \tau) \right\} \right] \end{aligned} \quad (2.3.21)$$

where,  $R_d$  is the responsivity of the photodetector.

Similarly, the output current at the lower photodetector can be expressed as

$$i_1(t) = R_d |E_1(t)|^2 \quad (2.3.22)$$

$$= \frac{R_d P_s}{2} \left[ 1 + \cos \left\{ 2\pi f_c \tau + 2\pi \Delta f \int_{t-\tau}^t \sum_k a_k p(t_1 - kT) dt_1 + \Delta \phi_n(t, \tau) \right\} \right]$$

The output of the balanced photodetectors is then found as

$$i = i_1 - i_2 \quad (2.3.23)$$

$$= R_d P_s \cos \left[ \omega_c \tau + \Delta \phi_s(t, \tau) + \Delta \phi_n(t, \tau) + \phi_0 \right]$$

where,  $\Delta \phi_n(t, \tau) = \phi_n(t) - \phi_n(t - \tau)$  is the phase change due to phase noise during the interval  $\tau$ ,  $\Delta \phi_s(t, \tau) = 2\pi \Delta f \int_{t-\tau}^t \sum_k a_k p(t_1 - kT) dt_1$  is the phase change due to signal component and  $\phi_0$  is the phase offset due to mismatch between  $f_c$  and MZI center frequency. For the ideal demodulation of CPFSK signal  $\tau$  is so chosen that [14].

$$\tau = \frac{T}{2h} \quad (2.3.24)$$

and

$$\omega_c \tau = (2n + 1) \frac{\pi}{2} \quad (2.3.25)$$

Then

$$2\pi \Delta f \tau = \frac{\pi}{2} \quad (2.3.26)$$

The phase offset  $\phi_0$  is assumed to be zero.

For the case of a " mark " transmission  $a_0 = +1$ , and the total phase change due to signal component  $\Delta \phi_n(t, \tau)$  during the interval  $\tau$  is  $2\pi \Delta f \tau$ . Under the chosen conditions, the signal current at the balanced photodetector output corresponding to bit ' 1 ' (mark), can be expressed as

$$i_m(t) = R_d P_s \cos[\Delta \phi_n(t, \tau)] \quad (2.3.27)$$

$$= R_d P_s x(t)$$

where,

$$x(t) = \cos[\Delta \phi_n(t, \tau)] \quad (2.3.28)$$

Similarly, for ' space ' transmission, the output of the balanced photodetector is

$$i(t) = -R_d P_s x(t)$$

The total noise power at the photodetector output consists of shot noise  $N_{shot}$ , excess noise due to laser phase  $N_{excess}$ , and thermal noise  $N_{th}$ . The power spectral density (PSD) and corresponding power of different noise components are derived in Ref. 18. which are as follows :

$$N_{shot} = 2eB_e R_d P_s \quad (2.3.29)$$

$$N_{excess} = \frac{1}{2}(R_d P_s)^2 \sigma_x^2 \quad (2.3.30)$$

where,

$$\sigma_x^2 = 2\pi\Delta\nu T \quad (2.3.31)$$

and

$$N_{th} = \frac{4KT_r F_e B_e}{R_L} \quad (2.3.32)$$

where,  $e$  is the charge of an electron,  $K$  is the Boltzmann's constant,  $T_r$  is the receiver temperature in degree kelvin,  $F_e$  is the receiver noise figure,  $B_e$  is the effective bandwidth of the baseband filter,  $R_L$  is the load resistance of the amplifier,  $P_s$  is the received signal power and  $\Delta\nu T$  is the transmitting laser linewidth.

Hence the total noise power at the photodetector (PD) output can be expressed as

$$N = N_{shot} + N_{excess} + N_{th} \quad (2.3.33)$$

For a given value of  $\Delta\phi_n(t, \tau) = \Delta\phi_n$ , the signal to noise ratio at the output of the photodetector is given by

$$Q(\Delta\phi_n) = \frac{i_m - i_s}{\sqrt{N}} = \frac{[2R_d R_e \cos \Delta\phi_n]}{\sqrt{N}} \quad (2.3.34)$$

The conditional bit error rate (BER) for the FSK-DD receiver conditioned on a given value of  $\Delta\phi_n$  is obtained as [15]

$$\begin{aligned} BER(\Delta\phi_n) &= \frac{1}{\sqrt{2\pi}} \int_Q^\infty e^{-\frac{x^2}{2}} dx \\ &= \frac{1}{2} \operatorname{erfc} \left\{ \frac{Q(\Delta\phi_n)}{\sqrt{2}} \right\} \end{aligned} \quad (2.3.35)$$

where,  $\operatorname{erfc}(x)$  represents the complementary error function defined as

$$\operatorname{erfc}(x) = 1 - \operatorname{erf}(x) = \frac{2}{\sqrt{\pi}} \int_x^\infty e^{-x^2} dx \quad (2.3.36)$$

The unconditional BER can be obtained by averaging the conditional BER over the distribution of  $\Delta\phi_n$ . Then

$$BER = E_{\Delta\phi_n} \left[ \frac{1}{2} \operatorname{erfc} \left\{ \frac{Q(\Delta\phi_n)}{\sqrt{2}} \right\} \right] \quad (2.3.37)$$

where,  $E_{\Delta\phi_n}$ , denotes the expectation of  $\Delta\phi_n$ . Using (2.33) and (2.36) the final form of bit error rate can be expressed as

$$BER = \frac{1}{2} \int_{-\infty}^{\infty} \operatorname{erfc} \left[ \frac{2R_d P_r \cos \Delta\phi_n}{\sqrt{2N}} \right] p(\Delta\phi_n) d(\Delta\phi_n) \quad (2.3.38)$$

where,  $p(\Delta\phi_n)$  represents the probability density function (PDF) of  $\Delta\phi_n$  which is Gaussian with zero mean and variance  $2\pi\Delta\nu\tau$  [20]. Thus

$$p(\Delta\phi_n) = \frac{1}{2\pi\sqrt{\Delta\nu\tau}} \exp \left\{ \frac{-[\Delta\phi_n(t, \tau)]^2}{4\pi\Delta\nu\tau} \right\} \quad (2.3.39)$$

where,  $\Delta\nu$  is the linewidth of the transmitting laser.

## 2.4 Theoretical analysis for coded optical FSK :

### 2.4.1 Coding topologies :

The optimum detection techniques for signals is corrupted by different types of channel noise. Shannon's Channel Capacity theorem states :

$$C = W \log_2 (1 + S/N) \text{ bits} \quad (2.4.1.1)$$

where  $C$  = channel capacity

$N$  = noise power

$S$  = signal power

$W$  = channel bandwidth

Since for PSK signaling with no coding,  $P_e = 10^{-5}$  for  $E_b/N_o = 9.6$  dB and from the above equation  $P_e \rightarrow 0$  for  $E_b/N_o = -1.6$  dB with ideal coding and  $W \rightarrow \infty$ , the capacity theorem promises a potential coding gain of 11 dB. Since the publication of Shannon's results in 1948, the systems designers have been constantly searching for coding methods to improve the rate of transmission in noisy channels. In a practical communication system, shown in the following figure, the ultimate efficiency in transmission may be obtained either by using forward-error-control techniques (FEC)

or by using a feedback channel along with error detection and retransmission techniques (ARQ). The ARQ method is used when the accuracy requirement is severe and some delay is permissible, e.g. in data transmission systems.

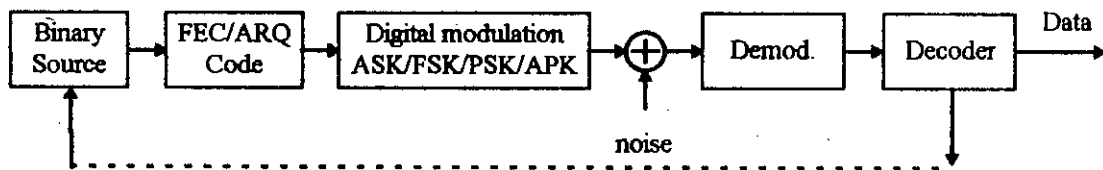
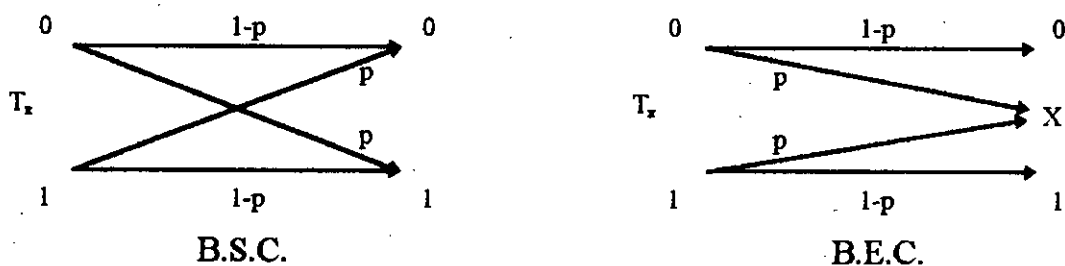


Fig. 2.4 Aux. channel for ARQ

If however, the time delay is not permissible and the transmission-reception has to be continuous as in, say, satellite links and long distance telephone channels, then FEC methods have to be used.

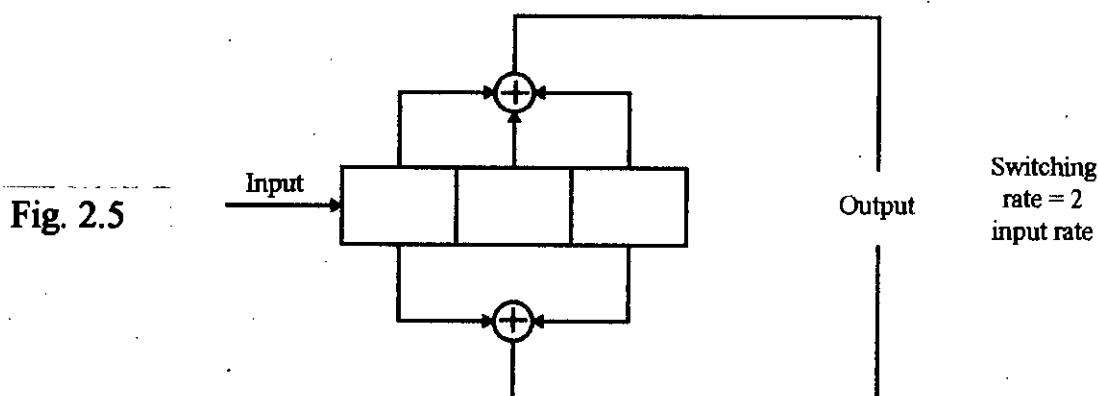
The channels are modeled as either a binary symmetric channel (BSC) or a binary erasure channel (BEC), as shown in the following figure. FEC is generally used in a BSC and ARQ in a BEC.



Errors occur in the channel either in a random manner or in bursts, e.g., in telephone channels and high frequency telephone channels. Specific burst-error correcting codes have been developed for bursty channels.

In Convolutional coding, the information data is passed through a linear shift register with  $M$  stages which shift  $k$  bits at time. For every  $M$  information bits stored in the shift register, there are  $n$  linear logic circuits which operate on the shift register contents to produce  $n$  coded bits as output of the encoder. The code rate  $R$  is therefore  $R = k / n$ . Because a particular information bit remains in the shift register for  $M/k$  shifts, it influences the value of  $nM / k$  coded bits. Thus, the Convolutional encoder is a device with memory. Typical values for  $k$  and  $n$  are in the range of 1 to 8, for  $R$  in

the range of 1/4 to 7/8, and for  $M$  in the range of 5 to 70. A Convolutional encoder with  $M = 3$ ,  $k = 1$  and  $n = 2$  is shown the figure below.



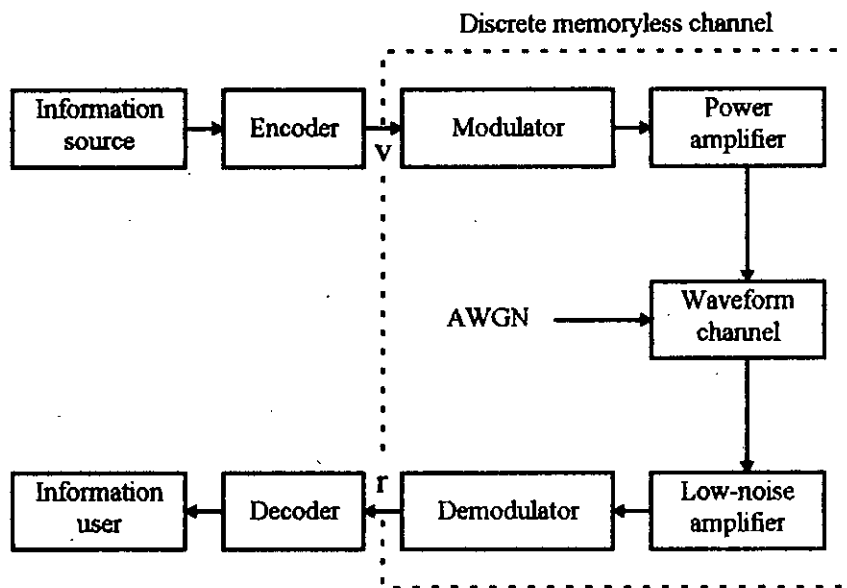
Form the above discussion it is seen that error-correction coding requires more capacity. This can be in the form of a wider bandwidth in a FDMA channel or a longer subburst in a TDMA channel.

In the following discussion some more concepts involving a coded system will be represented: *hard-decision*, *soft-decision*, and *maximum likelihood decoding* etc.. Consider a coded system operating on an AWGN waveform channel, from the viewpoint of the encoder and decoder, the *discrete memoryless channel* (DMC) is the most important. It is characterized by a set of  $M$ -ary input symbols,  $Q$ -ary output symbols, and *transition probabilities*  $\Pr(j|i)$ ,  $0 \leq i \leq (M - 1)$ ,  $0 \leq j \leq (Q - 1)$ , (where  $i$  is a modulator input symbol,  $j$  is a demodulator output symbol and probability  $\Pr(j|i)$  is the probability of receiving  $j$  given that  $i$  was transmitted) that are time-invariant and independent from symbol to symbol. The most commonly encountered case of a DMC is a *binary symmetric channel* (BSC) where ( 1 ) binary modulation is used ( $M = 2$ ) ; ( 2 ) the demodulator output is quantized to  $Q = 2$  levels and ( 3 )  $\Pr(0|1) = \Pr(1|0) = p$  and  $\Pr(0|0) = \Pr(1|1) = 1 - p$ . The *transition probability*  $p$  can be calculated from a knowledge of the waveform used, the probability density function of noise and the output quantization threshold of the demodulator. For example, when coherent PSK is used with binary output quantization, the BSC transition probability is just the PSK average probability of bit error with equally likely transmitted symbols 0 and 1 given by  $p = Q\sqrt{(2RE_b/N_o)}$ . The optimum threshold is 0 and the demodulator output is a 0 if the output voltage of the matched filter is negative. Otherwise, the output is a 1.



When binary demodulator output quantization is used ( $Q = 2$ ), the decoder has only binary inputs. In this case, the demodulator is said to make hard decisions and the decoding process is termed *hard-decision decoding*. Many coded digital communications systems use binary encoding with hard-decision decoding because of its simplicity.

In some binary-encoded systems where  $Q$ -ary demodulator output quantization is used ( $Q > 2$ ) or the output is left unquantized, the demodulator is said to make soft decisions. In this case the decoder accepts multilevel (or analog) inputs and the decoding process is termed *soft-decision decoding*. A soft-decision decoder is more complex than a hard decision decoder, as an automatic gain control is needed and  $\log_2 Q$  bits have to be manipulated for every channel bit.



Coded communication channel

Fig. 2.6

But soft-decision decoding offers an additional coding gain of about 2 dB at realistic values of  $E_b / N_o$  over hard-decision decoding. In practice eight-level quantization ( $Q = 8$ ) is commonly used because there is only a small difference in performance between the eight-level quantization scheme and the unquantized case. The eight-level quantized outputs involve one decision threshold and three pairs of confidence threshold.

*Hamming codes* have the following parameters.

Code length :  $n = 2^m - 1$

Information block length :  $k = 2^m - 1 - m = n - m$

Minimum distance :  $d_{min} = 3$

Error correcting capability :  $t = 1$

Hamming codes are examples of the few known perfect codes. We note that a perfect code must satisfy the following equation :

$$\sum_{i=0}^t \binom{n}{i} \leq 2^{n-k} \quad (2.4.1.2)$$

which for hamming code is :

$$1 + n = 2^{n-k} \quad (2.4.1.3)$$

since  $n = 2^{n-k} - 1$  for these codes, they are obviously perfect. Hamming codes comprises one of the few classes of codes for which the complete weight structure is known. The number of code words of weight  $i$ ,  $A_i$  is simply the coefficient of  $x^i$  in the expansion of the following weight enumerator polynomial.

$$A(x) = \frac{1}{n+1} \left[ (1+x)^n + n(1-x)(1-x^2)^{(n-1)/2} \right] \quad (2.4.1.4)$$

For example, let  $m = 3$ ,  $n = 2^3 - 1 = 7$ ,  $k = 7 - 3 = 4$ ; then the weight enumerator polynomial for the (7, 4) Hamming code is

$$A(x) = \frac{1}{8} \left[ (1+x)^7 + 7(1-x)(1-x^2)^3 \right] = 1 + 7x^3 + 7x^4 + x^7 \quad (2.4.1.5)$$

Therefore the weight structure for the (7, 4) Hamming code is  $A_0 = 1$ ,  $A_3 = A_4 = 7$  and  $A_7 = 1$ .

Golay codes represent another class of perfect codes and have the following parameters.

Code length :  $n = 23$

Information block length :  $k = 12$

Minimum distance :  $d_{min} = 7$

Error-correcting capability :  $t = 3$

The extended (24,12) Golay-code is widely used with a minimum distance of 8 by adding an extra redundant bit and has the exact code rate  $R_c = 1/2$ . The weight enumerator polynomial of the (23,12) Golay code is

$$A(x) = 1 + 253(x^7 + 2x^8 + 2x^{15} + x^{16}) + 1288(x^{11} + x^{12}) + x^{23} \quad (2.4.1.6)$$

The weight enumerator of the extended (24,12) Golay code is

$$A(x) = 1 + 759(x^8 + x^{16}) + 2576x^{12} + x^{24} \quad (2.4.1.7)$$

Bose-Chaudhuri-Hocquenghem (BCH) codes are basically binary cyclic block codes that have the capabilities of multiple-error correction and detection. They have sufficient structure so that encoding and decoding may be accomplished with straightforward combinational circuits (for example, shift registers). The familiar Hamming code is simply a special case of a BCH code which can correct all 1 bit errors. For any positive integer  $m > 3$  and  $t < 2^m - 1$  there exists a binary BCH code with the following parameters.

Code length :  $n = 2^m - 1$

Information block length :  $k \geq n - mt$

Minimum distance :  $d_{min} \geq 2t + 1$

Error-correcting capability :  $t$  bits

The weight structure BCH codes is still unknown in general, except for double-error and triple-error correcting and for some low-rate BCH codes. The (127, 112) BCH code is used in the *INTELSAT V* TDMA system.

Reed-Solomon's codes are linear, cyclic symbol error-correcting block codes and can be thought of as nonbinary BCH codes [5],[6] (i.e.  $n$  and  $k$  represent the number of  $s$ -bit symbols and not the number of bits). Reed-Solomon's codes are very powerful in that, for a given number of redundant symbols  $r = n - k$ , the error-correcting capability achieves the maximum. However Reed-Solomon's codes are considerably more complex due to their nonbinary structure. Also the computation of the

postdecoding bit error rate is considerably more difficult. The parameters for Reed-Solomon's code are :

Symbol length :  $m$  bits per symbol

Code length :  $n = 2^m - 1$  symbols

Information block length :  $k = n - 2t$  symbols

Minimum distance :  $d_{min} = 2t + 1$  symbols

Error-correcting capability :  $t$  symbols

Reed-Solomon's codes provide correction for  $2^m$  symbols, hence for burst errors. The weight for an  $(n, k)$  Reed-Solomon's code is

$$A_0 = 1$$

$$A_j = 0 \quad 1 \leq j \leq n-k$$

$$A_j = \binom{n}{C_j} \sum_{h=0}^{j-1-n+k} (-1)^h \binom{j}{C_h} [2^{m(j-h-n+k)} - 1] \quad n-k+1 \leq j \leq n \quad (2.4.1.8)$$

*Maximal-length codes* have the following parameters.

Code length :  $n = 2^m - 1, m \geq 3$

Information block length :  $k = m$

Minimum distance :  $d_{min} = 2^{m-1}$

A maximal-length code has  $2^m - 1$  nonzero code words of the same weight  $2^{m-1}$ .

The theory of encoding and decoding for linear block codes is well-developed. The reader can refer to the excellent texts [5,7,8].

Among various types of convolution codes we will assume Viterbi decoding (i.e. maximum likelihood decoding) based on hard decisions. By hard decision we mean that the analogue value of the decoded output is not available, but is instead quantized so that only zero and ones are used in decoding process. The computation of the performance of convolution codes is quite difficult and will not be discussed here.

## 2.4.2 FSK with Convolution code :

- *Hard decision decoding*

For hard decision decoding of Convolutional codes, the metrics in the Viterbi algorithm are the hamming distances between the received sequence and the surviving

sequences at each node of the trellis. Since the codes are linear codes, the all-zero sequence may be assumed to be transmitted. A first event error is made at the  $i$ -th received branch if the all-zero path is eliminated at this point by another path merging with it. A union bound on the probability of a first event error  $P_e$  at branch  $i$  may be obtained by summing the error probabilities for all possible paths which merge with the all-zero path at this point. This bound is given by

$$P_e < \sum_{j=0}^{\infty} n_j P_2(j) \quad (2.4.2.1)$$

where  $n_j$  denotes the number of paths of distance  $j$  from the all-zero path and  $P_2(j)$  is the probability that another path which is at a distance  $j$  from the all-zero path and has a metric that exceeds the metric of all-zero path.

An upper bound on the probability of bit error  $P_b$  may be obtained by weighing each term by the corresponding numbers of bit errors. For a rate  $k/n$  code, there are  $k$ -symbols decoded on each branch. Thus  $P_b$  is bounded by

$$P_b < \frac{1}{k} \sum_{j=d_{f \min}}^{\infty} W_j P_2(j) \quad (2.4.2.2)$$

where  $W_j$  is the number of bit error associated with one another path which is at a distance  $j$  from the all-zero path and  $d_{f \min}$  is the minimum free distance of the code. For a binary symmetric channel (BSC),  $P_2(j)$  is upper bounded by

$$P_2(j) < D_0^j$$

with  $D_0 = [2\sqrt{p(1-p)}]$  (2.4.2.3)

where,  $p$  is the probability of a bit error for the BSC. For a rate  $-1/2$  CC, the weights  $W_j$  and the  $d_{f \min}$  corresponding to two typical values of the constraint length  $k$  are :

$K = 4, d_{f \min} = 6, \{W_j\} = 2, 7, 18, 130, 333, 836, 2069, 5060, 12255.$

$K = 7, d_{f \min} = 10, \{W_j\} = 36, 0, 211, 0, 1404, 0, 11633, 76628, 469991.$

The IF bandwidth expansion factor for the coded system is defined as  $F = L/r$ ; where  $r$  is the rate of the employed code and  $L = T/T'$  is the ratio of the IF bandwidth to the transmission rate as defined earlier. The computer program for the BER evaluation is given in appendix A and B.

### 2.4.3 FSK with Reed-Solomon's code

The RS code is a maximum-distance-separable (MDS) code which means that for a given code rate and codeword length, the RS code has the largest possible minimum distance between codewords. A rate  $k/n$  RS code  $(n,k)$  has minimum distance given by  $d_{\min} = n-k+1$ . However, the complexity of the error correcting algorithm for RS codes is a function of the block length and increases for a given code rate with the alphabet size.

When the number of words in error within the RS codeword exceeds  $d_{\min}/2$ , the output may appear closer to a different RS codeword and, in general, the decoder makes an error ( $e$ ). When erasures ( $s$ ) are also present i.e., no decision is made by the demodulator, the decoder can correct patterns of errors ( $e$ ) and erasures ( $s$ ) such that  $2e+s < n-k+1$ , multiplied by the corresponding probability of each event occurring.

The probabilities of having  $e$  specified words in error,  $s$  specified erasures and  $n-e-s$  correct words are  $(P_e)^e$ ,  $(P_s)^s$  and  $(P_c)^{n-e-s}$  respectively where  $P_e$ ,  $P_s$ ,  $P_c$  are the probabilities that the word is in error, in erasure or is correct respectively. The number of ways to obtain  $e$  errors,  $s$  erasures and  $n-e-s$  correct words is [2-3].

$$\left[ \begin{matrix} n \\ e \end{matrix} \right] \left[ \begin{matrix} n-e \\ s \end{matrix} \right] = \frac{n!}{(n-e-s)!e!s!} \quad (2.4.3.1)$$

where, the brackets represent binomial coefficients. Thus for choices of  $2e+s < d_{\min}$ ,  $P(e, s, n)$ , the probability that the correct RS character can not be detected, is given by[2]

$$P(e, s, n) = \frac{n!}{(n-e-s)!e!s!} (P_e)^e (P_s)^s (P_c)^{n-e-s} \quad (2.4.3.2)$$

where,  $2e+s \geq d_{\min}$ . The relevant computer program is given in appendix C. The fraction of the output symbols which are in error (or erased) is upper bounded by  $(e+s)/n$ .

If we now sum over all combinations of errors and erasures such that  $2e+s \geq d_{\min}$ , the bit error probability for the RS decoder with *hard-decision decoding* scheme, in which no erasure is formed, the bit error probability is given by[2-9].

$$P_b = \sum_{e=0}^n \binom{n}{e} (P_e)^e (P_e)^{n-e} \quad (2.4.3.3)$$

## 2.5 Results and discussion

Following the theoretical analysis presented in section 2.3, the performance results of optical direct detection FSK system are evaluated at a bit rate of 2.5 Gb/s with and without forward error correction coding. In the latter case we employed two encoding techniques, viz. Convolutional coding (CC) and Reed-Solomon's (RS) coding. The computations of the performance results are carried out for several values of normalized laser linewidth  $\Delta\nu T$  and modulation index  $h = 2\Delta\nu T$ .

Figure 2.7 depicts the bit error rate ( $P_b$ ) performance of coded and uncoded FSK as a function of the optical signal power  $P_s$  (dB<sub>m</sub>). The coded results are presented for rate 1/2 Convolutinal coding with hard decision decoding for two values of the code constraint length  $k = 4, 7$  when the normalized laser linewidth  $\Delta\nu T = 0.0$  and modulation index  $h = 0.5$ . The plots reveal that the bit error rate  $P_b$  decreases more sharply for coded case than for uncoded case. The results are provided for the same information rate.

It is also evident from the curves that to attain a specified bit error rate, say  $P_b = 10^{-9}$ , the required signal power  $P_s$  is less for the coded FSK system compared to uncoded FSK.

When the normalized linewidth  $\Delta\nu T$  is increased to 0.005 keeping the modulation index unchanged ( $h = 0.5$ ) the performance results are shown in Fig. 2.8. Compared to Fig. 2.7 it becomes clear that the error rate curves move slightly upward due to impact of laser phase noise. Similar results are provided in Fig. 2.9, Fig. 2.10 and Fig. 2.11. Comparison of these curves with Fig. 2.7 shows that the bit error rate increases with increasing value of the normalized linewidth  $\Delta\nu T$  and bit error floor occurs

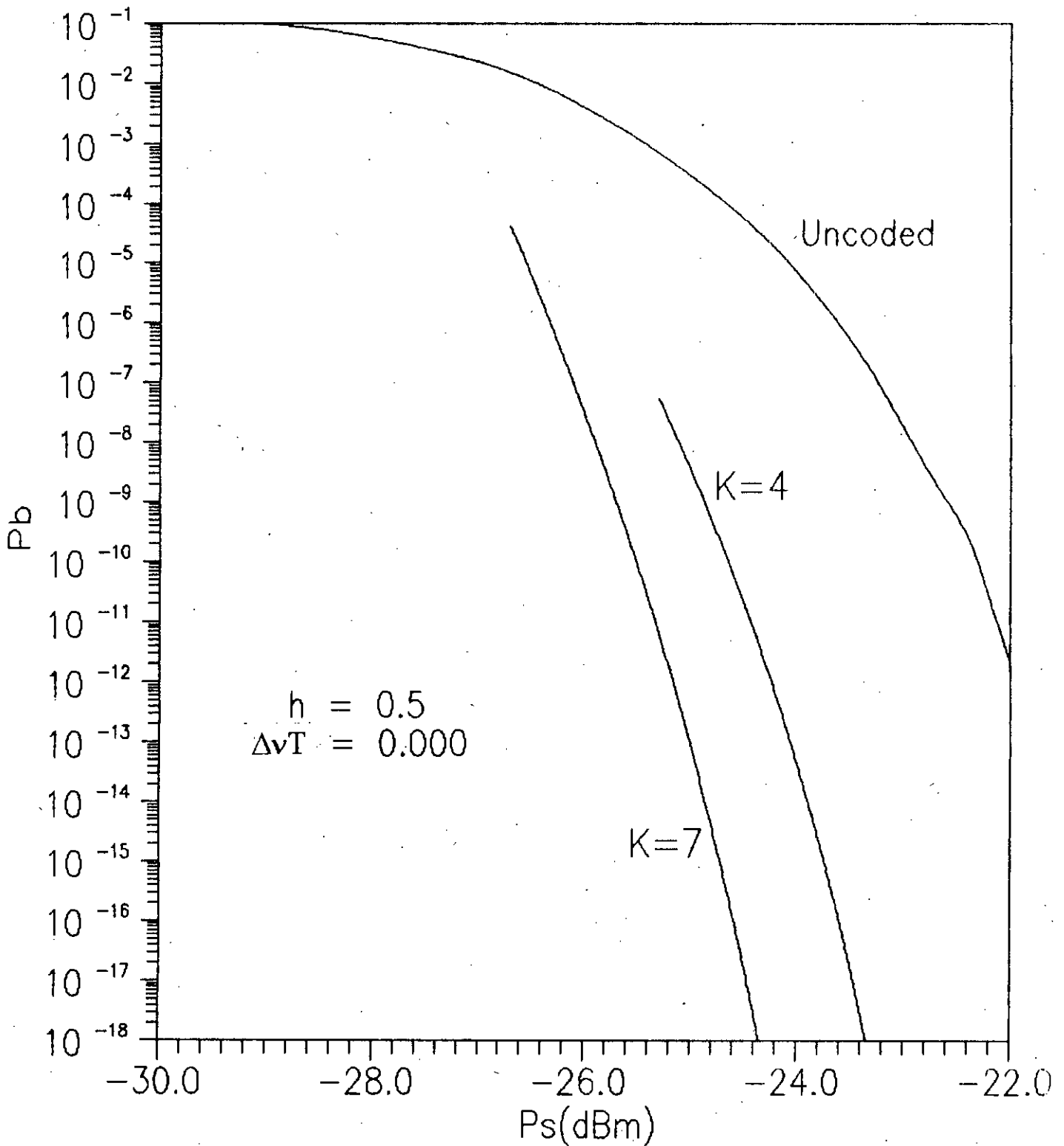


**Fig. 2.7** Plots of bit error probability  $P_b$  vs transmitted signal power  $P_s$ (dB<sub>m</sub>) for uncoded and rate 1/2 convolutionally coded ( $K = 4, 7$ ) FSK with modulation index  $h = 0.5$  and laser linewidth  $\Delta\nu T = 0.000$



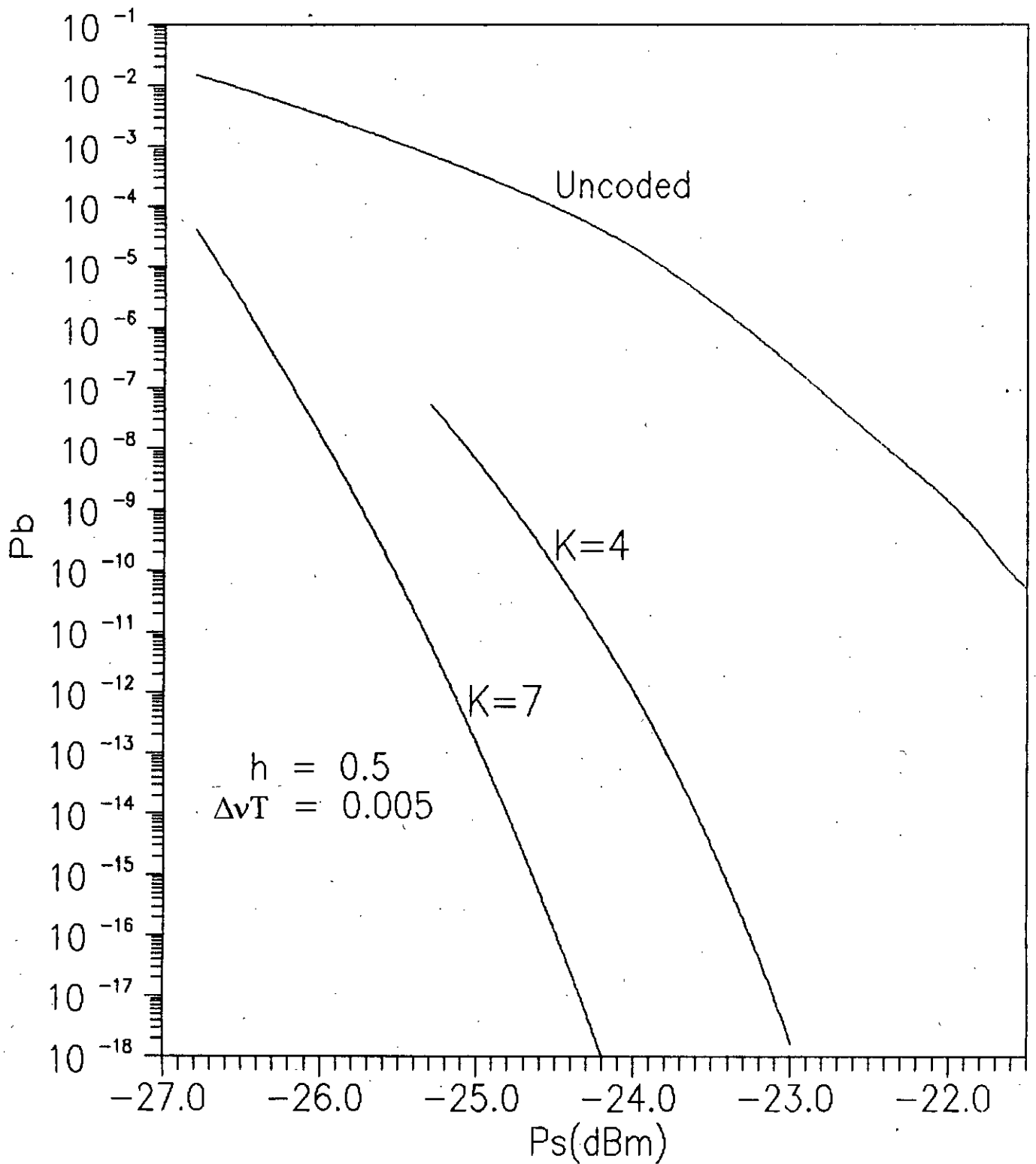


**Fig. 2.8** Plots of bit error probability  $P_b$  vs transmitted signal power  $P_s$ (dB<sub>m</sub>) for uncoded and rate 1/2 convolutionally coded ( $K = 4, 7$ ) FSK with modulation index  $h = 0.5$  and laser linewidth  $\Delta\nu T = 0.005$

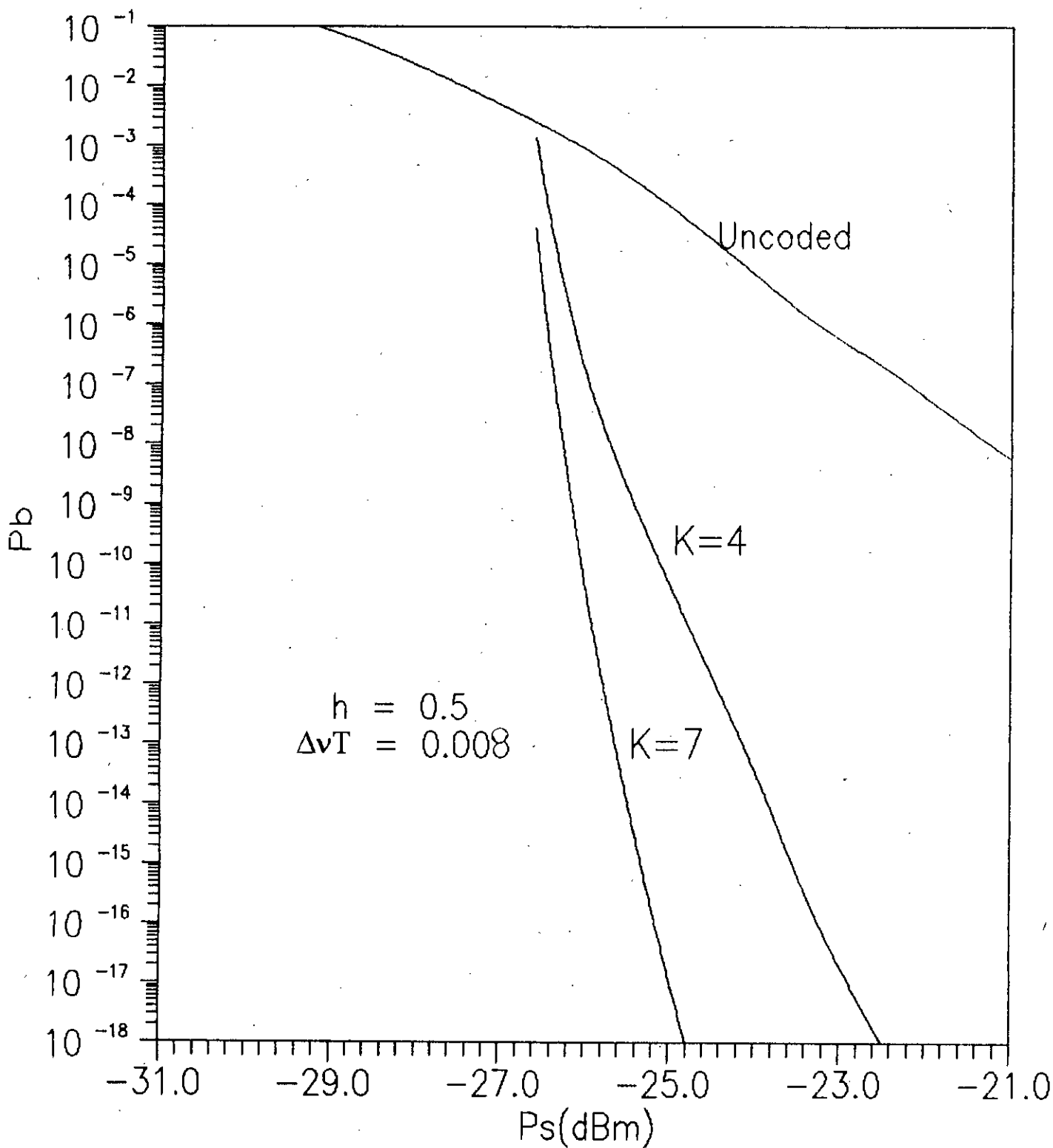


**Fig. 2.9** Plots of bit error probability  $P_b$  vs transmitted signal power  $P_s$ (dB<sub>m</sub>) for uncoded and rate 1/2 convolutionally coded ( $K = 4, 7$ ) FSK with modulation index  $h = 0.5$  and laser linewidth  $\Delta\nu T = 0.008$

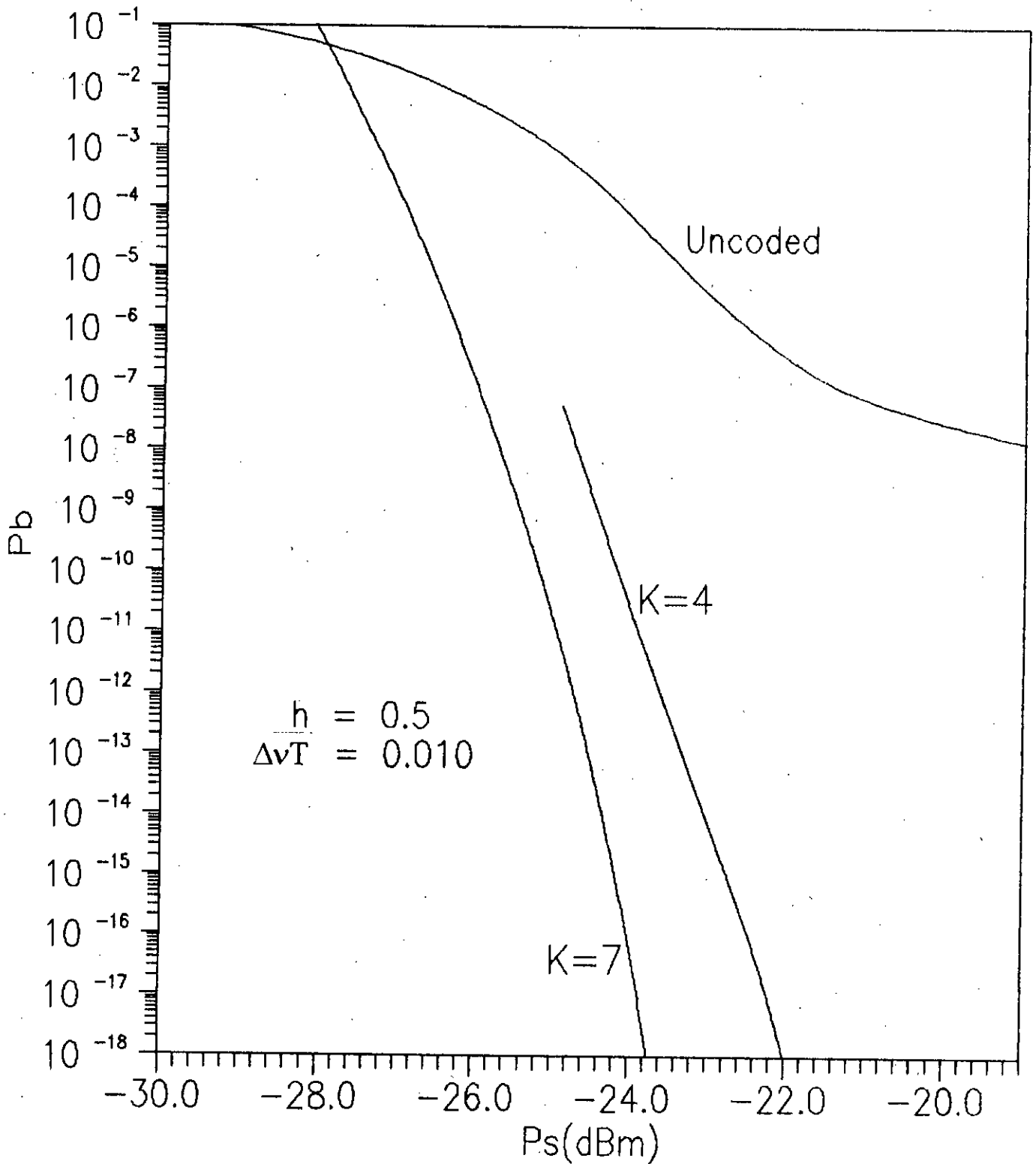
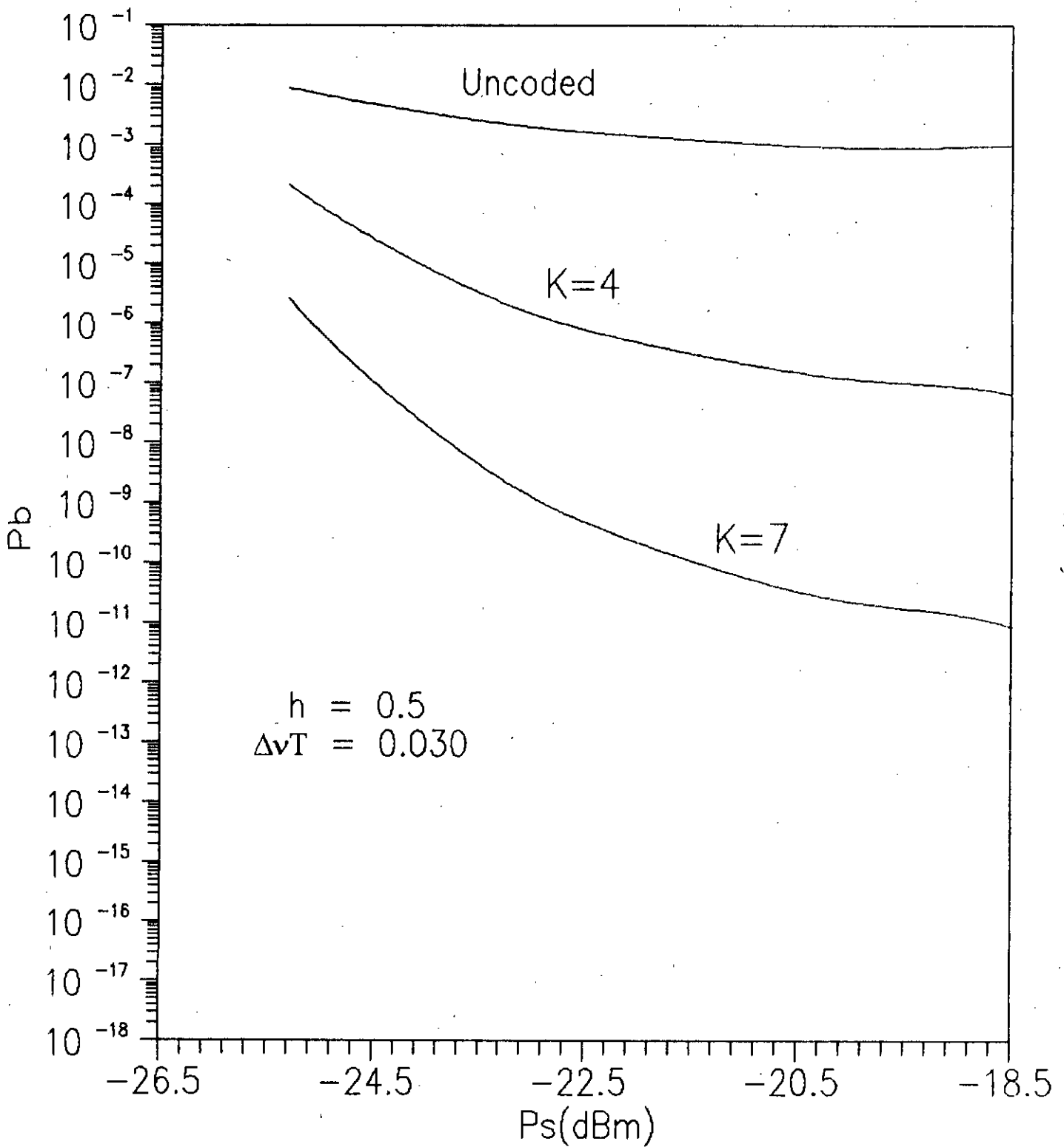


Fig. 2.10 Plots of bit error probability  $P_b$  vs transmitted signal power  $P_s$ (dB<sub>m</sub>) for uncoded and rate 1/2 convolutionally coded (K = 4, 7) FSK with modulation index  $h = 0.5$  and laser linewidth  $\Delta\nu T = 0.010$



**Fig. 2.11** Plots of bit error probability  $P_b$  vs transmitted signal power  $P_s$ (dB<sub>m</sub>) for uncoded and rate 1/2 convolutionally coded ( $K = 4, 7$ ) FSK with modulation index  $h = 0.5$  and laser linewidth  $\Delta\nu T = 0.030$

when  $\Delta\nu T \geq 0.01$  at or above  $10^{-8}$  for uncoded FSK. On the otherhand, for the coded case, no error rate floor occurs for  $\Delta\nu T = 0.01$  or less and at higher values of  $\Delta\nu T$ , floor occurs at a much smaller value of  $P_b$ . For example, in Fig. 2.11 the BER floor occurs around  $10^{-3}$  for the uncoded FSK whereas for the coded case floor occurs at around  $10^{-7}$  and  $10^{-11}$  corresponding to constraint length  $k = 4$  and  $7$  respectively.

The performance curves for coded and uncoded FSK are also provided in Fig. 2.12 through Fig. 2.16 with and without laser phase noise when  $h$  is increased to 1.0. It is noticed that the performance of the system becomes degraded with increasing value of non-zero linewidth  $\Delta\nu T$  as found earlier. However, for the same value of  $\Delta\nu T$  increased value of the modulation index provides better performance. Comparison of Fig. 2.13 with Fig. 2.10 reveals that the error rate curves become more steeper with increasing value of the modulation index  $h$ . Further, when Fig. 2.11 is compared with Fig. 2.16, it becomes evident that the BER floor is reduced by two to three orders of magnitude due to increase in  $h$ . For the coded case, the floor disappears due to increase of  $h$  from 0.5 to 1.0.

Similar performance results are provided in Fig. 2.17 through Fig. 2.20 for rate 1/2 CC with  $k = 4, 7$  for several values of normalized linewidth  $\Delta\nu T$  when  $h$  is equal to 2.0.

Further it is also noticed that there is a considerable reduction in the optical signal power for the coded FSK system to achieve a bit error rate of  $P_b = 10^{-9}$  compared to uncoded FSK. We term this reduction in signal power as the coding gain (CG).

When Reed-Solomon's (RS) coding is employed, performance results for coded FSK is presented in Fig. 2.21 through Fig. 2.25 for several values of the normalized linewidth  $\Delta\nu T$  with  $h = 0.5$ . As in the case of Convolutional coding, there is also considerable reduction in the required signal power to attain a specified bit error rate. Further the effect of laser phase noise is also less compared to uncoded system. It is also noticed that improvement in system performance is higher for (15,7) RS code than for (15,9) RS code by around 1 dB at  $P_b = 10^{-9}$ . Thus as the rate of the code is

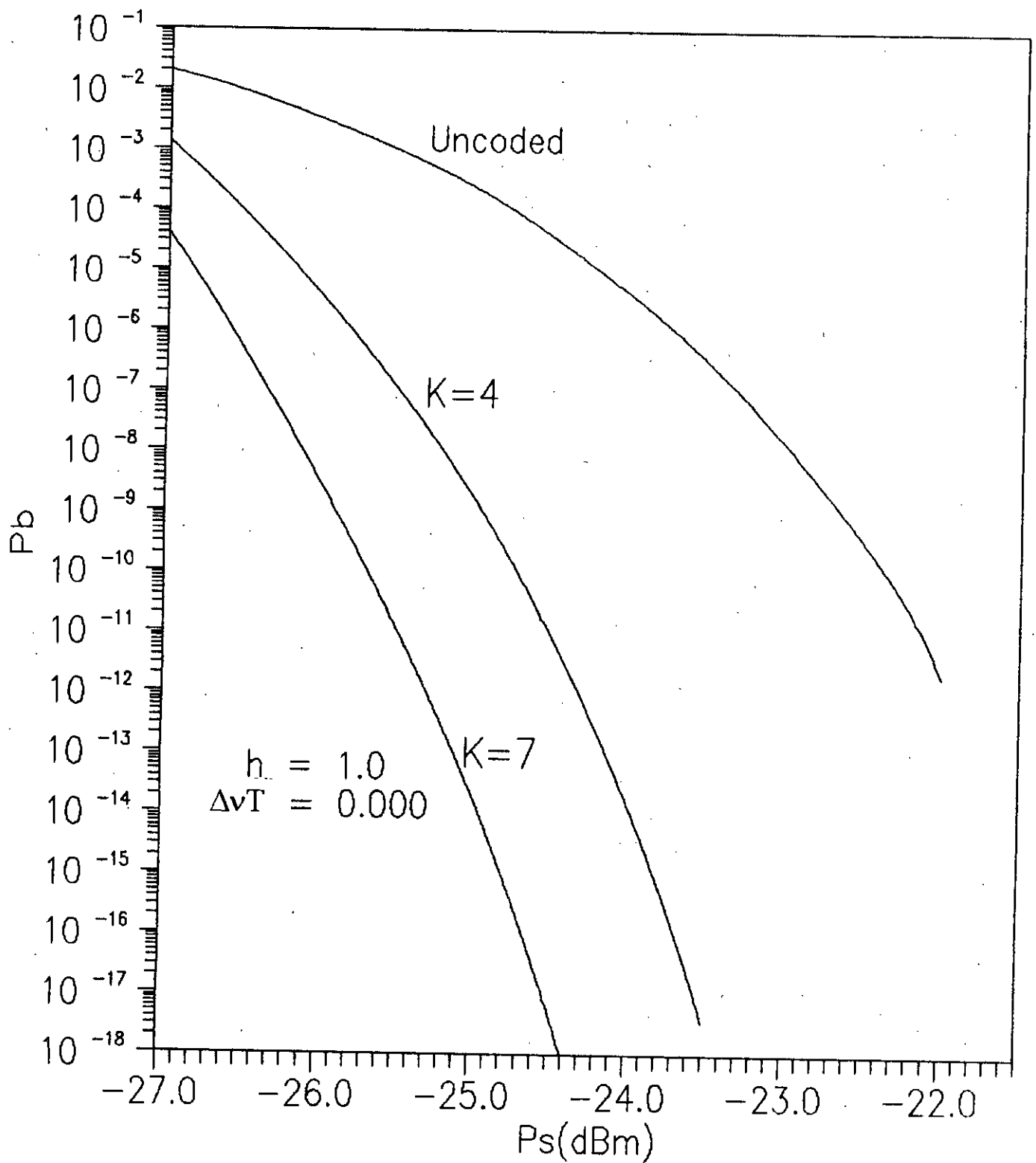
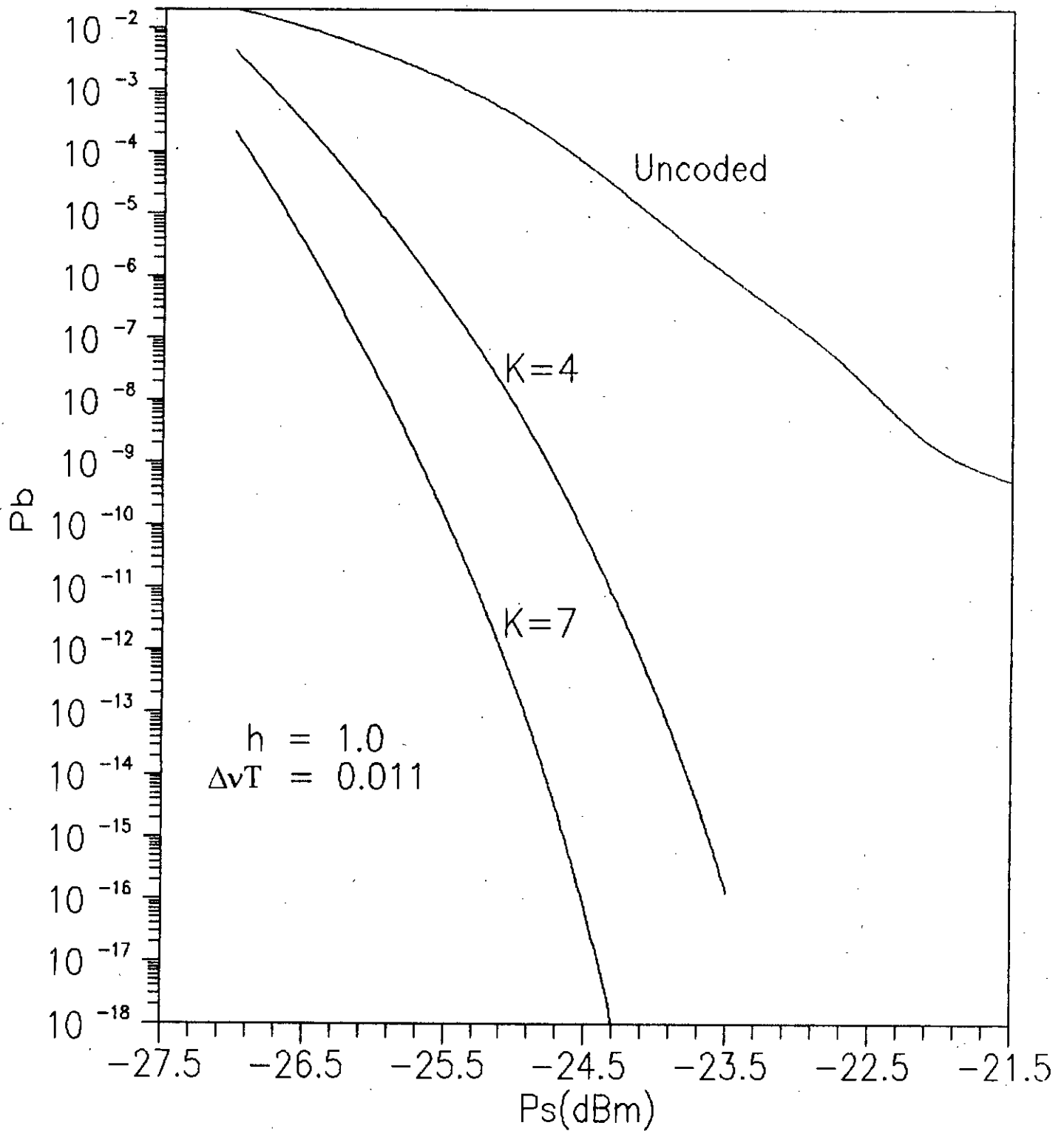


Fig. 2.12 Plots of bit error probability  $P_b$  vs transmitted signal power  $P_s(\text{dBm})$  for uncoded and rate 1/2 convolutionally coded ( $K = 4, 7$ ) FSK with modulation index  $h = 1.0$  and laser linewidth  $\Delta\nu T = 0.000$



**Fig. 2.13** Plots of bit error probability  $P_b$  vs transmitted signal power  $P_s$ (dB<sub>m</sub>) for uncoded and rate 1/2 convolutionally coded ( $K = 4, 7$ ) FSK with modulation index  $h = 1.0$  and laser linewidth  $\Delta\nu T = 0.011$

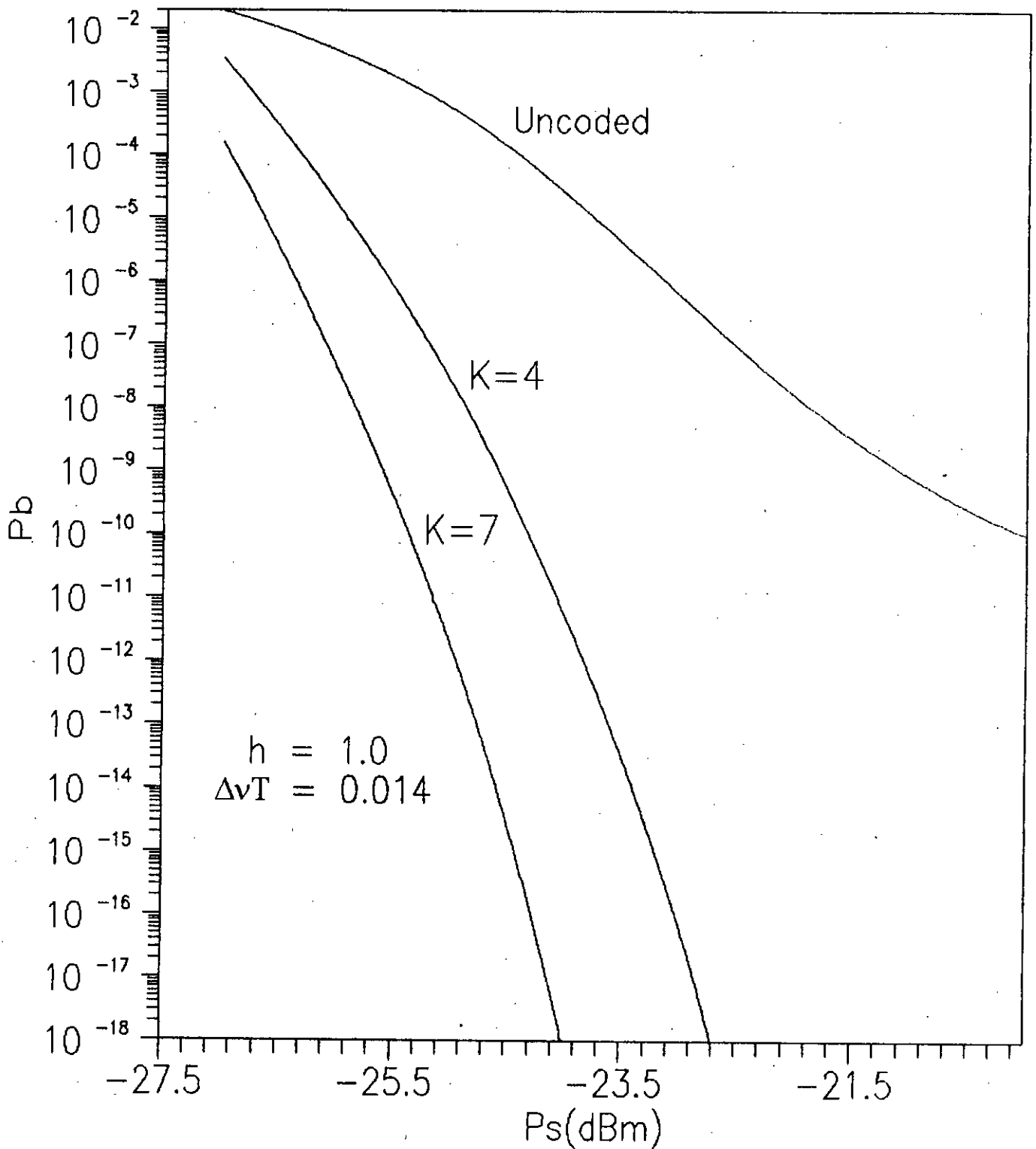


Fig. 2.14 Plots of bit error probability  $P_b$  vs transmitted signal power  $P_s$ (dB<sub>m</sub>) for uncoded and rate 1/2 convolutionally coded ( $K = 4, 7$ ) FSK with modulation index  $h = 1.0$  and laser linewidth  $\Delta\nu T = 0.014$



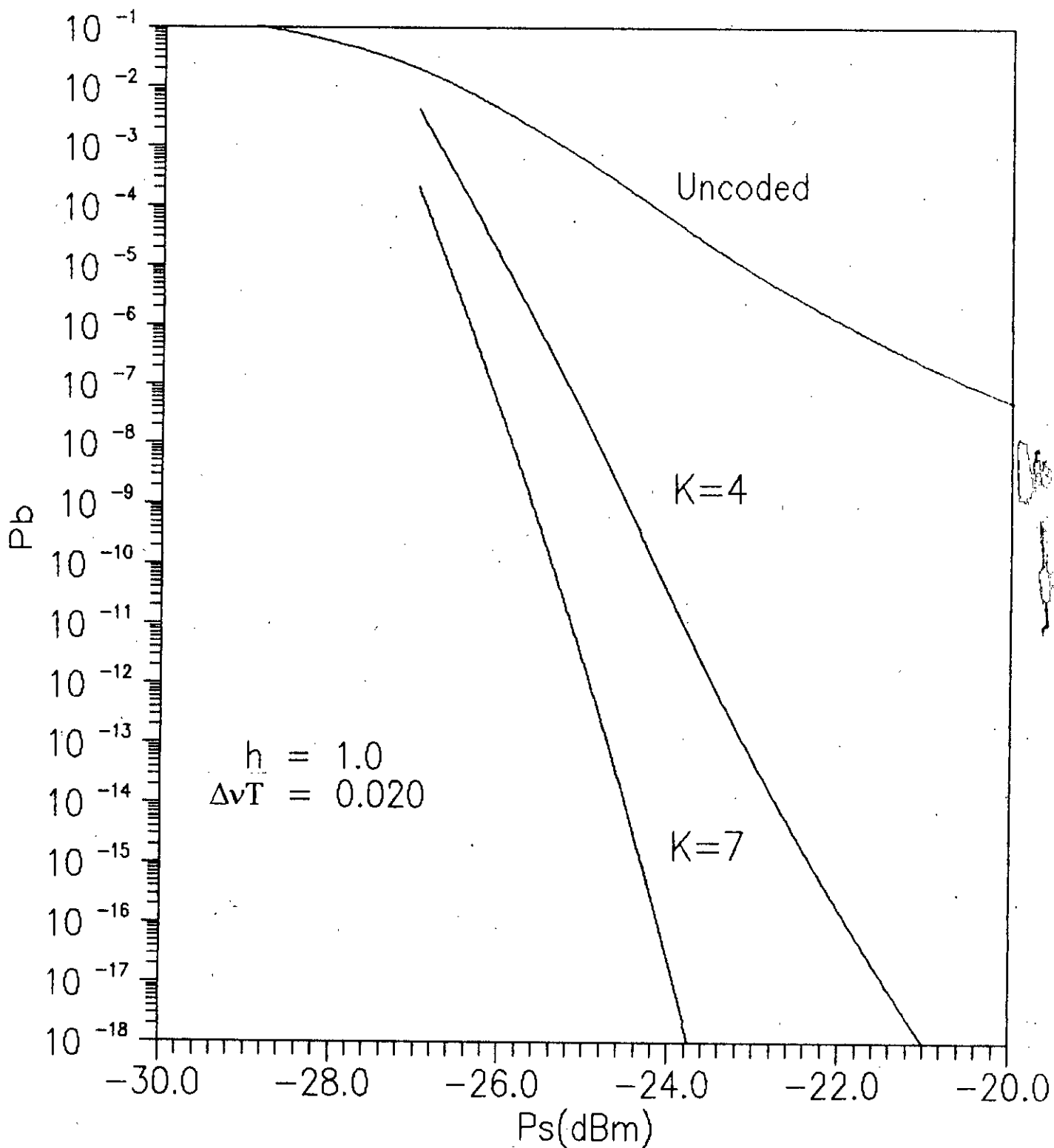
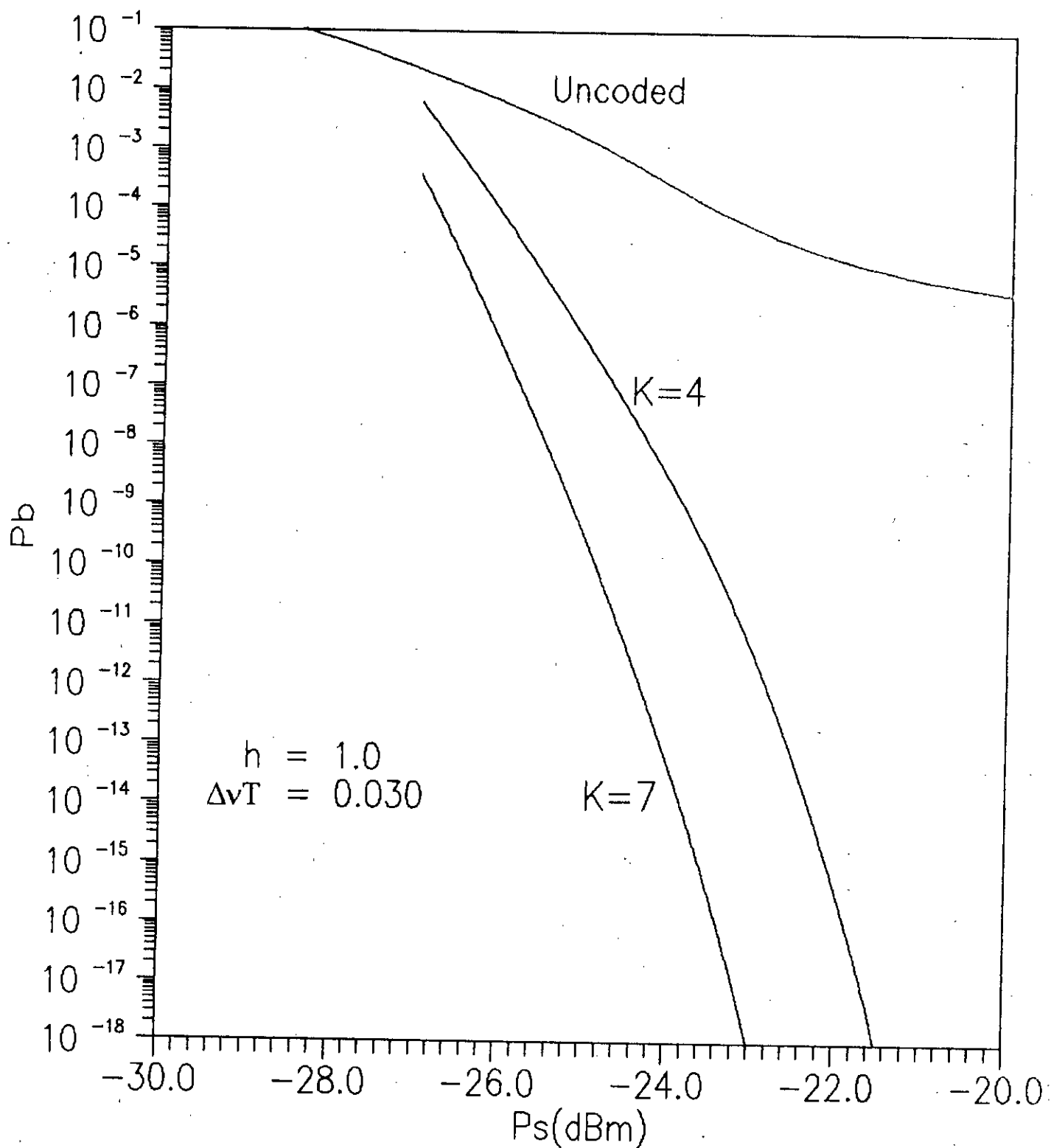
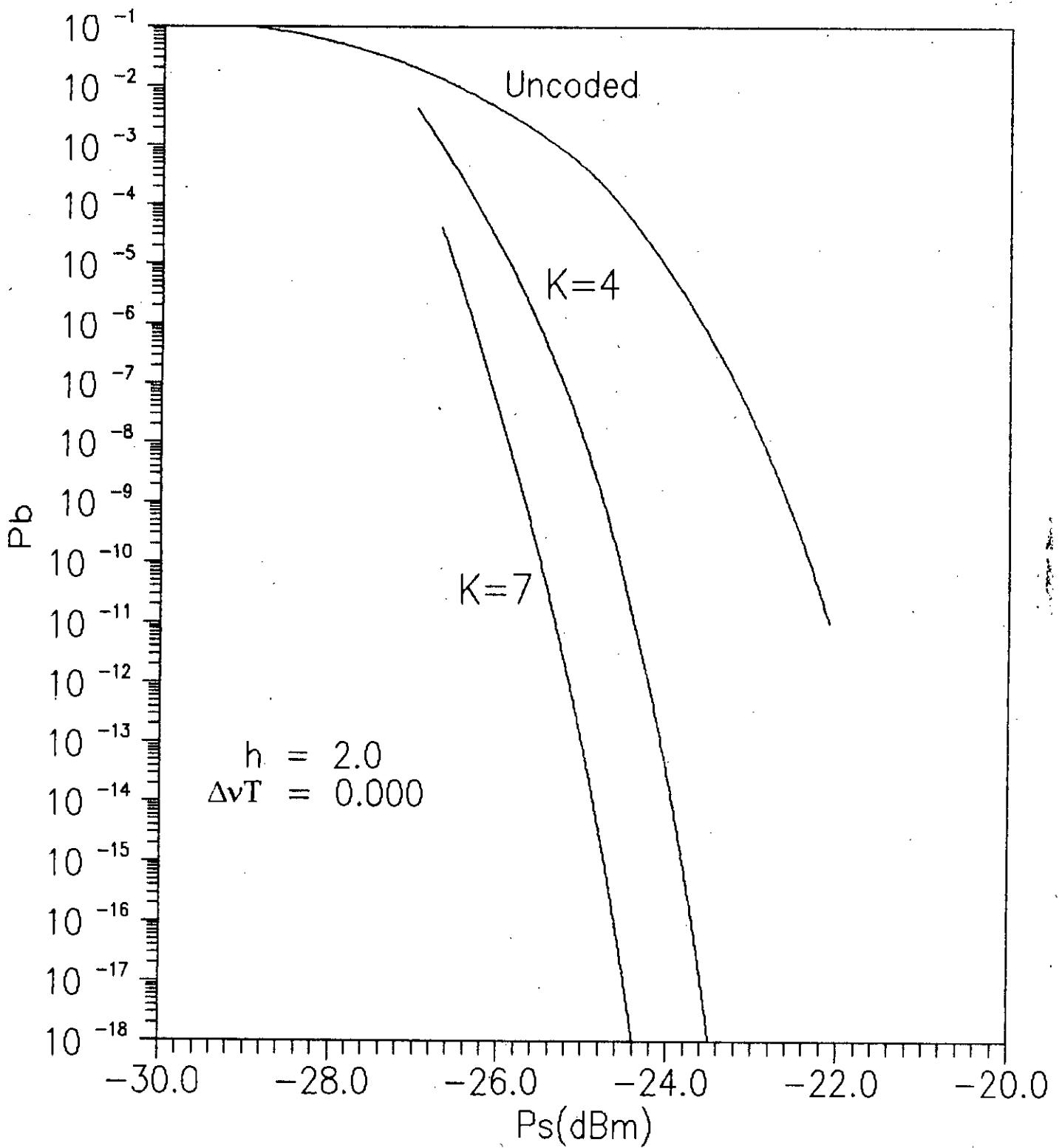


Fig. 2.15 Plots of bit error probability  $P_b$  vs transmitted signal power  $P_s$ (dB<sub>m</sub>) for uncoded and rate 1/2 convolutionally coded ( $K = 4, 7$ ) FSK with modulation index  $h = 1.0$  and laser linewidth  $\Delta\nu T = 0.020$



**Fig. 2.16** Plots of bit error probability  $P_b$  vs transmitted signal power  $P_s$ (dB<sub>m</sub>) for uncoded and rate 1/2 convolutionally coded ( $K = 4, 7$ ) FSK with modulation index  $h = 1.0$  and laser linewidth  $\Delta\nu T = 0.030$



**Fig. 2.17** Plots of bit error probability  $P_b$  vs transmitted signal power  $P_s(\text{dB}_m)$  for uncoded and rate 1/2 convolutionally coded ( $K = 4, 7$ ) FSK with modulation index  $h = 2.0$  and laser linewidth  $\Delta\nu T = 0.000$

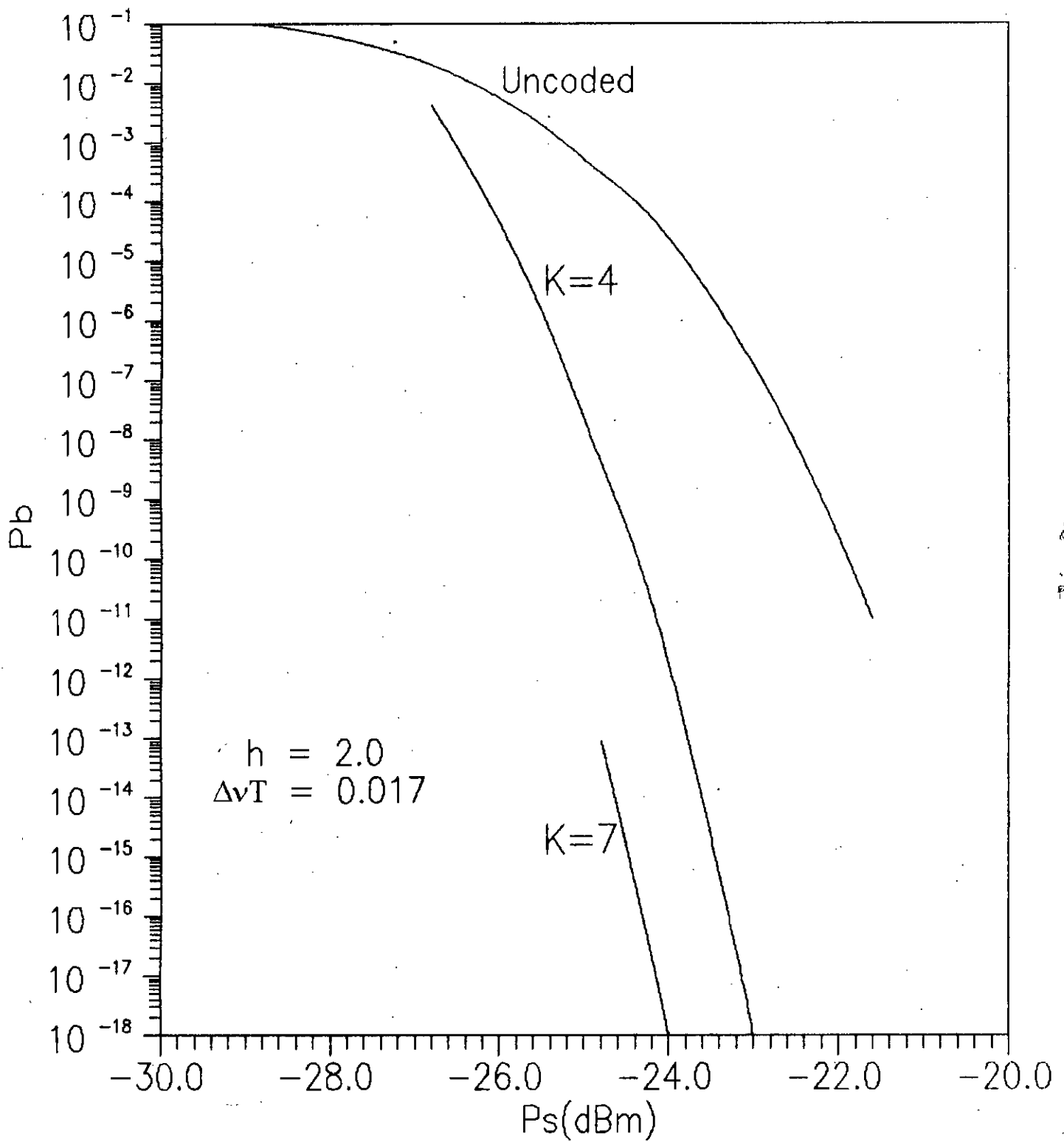


**Fig. 2.18** Plots of bit error probability  $P_b$  vs transmitted signal power  $P_s$ (dB<sub>m</sub>) for uncoded and rate 1/2 convolutionally coded ( $K = 4, 7$ ) FSK with modulation index  $h = 2.0$  and laser linewidth  $\Delta\nu T = 0.017$

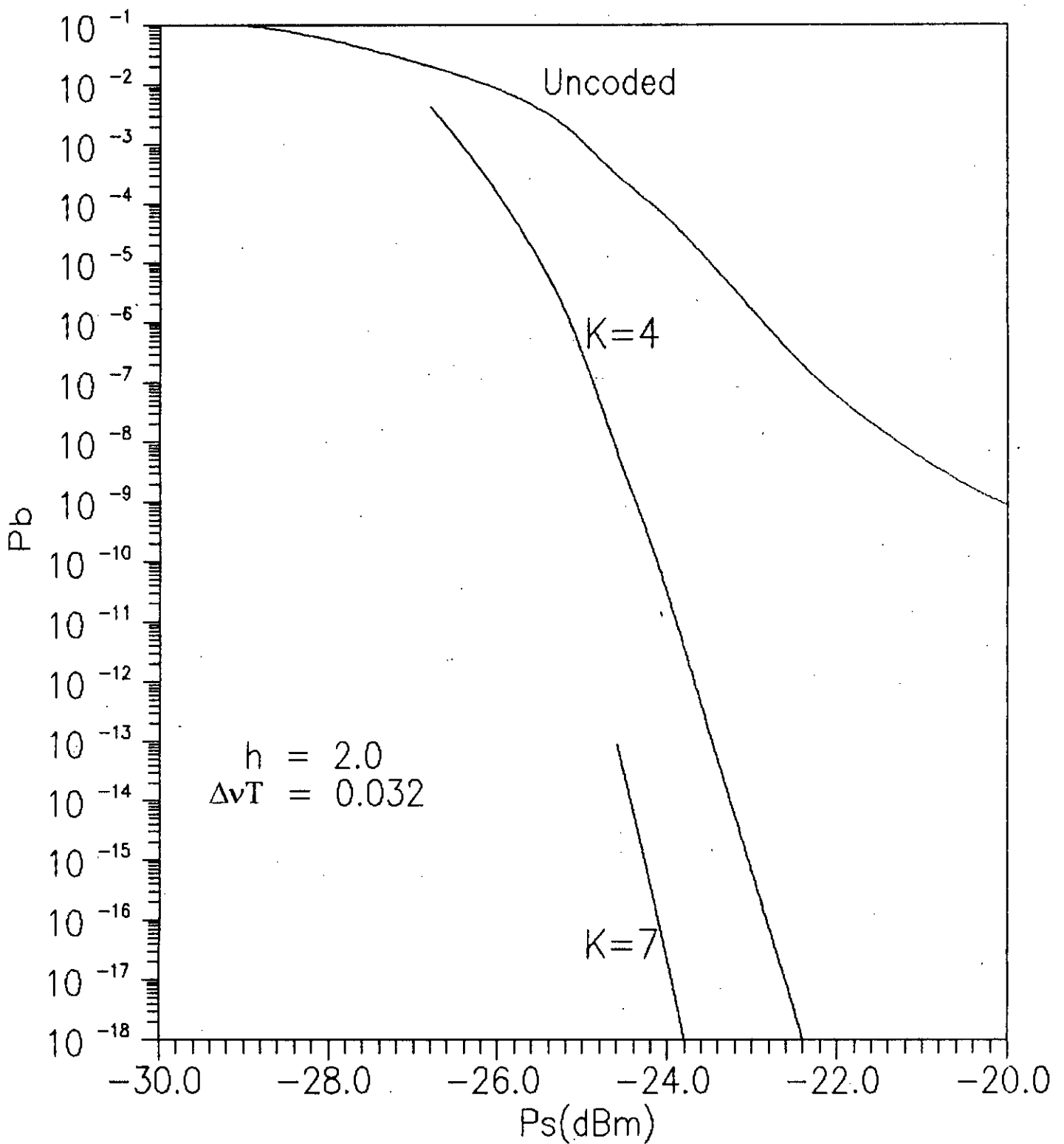


**Fig. 2.19** Plots of bit error probability  $P_b$  vs transmitted signal power  $P_s$ (dB<sub>m</sub>) for uncoded and rate 1/2 convolutionally coded ( $K = 4, 7$ ) FSK with modulation index  $h = 2.0$  and laser linewidth  $\Delta\nu T = 0.032$

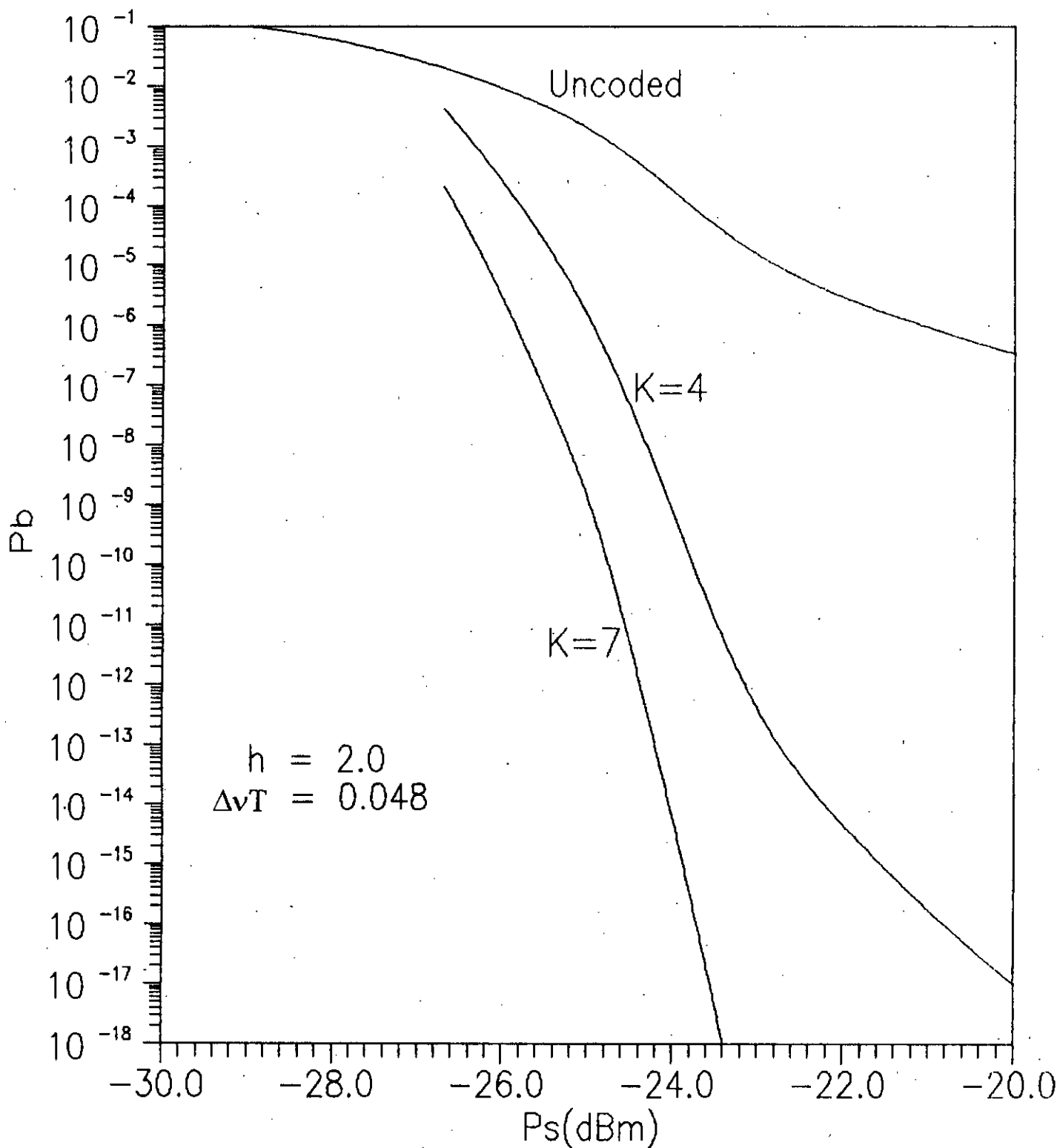


**Fig. 2.20** Plots of bit error probability  $P_b$  vs transmitted signal power  $P_s$ (dB<sub>m</sub>) for uncoded and rate 1/2 convolutionally coded ( $K = 4, 7$ ) FSK with modulation index  $h = 2.0$  and laser linewidth  $\Delta\nu T = 0.048$

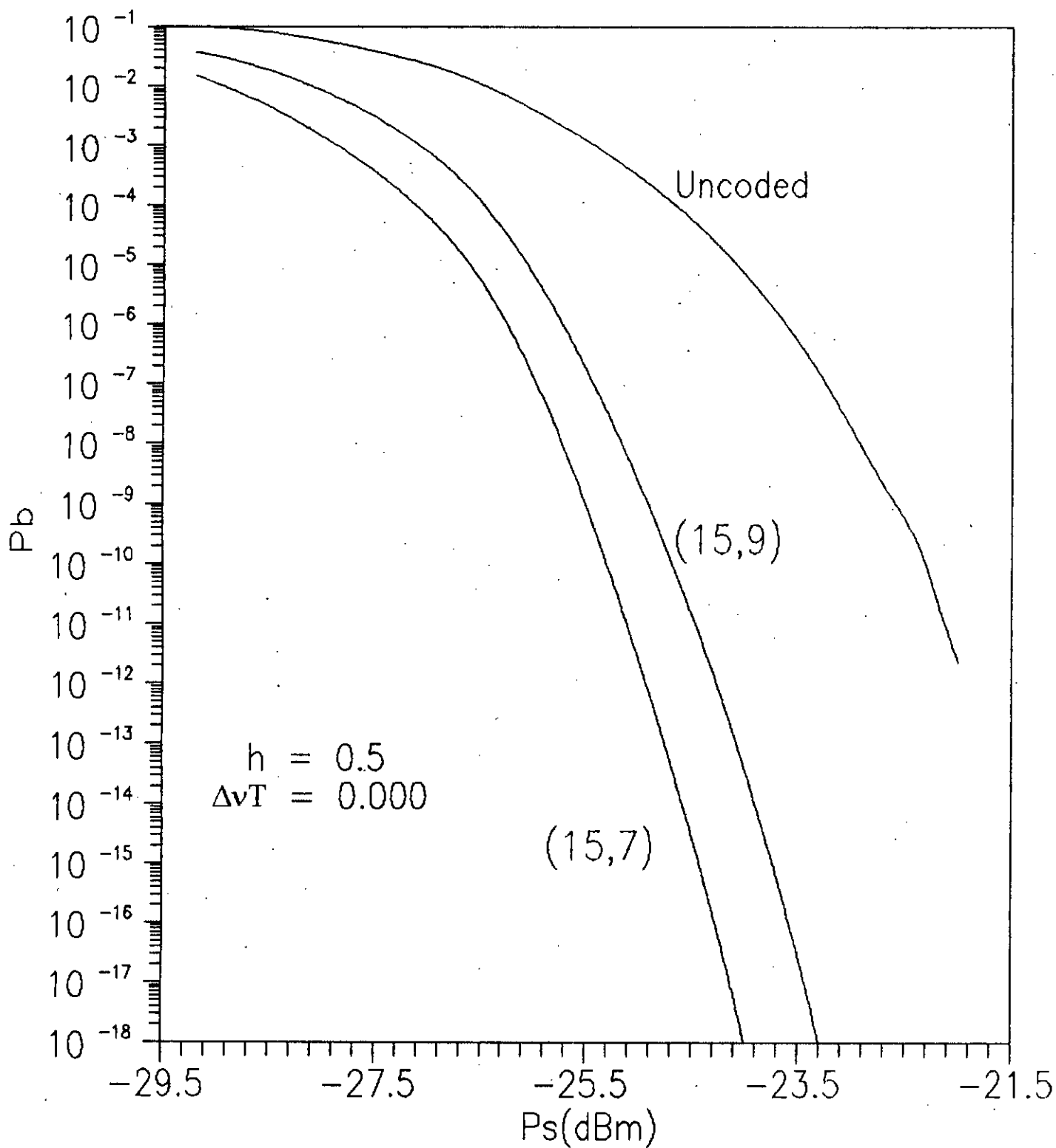


**Fig. 2.21** Plots of bit error probability  $P_b$  vs transmitted signal power  $P_s$ (dB<sub>m</sub>) for uncoded and Reed-Solomon's coded FSK with modulation index  $h = 0.5$  and laser linewidth  $\Delta\nu T = 0.000$

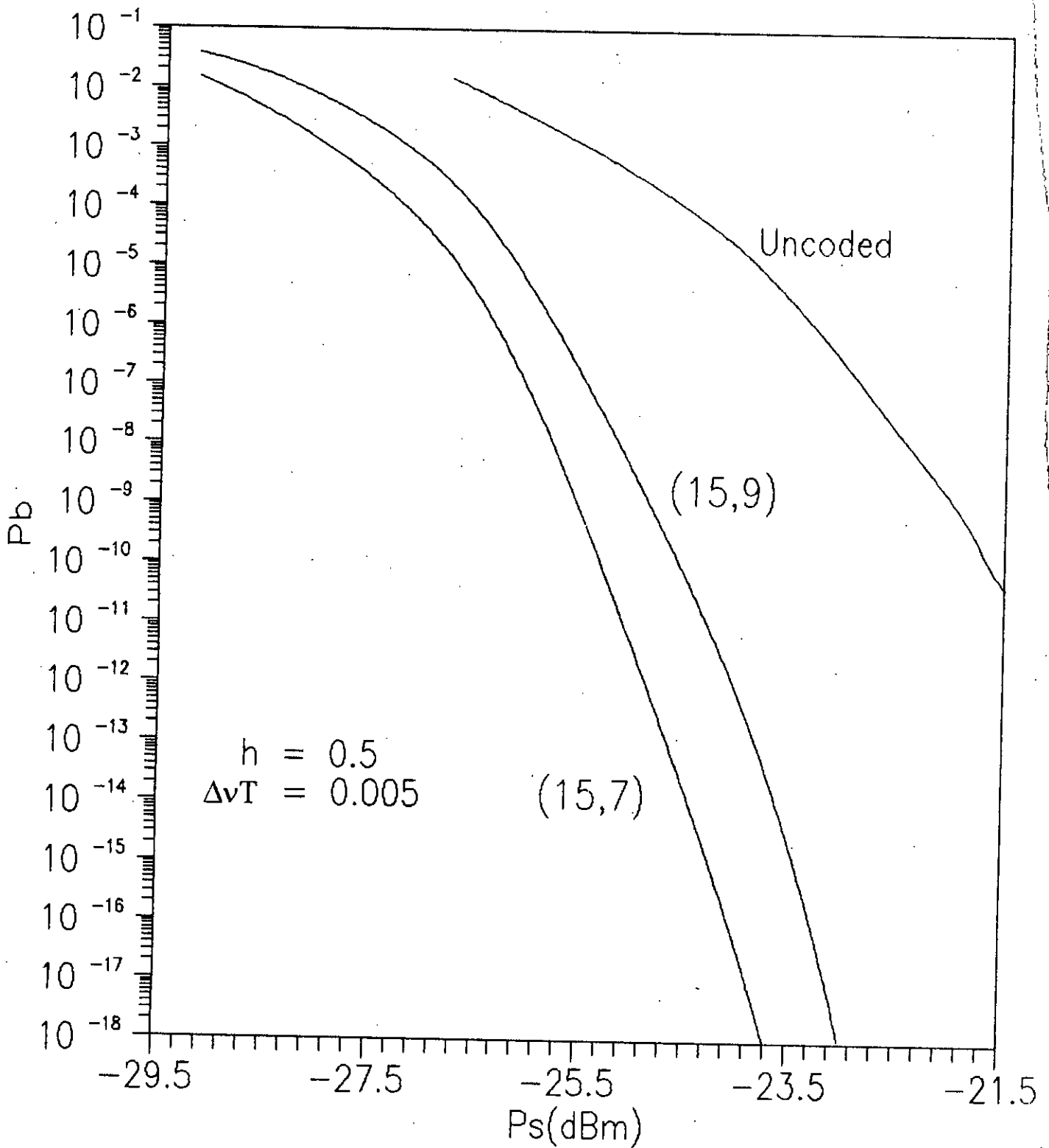
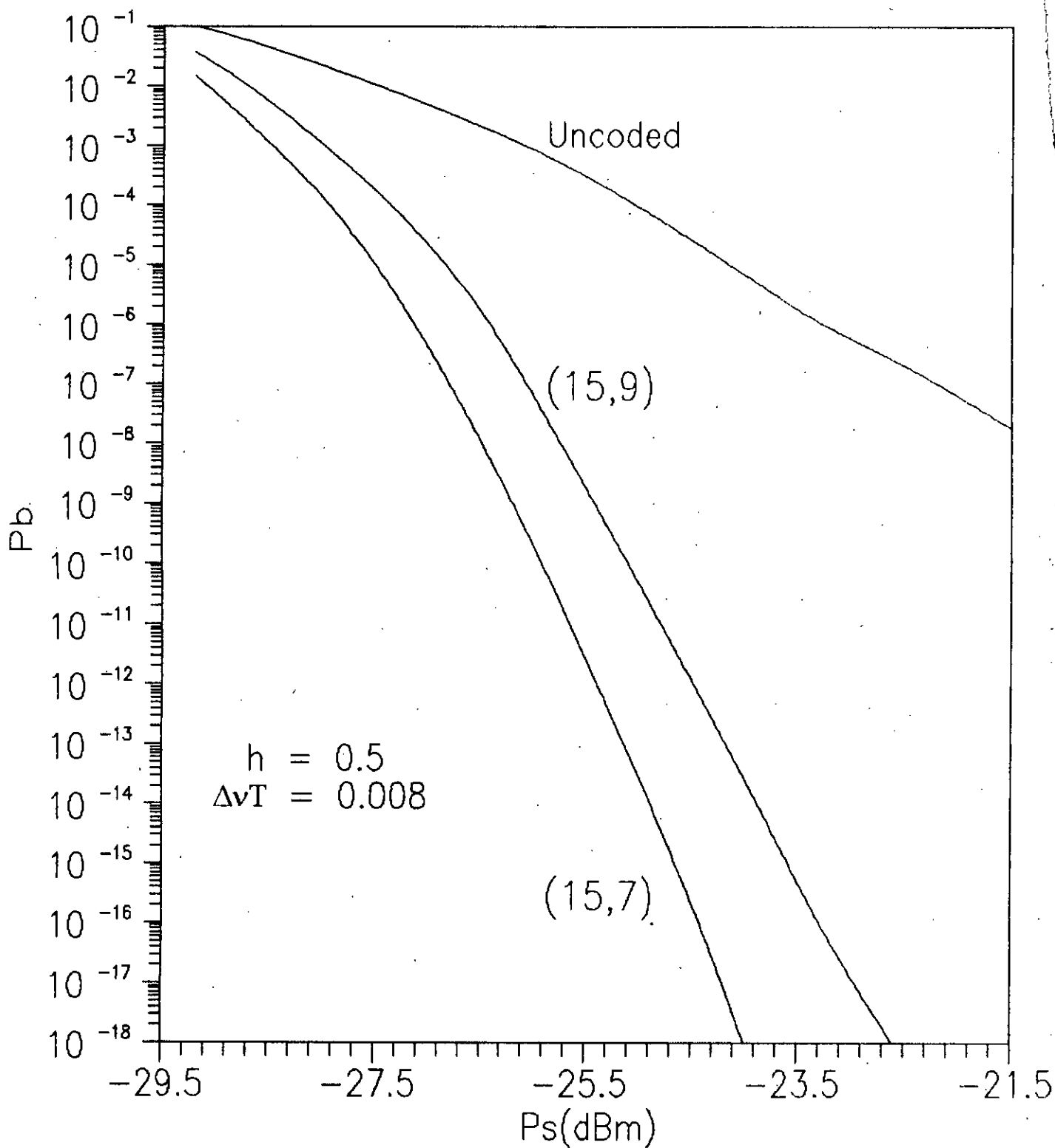
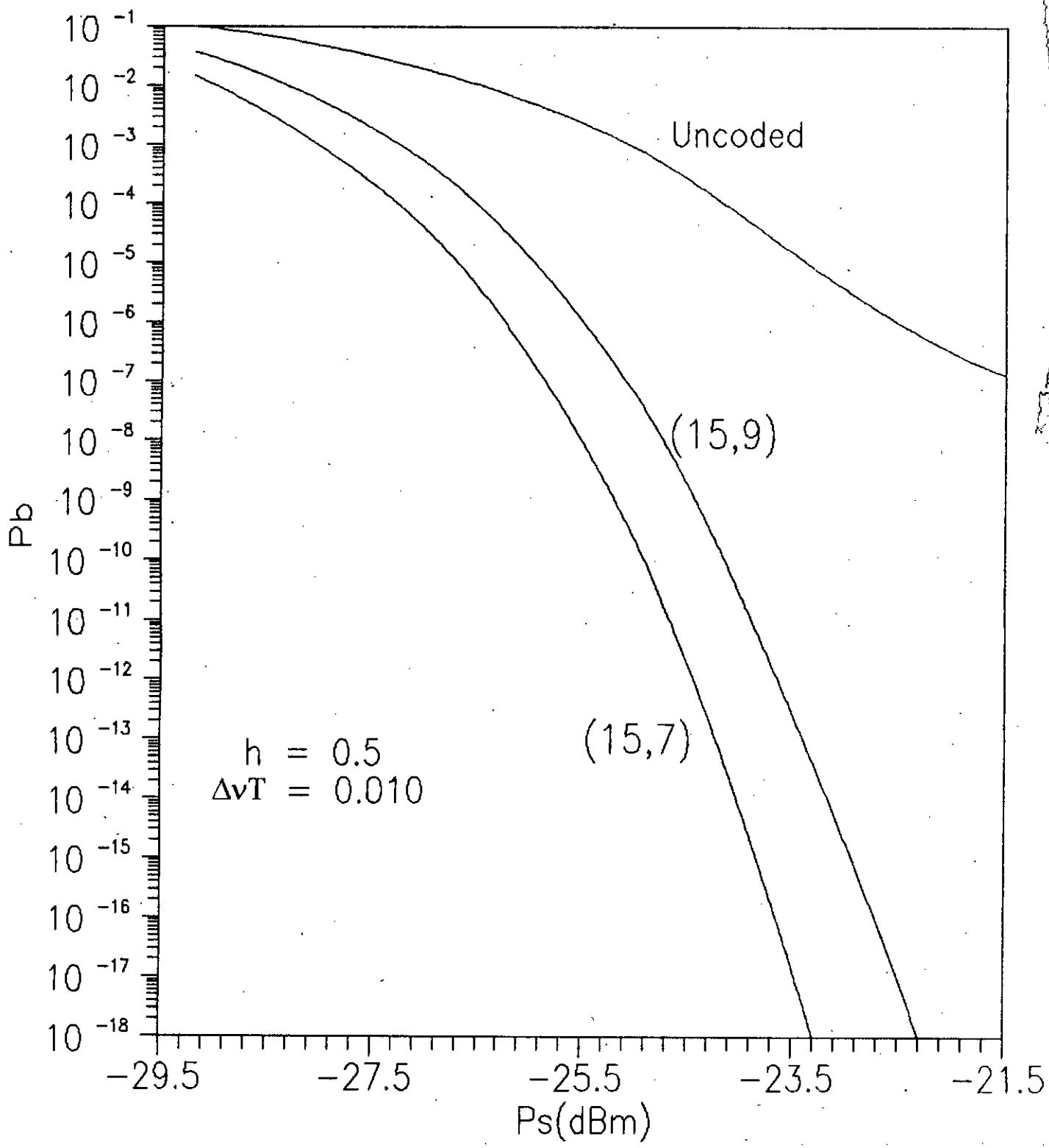


Fig. 2.22 Plots of bit error probability  $P_b$  vs transmitted signal power  $P_s$ (dB<sub>m</sub>) for uncoded and Reed-Solomon's coded FSK with modulation index  $h = 0.5$  and laser linewidth  $\Delta\nu T = 0.005$





**Fig. 2.23** Plots of bit error probability  $P_b$  vs transmitted signal power  $P_s$ (dB<sub>m</sub>) for uncoded and Reed-Solomon's coded FSK with modulation index  $h = 0.5$  and laser linewidth  $\Delta\nu T = 0.008$ .



**Fig. 2.24** Plots of bit error probability  $P_b$  vs transmitted signal power  $P_s$ (dB<sub>m</sub>) for uncoded and Reed-Solomon's coded FSK with modulation index  $h = 0.5$  and laser linewidth  $\Delta\nu T = 0.010$

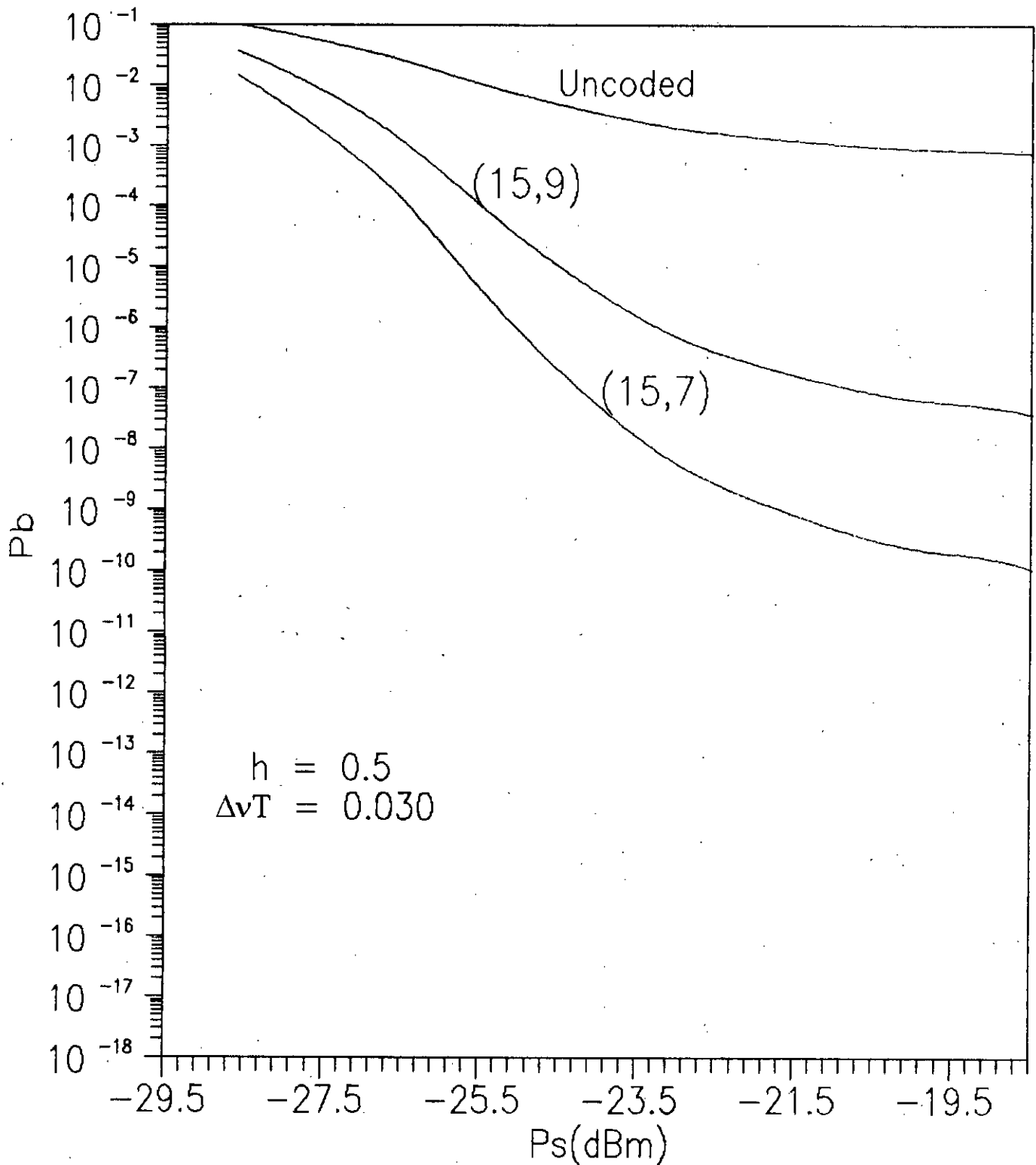


**Fig. 2.25** Plots of bit error probability  $P_b$  vs transmitted signal power  $P_s$ (dB<sub>m</sub>) for uncoded and Reed-Solomon's coded FSK with modulation index  $h = 0.5$  and laser linewidth  $\Delta\nu T = 0.030$

decreased, performance becomes better due to less expansion in transmission bandwidth.

Similar performance results are provided in Fig. 2.26 through Fig. 2.30 for  $h = 1.0$  and Fig. 2.31 through Fig. 2.34 for  $h = 2.0$  with several linewidth values.

The power penalty suffered by the uncoded FSK system due to non-zero laser linewidth is depicted in Fig. 2.35 as a function of the modulation index  $h$ . It is found that as the modulation index  $h$  increases the penalty reduces and is also less at smaller values of linewidth and particular values of  $h$ . Figure 2.36, 2.37 show similar results for convolutionally coded FSK with  $k = 4, 7$  respectively. It is observed that the power penalty is negligibly small for coded FSK system compared to uncoded system at particular values of modulation index  $h$  and normalized linewidth  $\Delta\nu T$ . For example, for uncoded case as is evident from Fig. 2.35, the penalty is about 3.2 dB when  $h = 0.5$  and  $\Delta\nu T = 0.01$  whereas the same is 0.2 dB and 0.05 dB corresponding to  $k = 4$  and 7 respectively for the coded case. Thus for the same power penalty, the allowable non-zero laser linewidth is higher for the coded system.

The penalty versus  $h$  plots for (15,9), (15,7) RS coded optical FSK system is provided in Fig. 2.38 and Fig. 2.39 respectively. Similar conclusions are also revealed from curves as in the case of Convolutionally coded FSK system.

As shown in Fig. 2.40, the variation of power penalty due to laser phase noise versus normalized laser linewidth  $\Delta\nu T$  for uncoded and rate 1/2 Convolutionally coded FSK system with  $k = 4, 7$  for  $h = 0.5$ , it is observed that the penalty is significantly reduced when coding is employed. The penalty can be further reduced by increasing the modulation index  $h$  as depicted in Fig. 2.41 and Fig. 2.42. Similar observations are also found for (15,9) and (15,7) RS coded FSK system as depicted in Fig. 2.43, Fig. 2.44 and Fig. 2.45.

The reductions in the required transmitted power over uncoded system to achieve a specified bit error rate of  $P_b = 10^{-9}$  is termed as the coding gain and is depicted in Fig. 2.46 and Fig. 2.47 for rate 1/2 CC and (15,9) and (15,7) RS coded systems

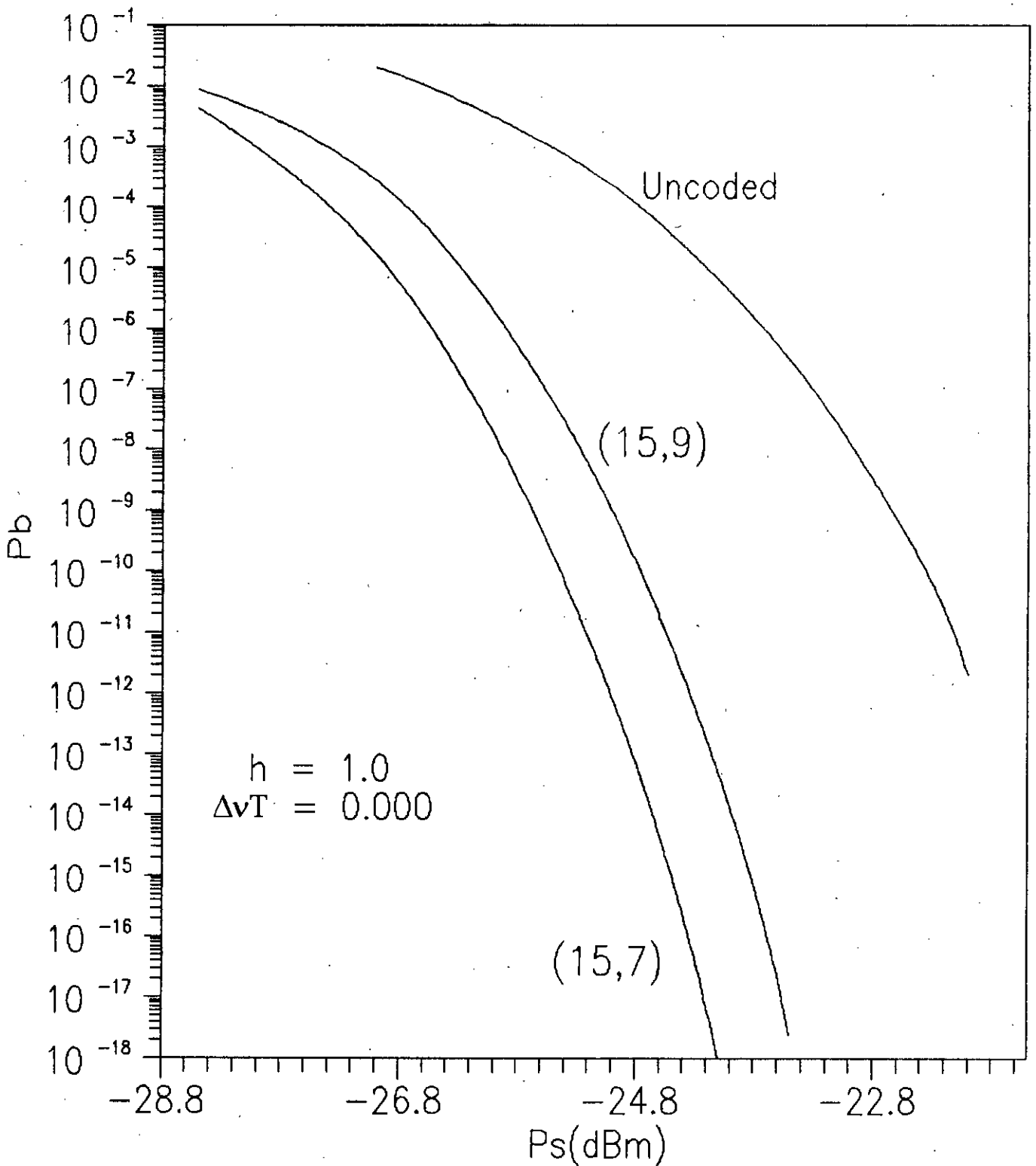


**Fig. 2.26** Plots of bit error probability  $P_b$  vs transmitted signal power  $P_s$ (dB<sub>m</sub>) for uncoded and Reed-Solomon's coded FSK with modulation index  $h = 1.0$  and laser linewidth  $\Delta\nu T = 0.000$

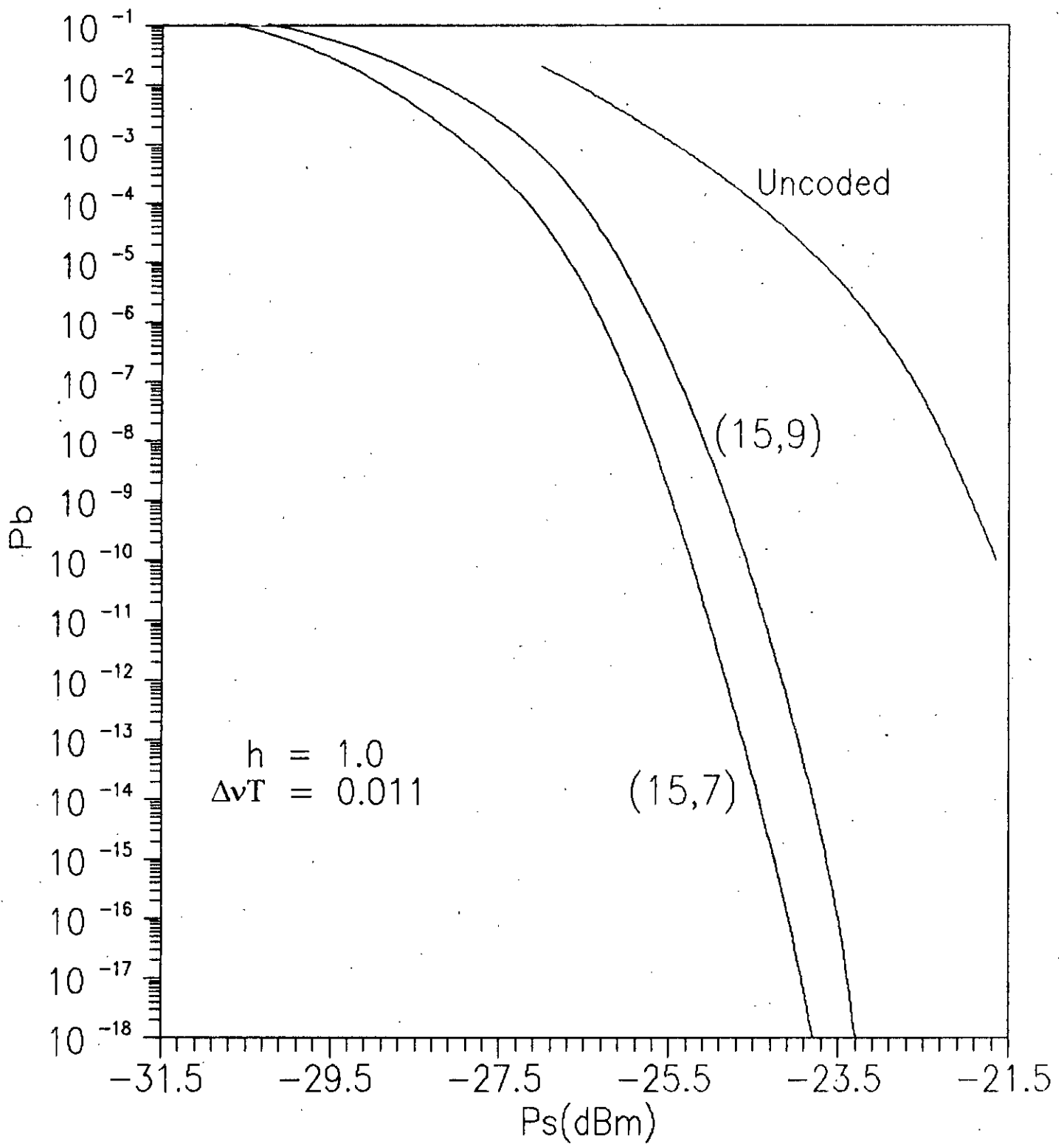


**Fig. 2.27** Plots of bit error probability  $P_b$  vs transmitted signal power  $P_s$ (dB<sub>m</sub>) for uncoded and Reed-Solomon's coded FSK with modulation index  $h = 1.0$  and laser linewidth  $\Delta\nu T = 0.011$

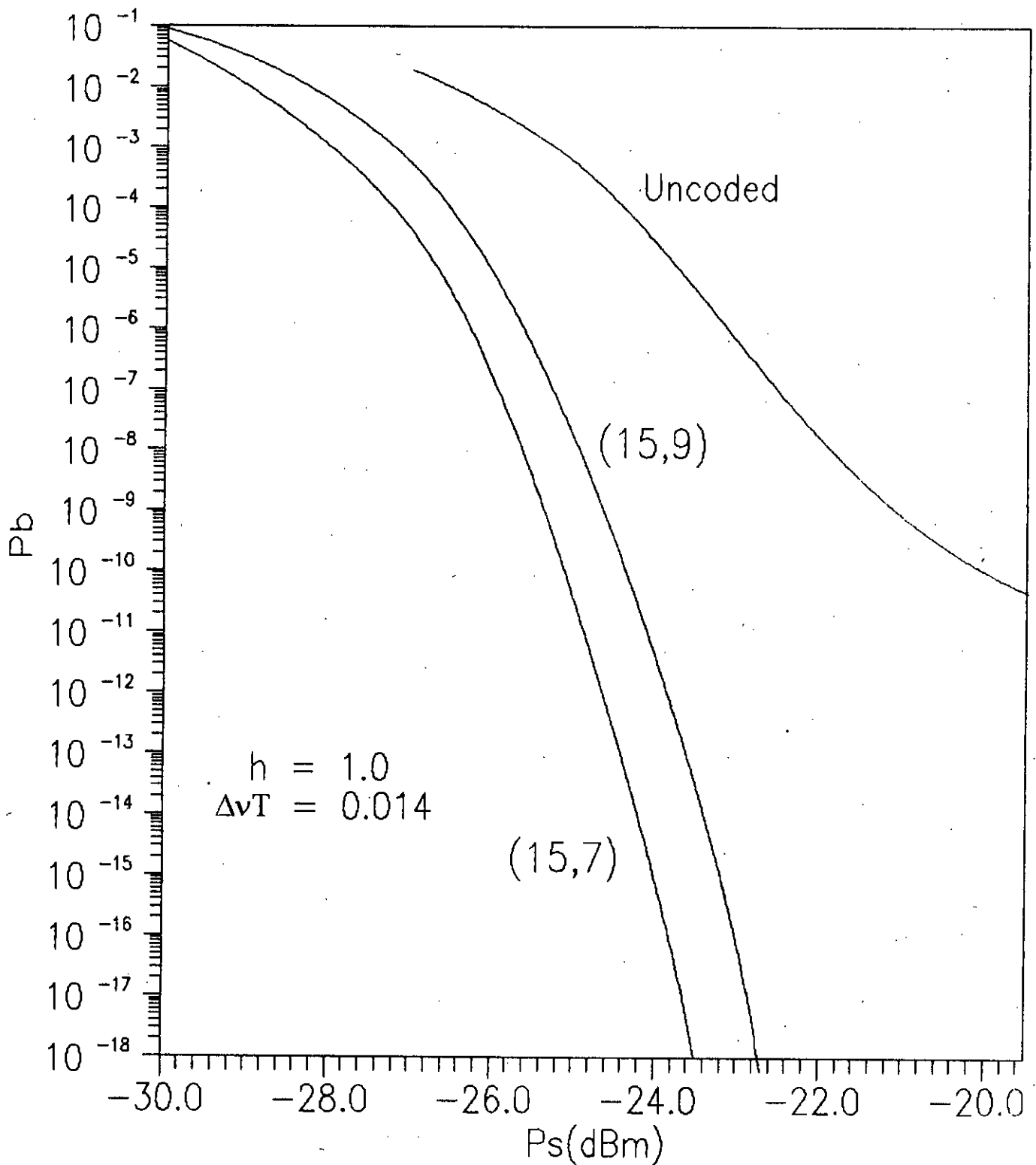


**Fig. 2.28** Plots of bit error probability  $P_b$  vs transmitted signal power  $P_s$ (dB<sub>m</sub>) for uncoded and Reed-Solomon's coded FSK with modulation index  $h = 1.0$  and laser linewidth  $\Delta\nu T = 0.014$

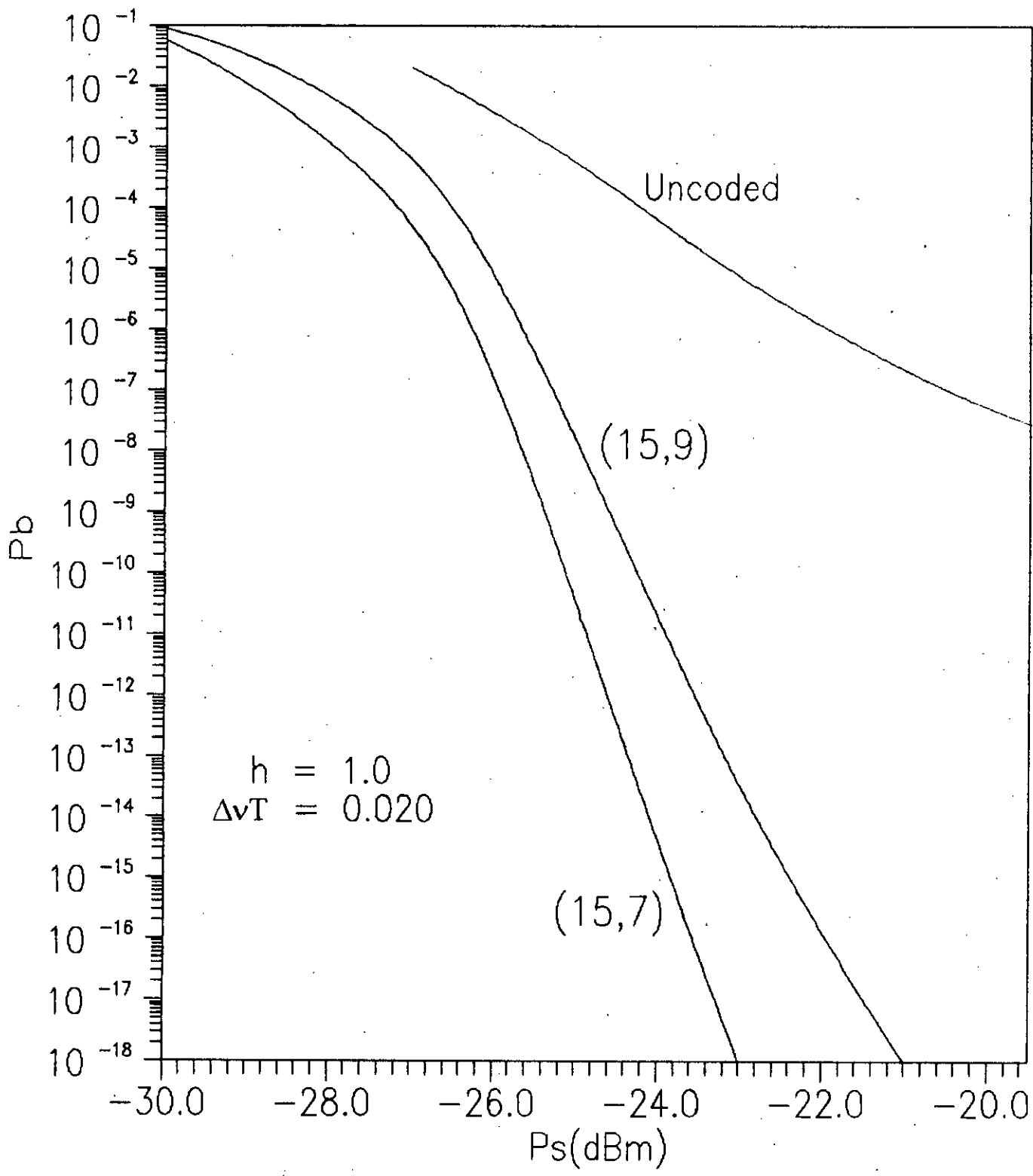


**Fig. 2.29** Plots of bit error probability  $P_b$  vs transmitted signal power  $P_s$ (dB<sub>m</sub>) for uncoded and Reed-Solomon's coded FSK with modulation index  $h = 1.0$  and laser linewidth  $\Delta\nu T = 0.020$



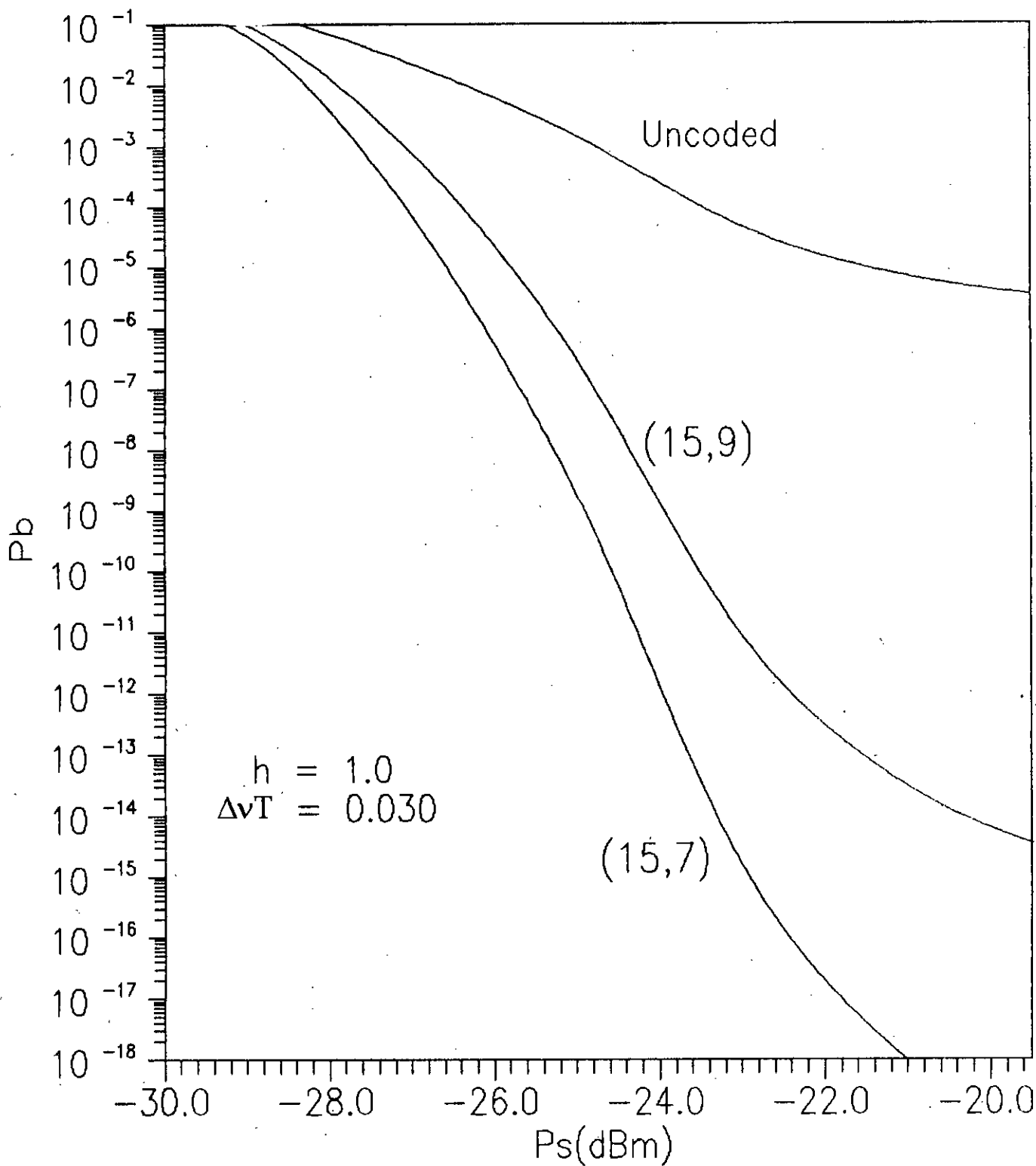


**Fig. 2.30** Plots of bit error probability  $P_b$  vs transmitted signal power  $P_s$ (dB<sub>m</sub>) for uncoded and Reed-Solomon's coded FSK with modulation index  $h = 1.0$  and laser linewidth  $\Delta\nu T = 0.030$

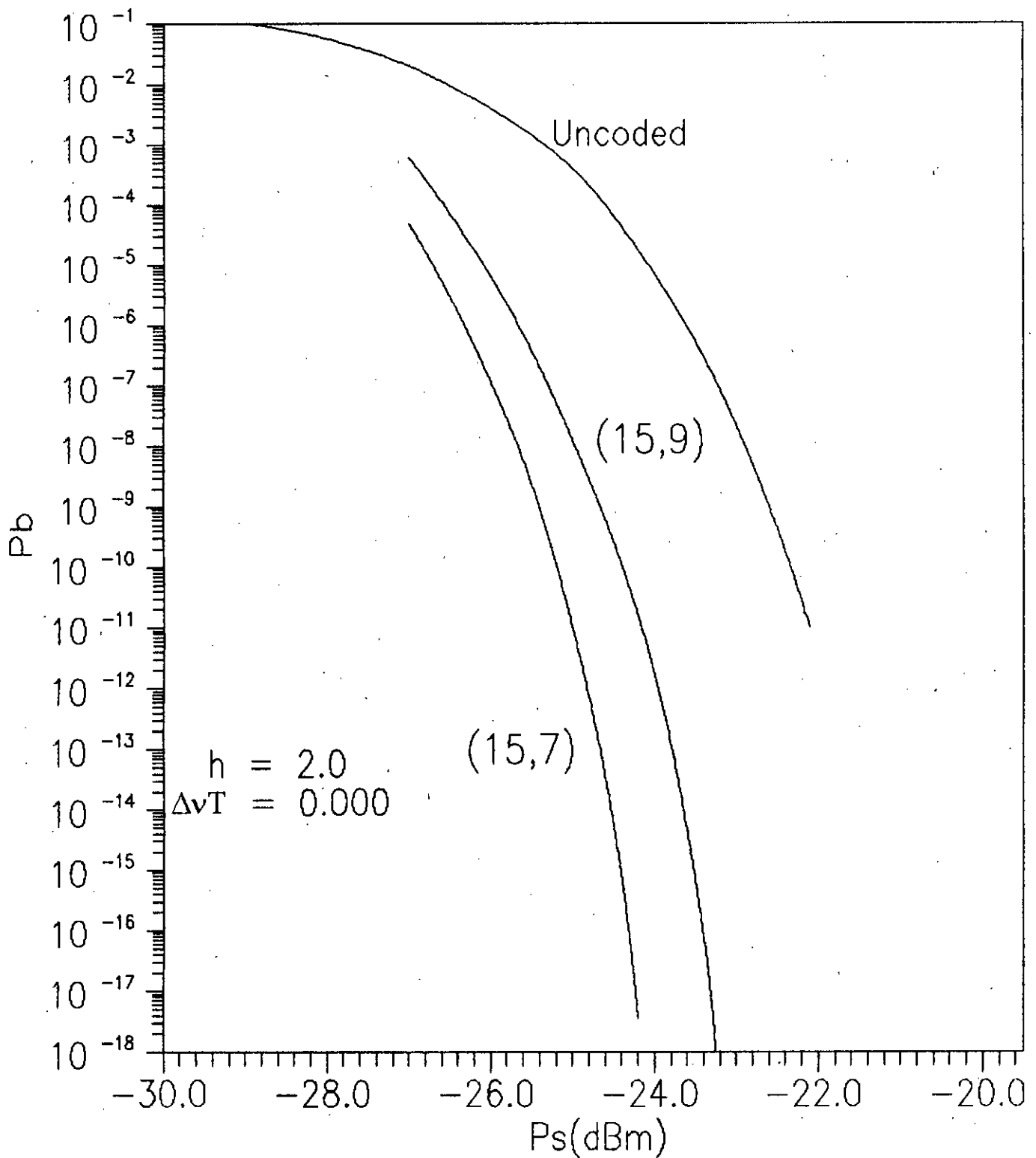
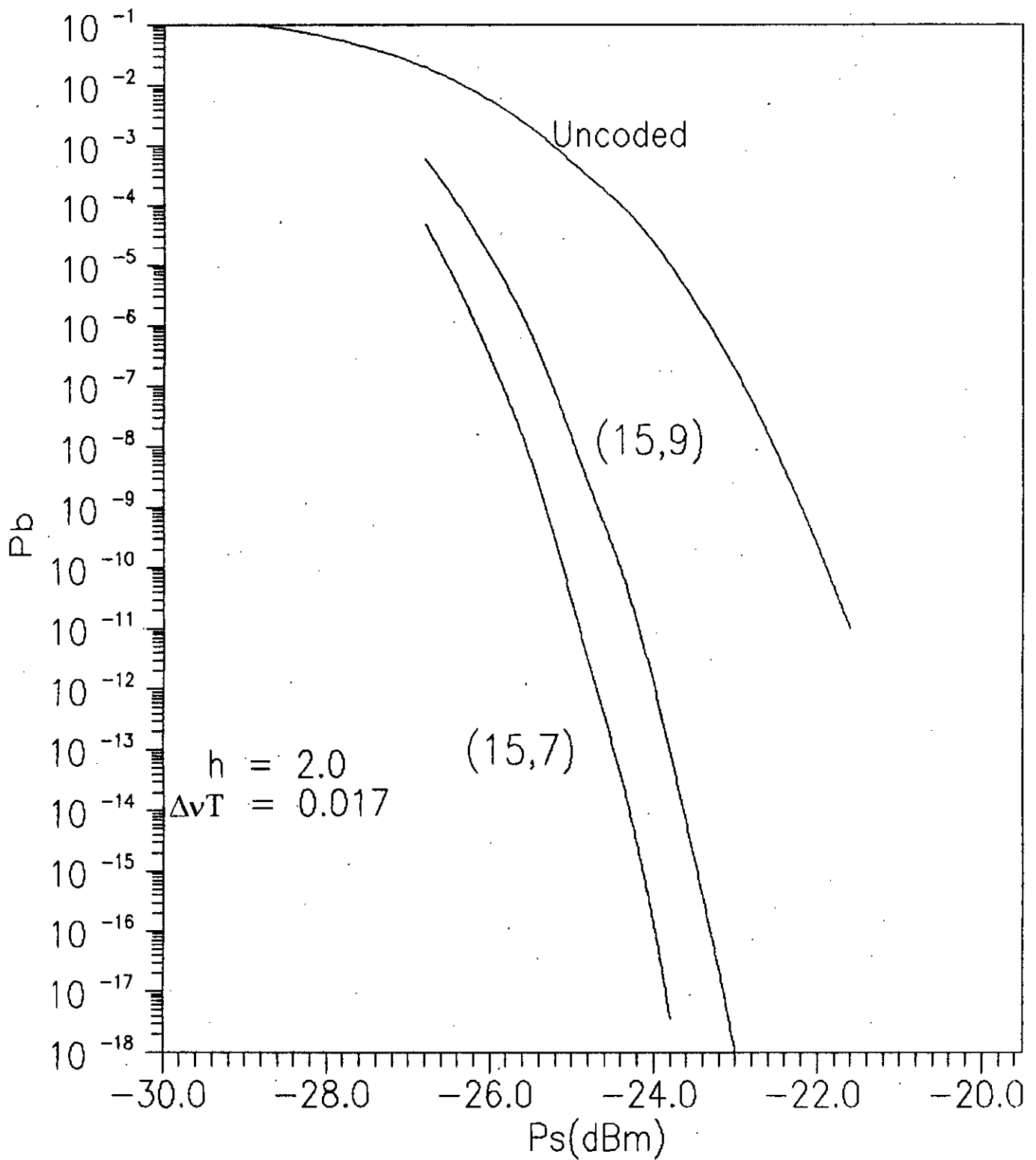
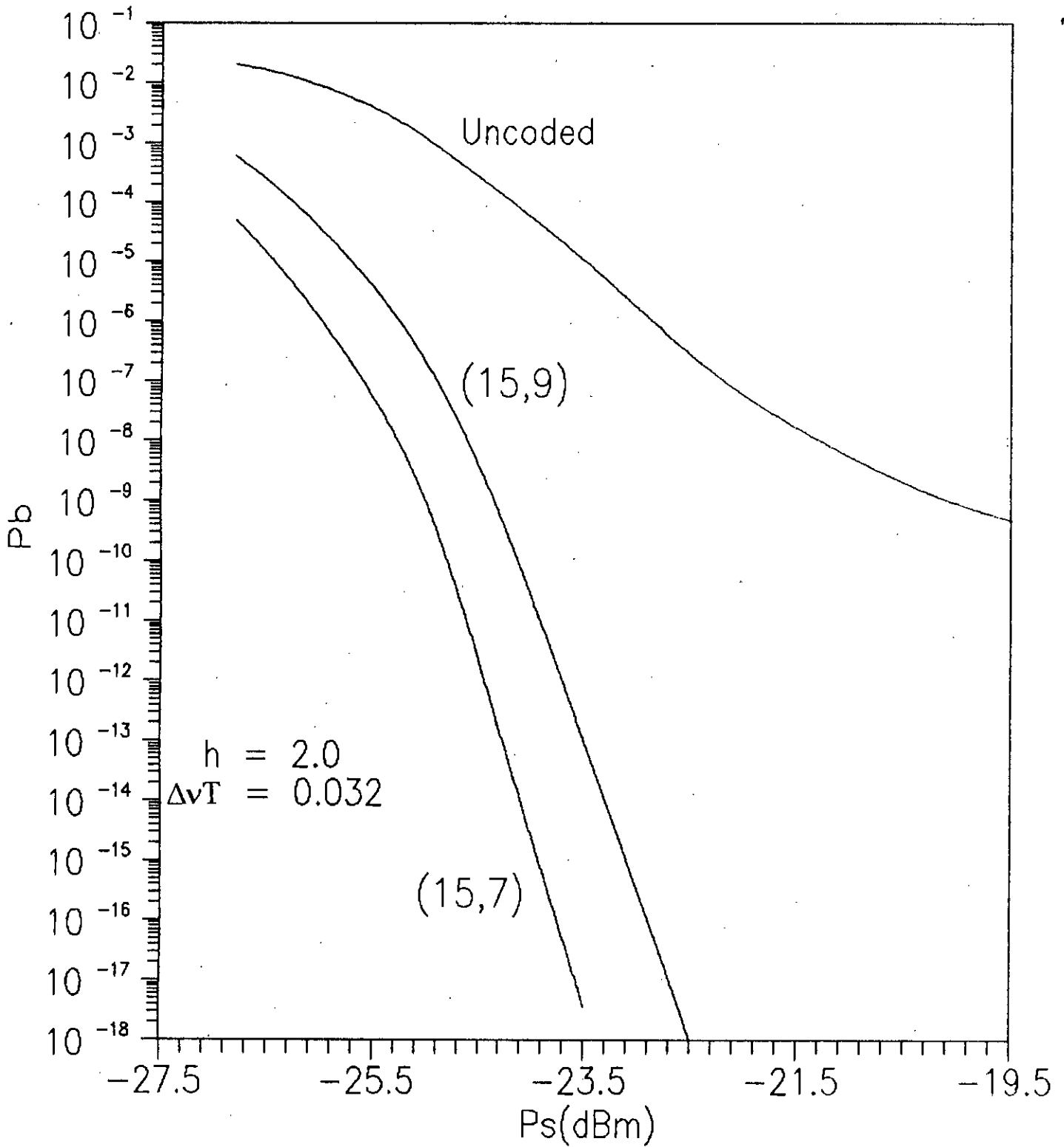


Fig. 2.31 Plots of bit error probability  $P_b$  vs transmitted signal power  $P_s$ (dB<sub>m</sub>) for uncoded and Reed-Solomon's coded FSK with modulation index  $h = 2.0$  and laser linewidth  $\Delta\nu T = 0.000$



**Fig. 2.32** Plots of bit error probability  $P_b$  vs transmitted signal power  $P_s(\text{dB}_m)$  for uncoded and Reed-Solomon's coded FSK with modulation index  $h = 2.0$  and laser linewidth  $\Delta\nu T = 0.017$



**Fig. 2.33** Plots of bit error probability  $P_b$  vs transmitted signal power  $P_s$ (dB<sub>m</sub>) for uncoded and Reed-Solomon's coded FSK with modulation index  $h = 2.0$  and laser linewidth  $\Delta\nu T = 0.032$

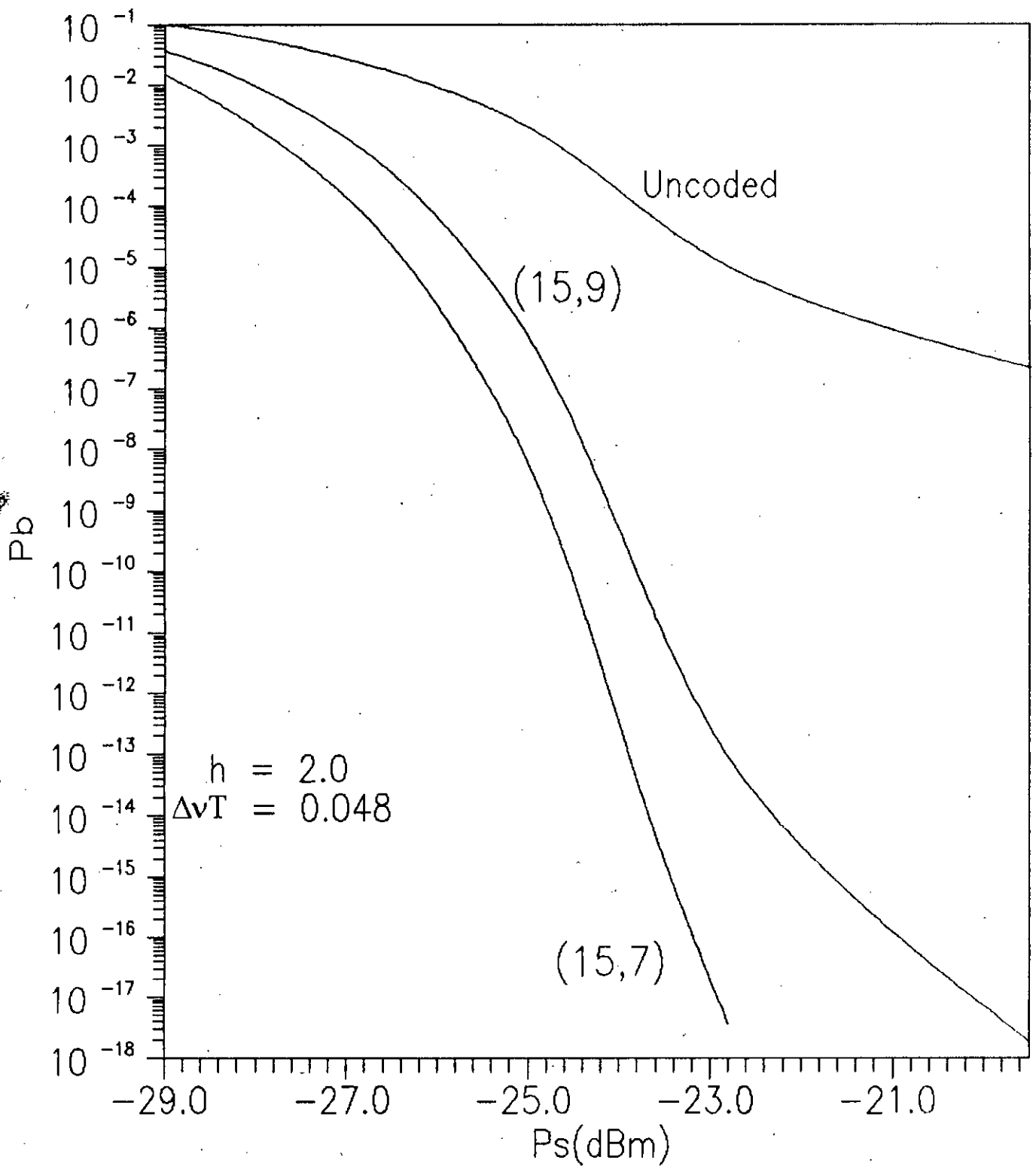


**Fig. 2.34** Plots of bit error probability  $P_b$  vs transmitted signal power  $P_s$ (dB<sub>m</sub>) for uncoded and Reed-Solomon's coded FSK with modulation index  $h = 2.0$  and laser linewidth  $\Delta\nu T = 0.048$

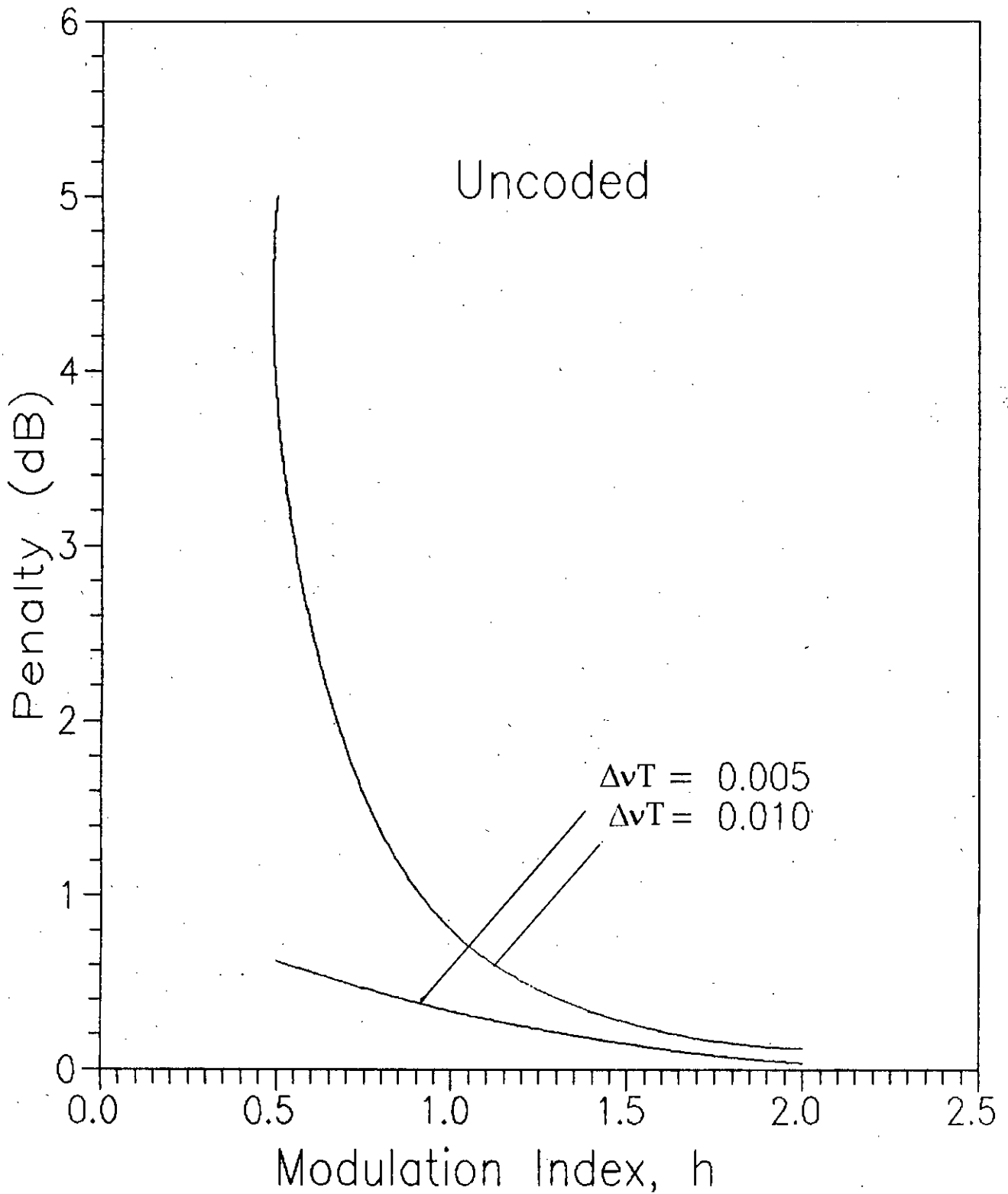


**Fig. 2.35** Plots of power penalty due to laser phase noise at bit error rate  $P_b = 10^{-9}$  as a function of the modulation index  $h$  with  $\Delta\nu T = 0.005$  and  $\Delta\nu T = 0.010$

89508

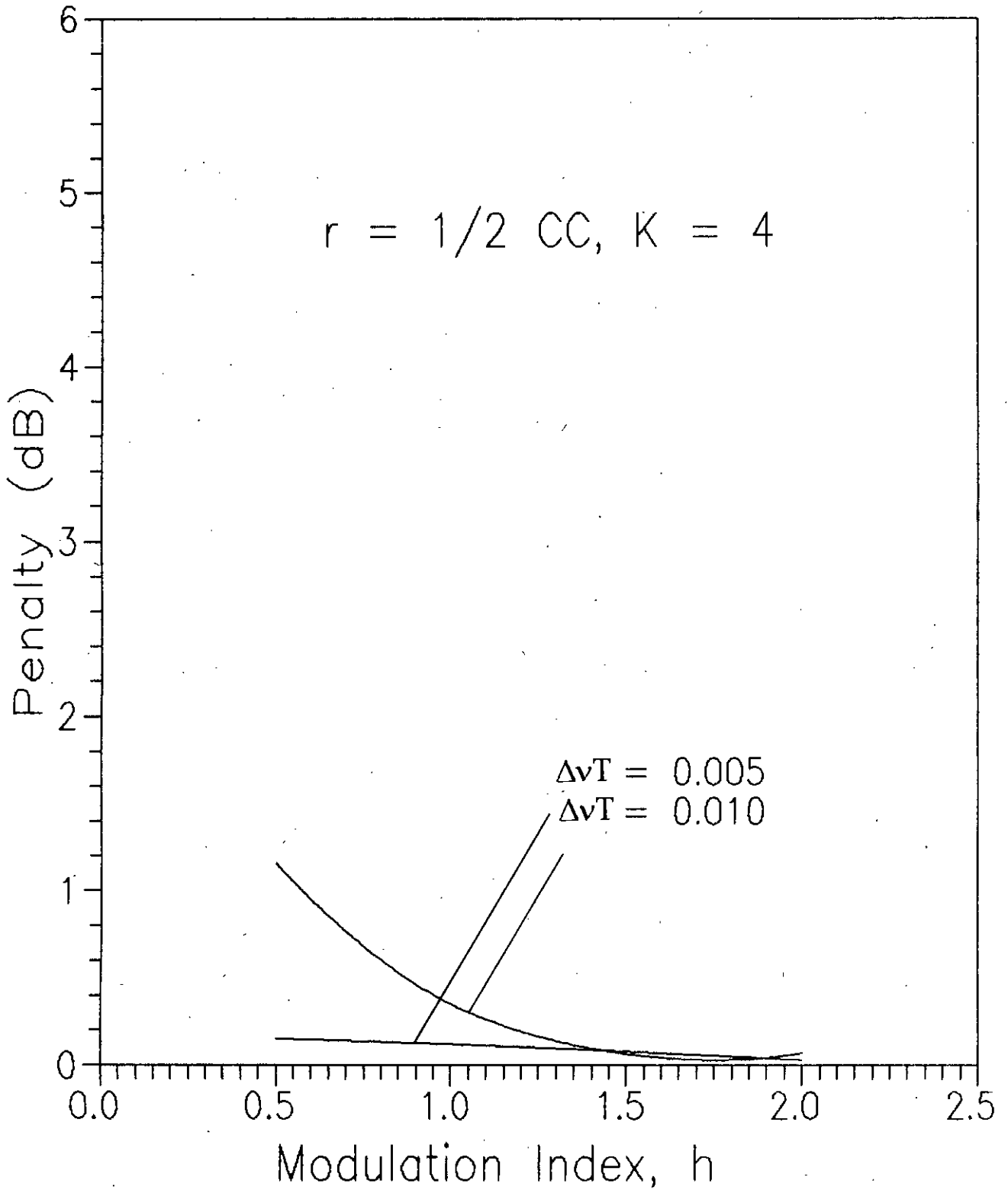


**Fig. 2.36** Plots of power penalty due to laser phase noise at bit error rate  $P_b = 10^{-9}$  for rate 1/2 convolutionally coded  $K = 4$  FSK with direct detection as a function of the modulation index  $h$  with  $\Delta\nu T = 0.005$  and  $\Delta\nu T = 0.010$

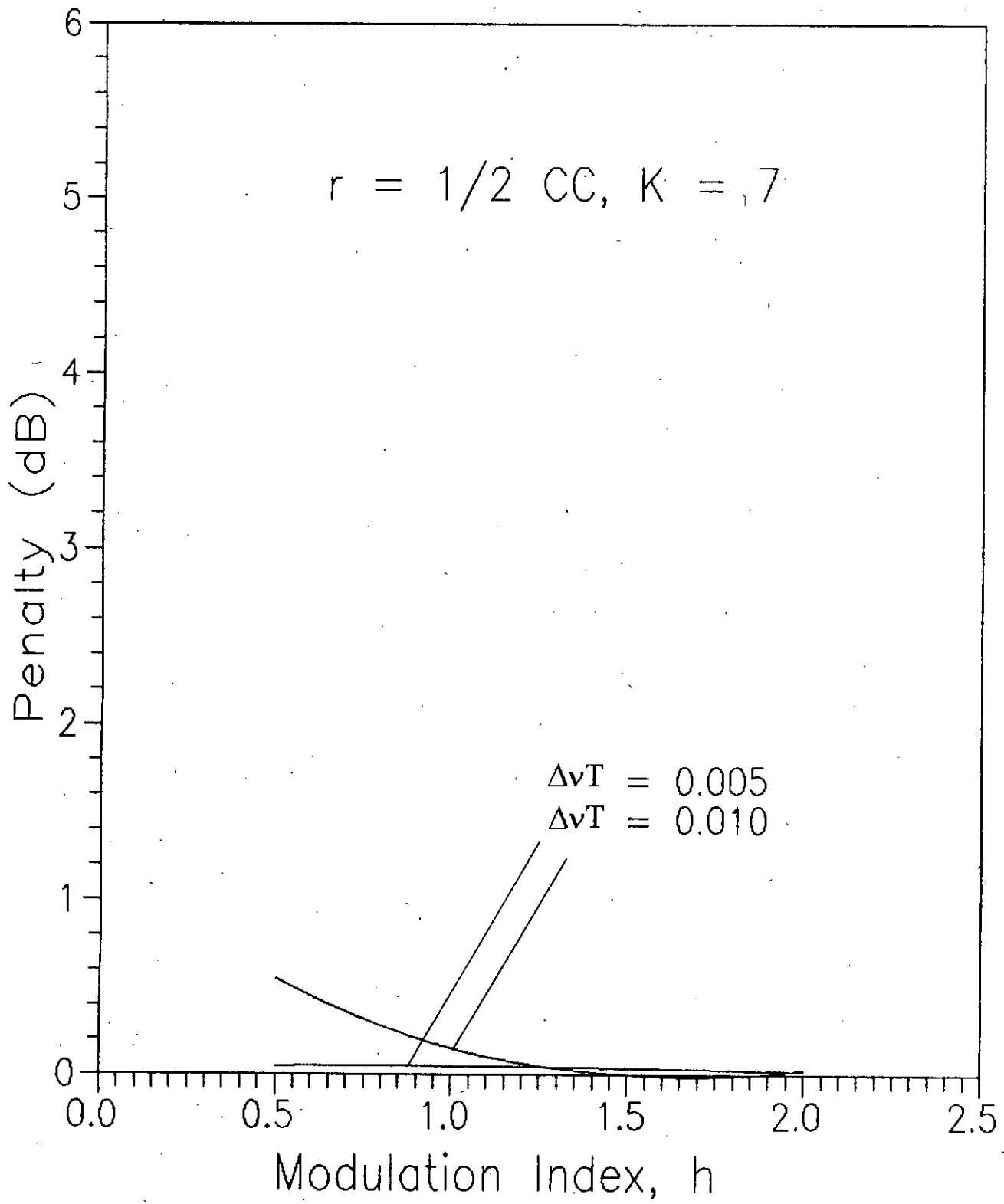


**Fig. 2.37** Plots of power penalty due to laser phase noise at bit error rate  $P_b = 10^{-9}$  for rate 1/2 convolutionally coded  $K = 7$  FSK with direct detection as a function of the modulation index  $h$  with  $\Delta\nu T = 0.005$  and  $\Delta\nu T = 0.010$



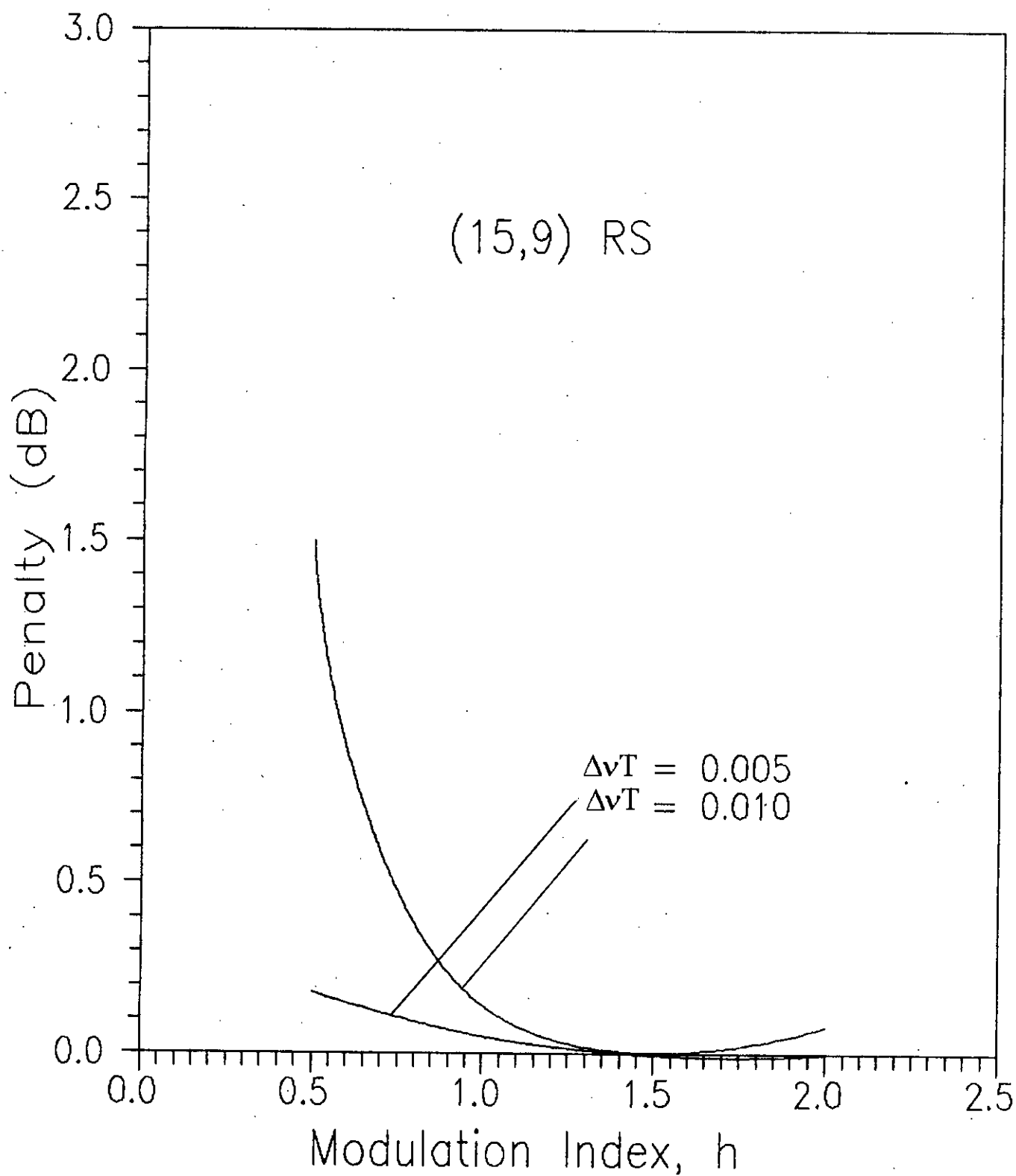


**Fig. 2.38** Plots of power penalty vs modulation index  $h$  (15, 9) Reed-Solomon coded FSK at bit error rate  $P_b = 10^{-9}$  for  $\Delta vT = 0.005$  and  $\Delta vT = 0.010$

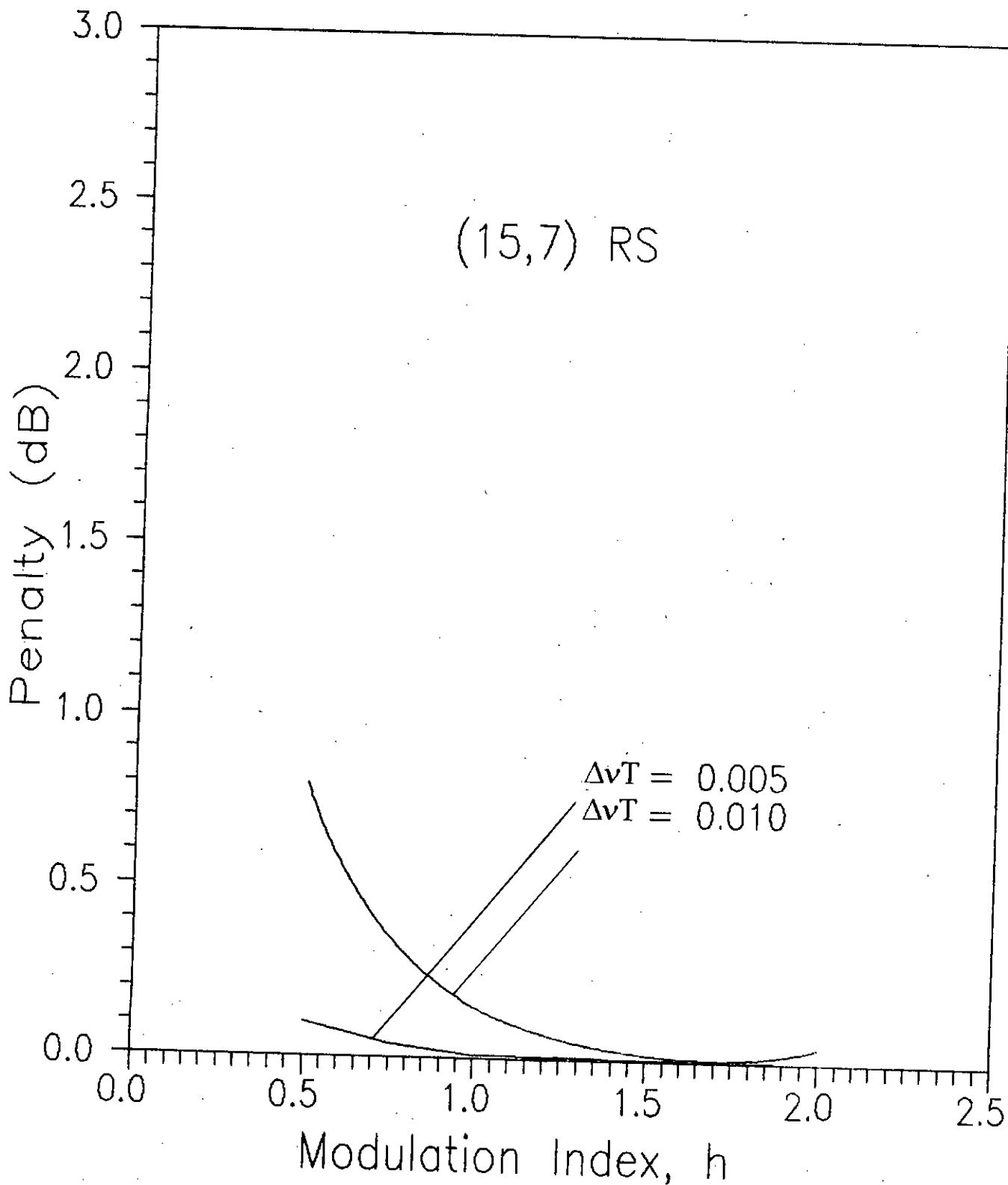


**Fig. 2.39** Plots of power penalty vs modulation index  $h$  (15, 7) Reed-Solomon coded FSK at bit error rate  $P_b = 10^{-9}$  for  $\Delta vT = 0.005$  and  $\Delta vT = 0.010$

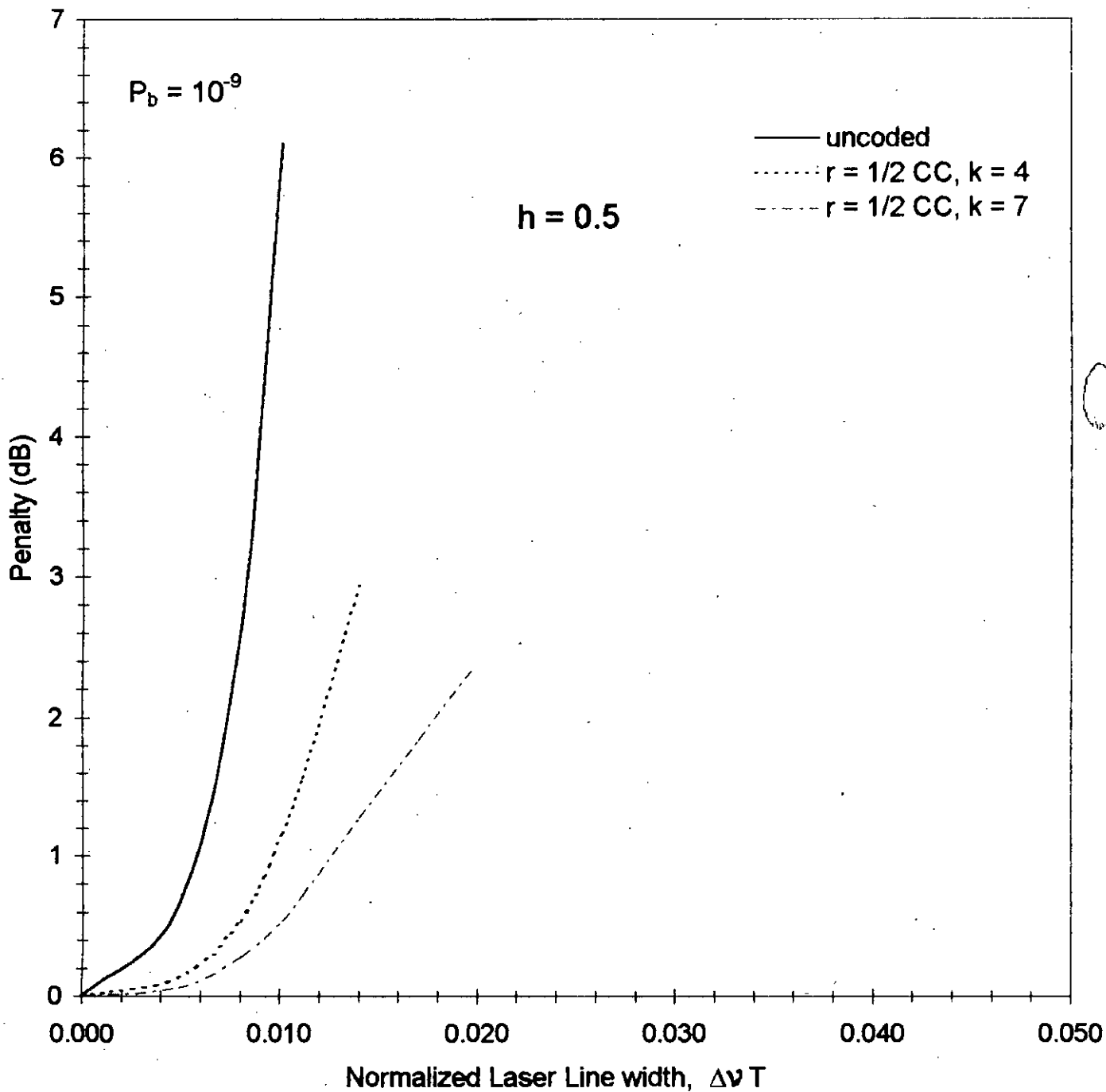


Fig. 2.40 Plots of power penalty due to phase noise at  $P_b = 10^{-9}$  for uncoded and rate 1/2 convolutionally coded FSK as a function of normalized laser linewidth  $\Delta\nu T$  for modulation index  $h = 0.5$

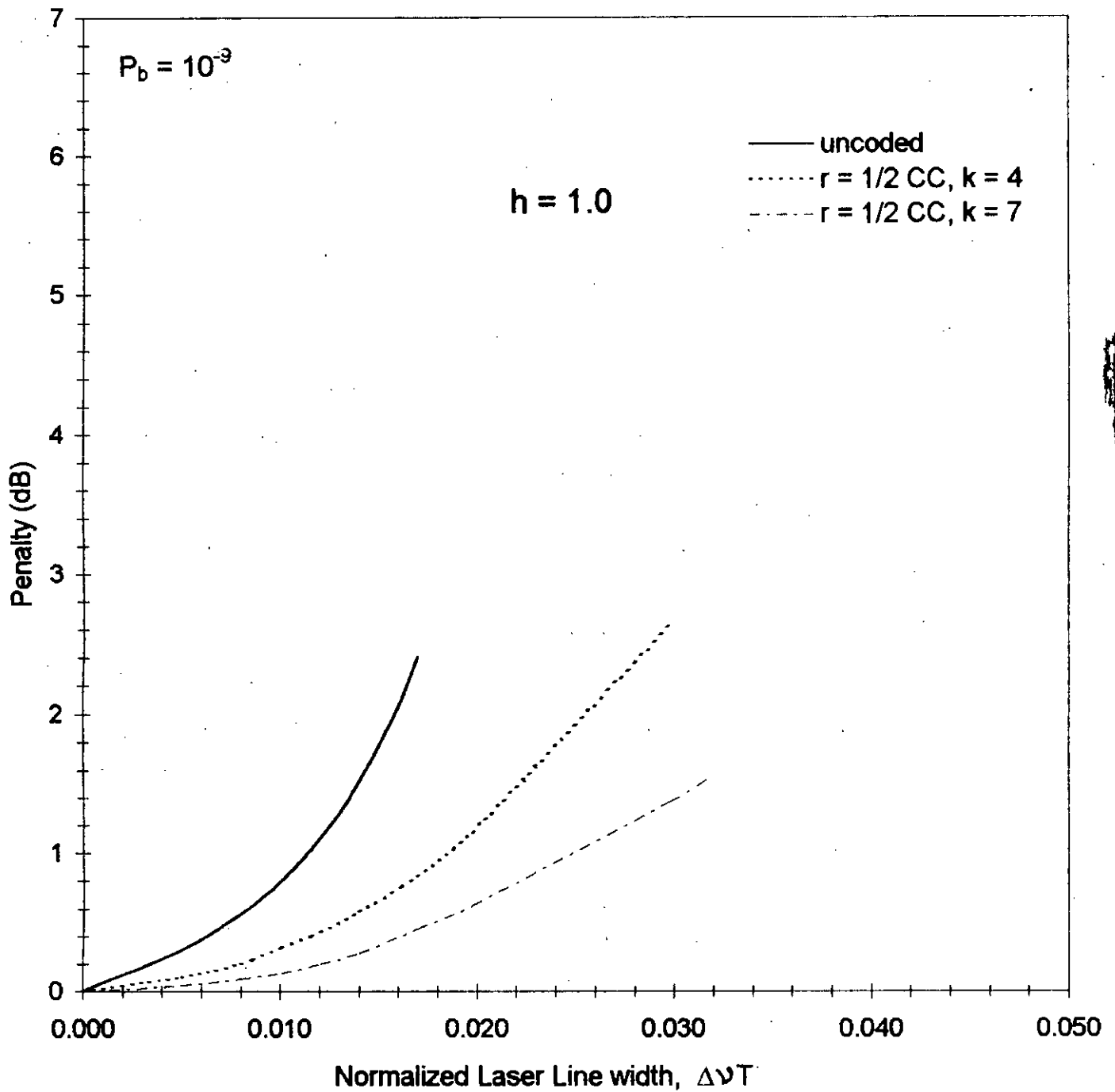


Fig. 2.41 Plots of power penalty due to phase noise at  $P_b = 10^{-9}$  for uncoded and rate 1/2 convolutionally coded FSK as a function of normalized laser linewidth  $\Delta\nu T$  for modulation index  $h = 1.0$

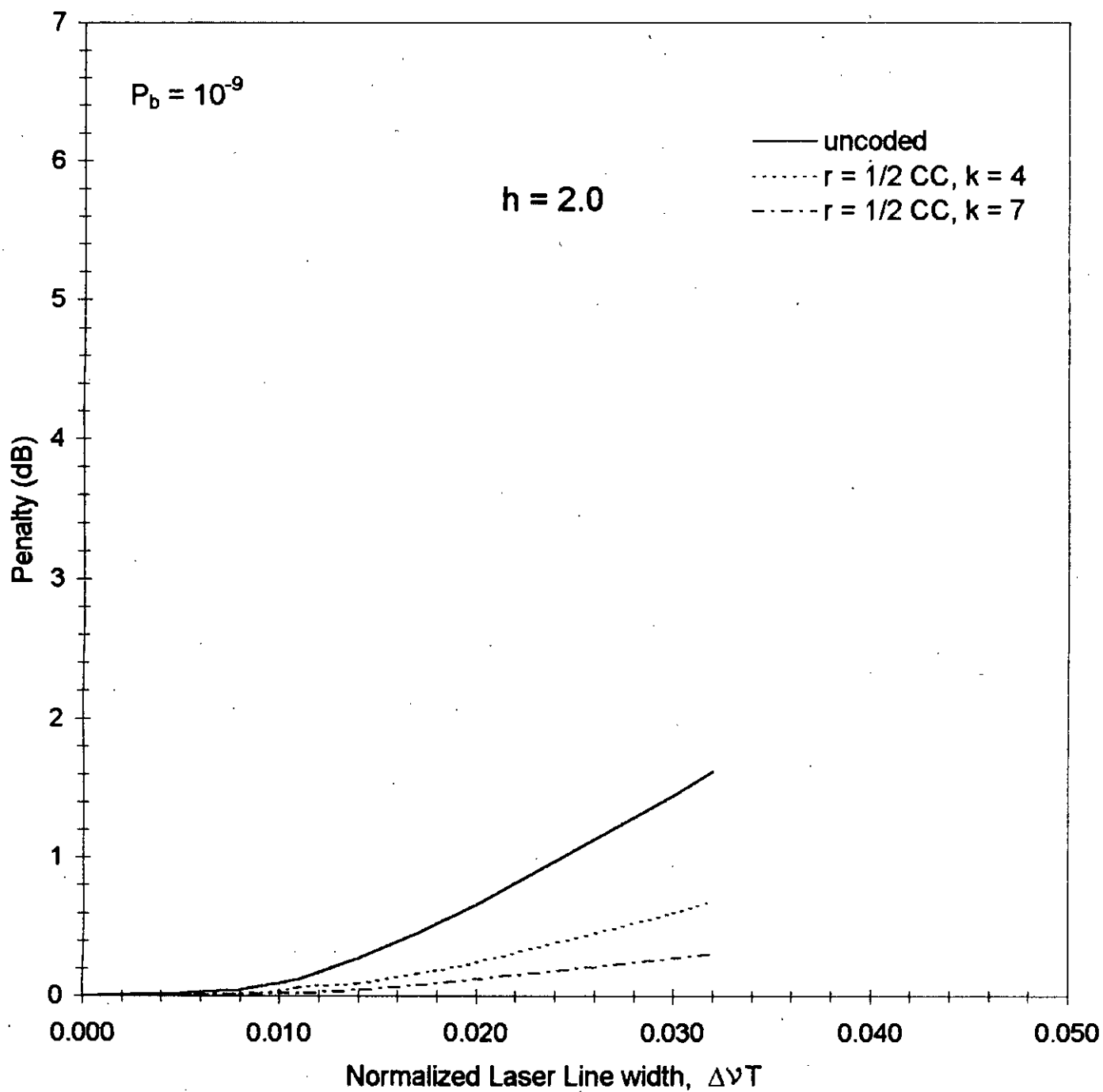


Fig. 2.42 Plots of power penalty due to phase noise at  $P_b = 10^{-9}$  for uncoded and rate 1/2 convolutionally coded FSK as a function of normalized laser linewidth  $\Delta\nu T$  for modulation index  $h = 2.0$

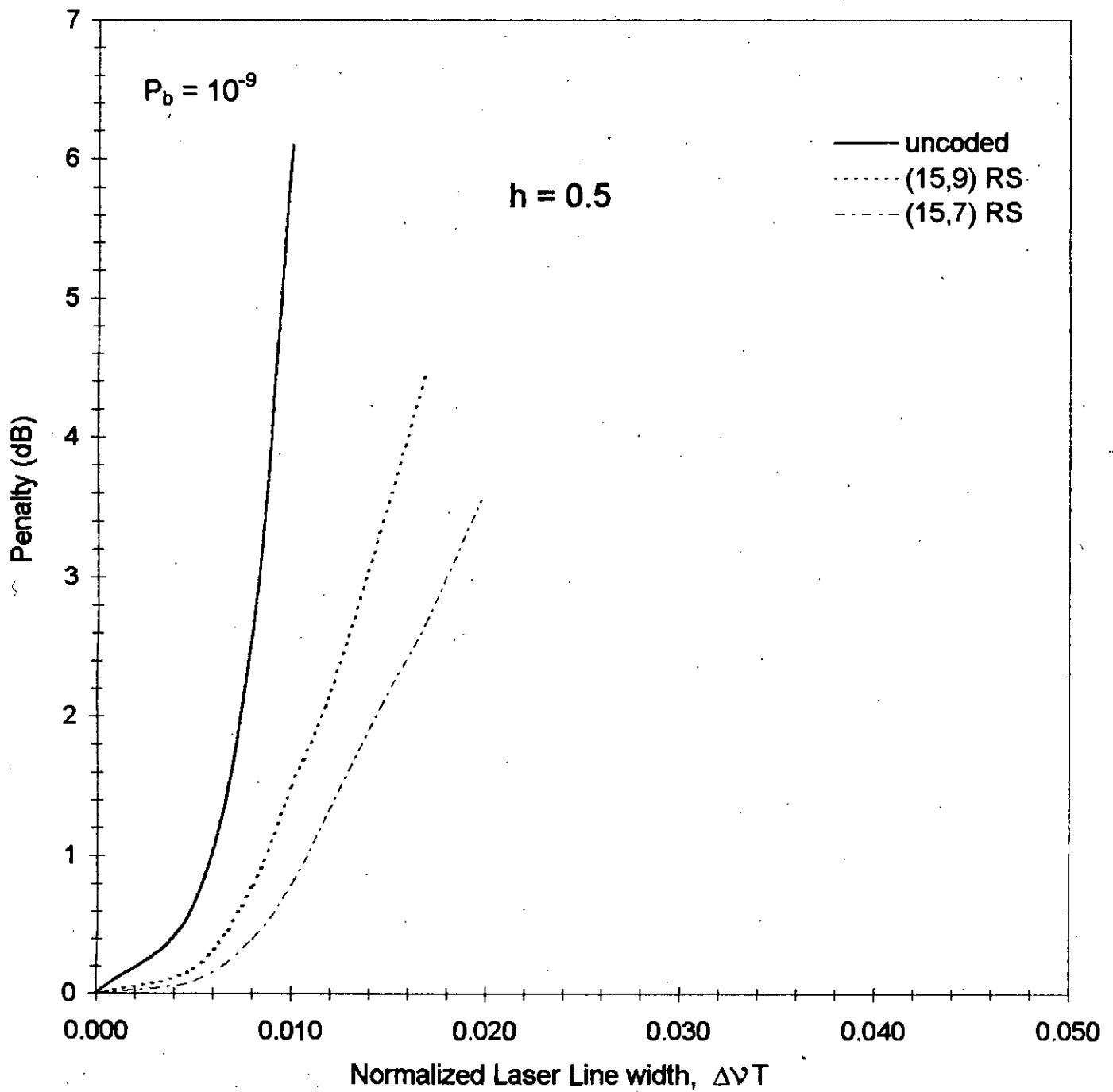


Fig. 2.43 Plots of power penalty due to phase noise at  $P_b = 10^{-9}$  for uncoded and Reed-Solomon's coded FSK as a function of normalized laser linewidth  $\Delta\nu T$  for modulation index  $h = 0.5$

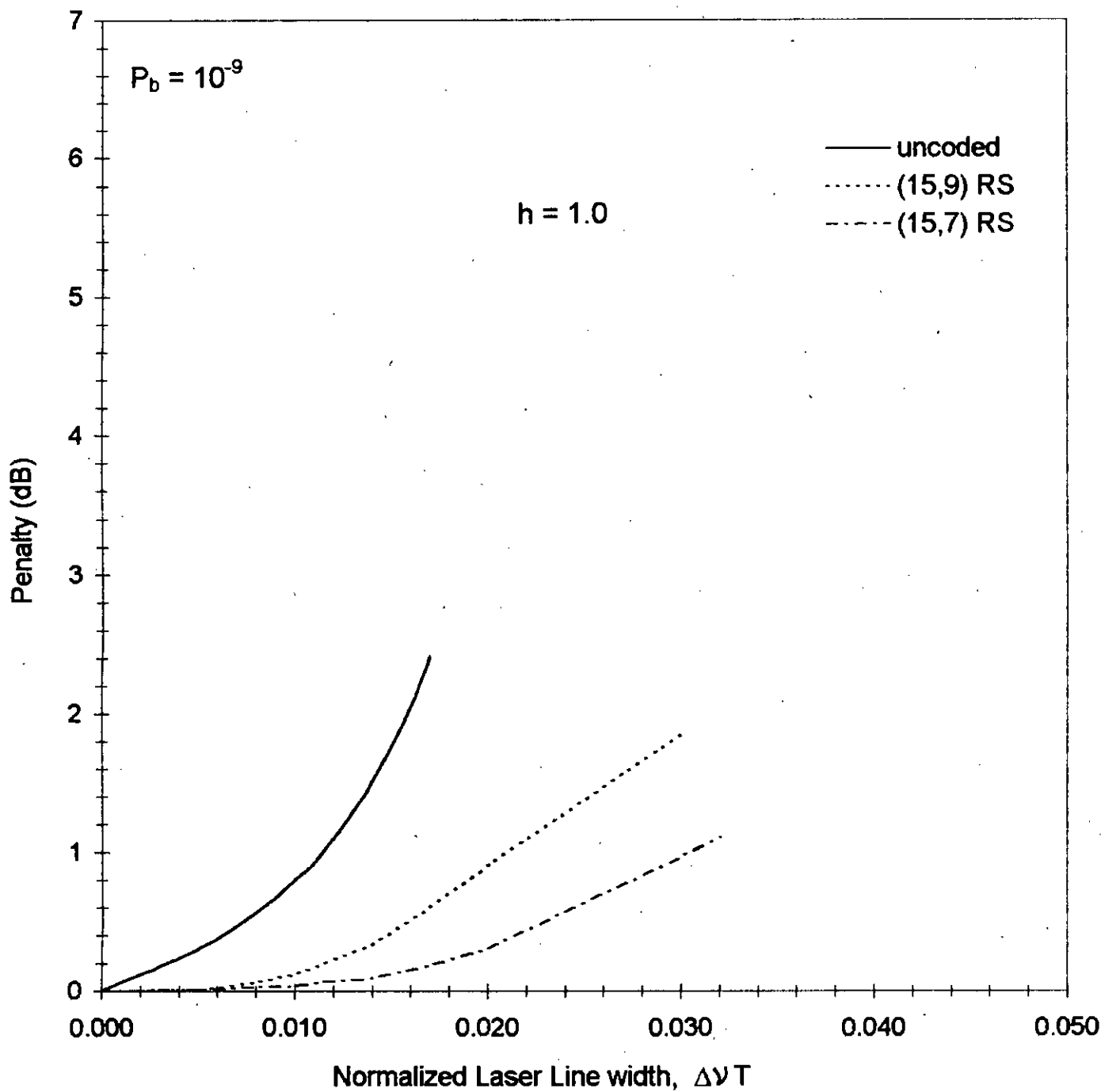


Fig. 2.44 Plots of power penalty due to phase noise at  $P_b = 10^{-9}$  for uncoded and Reed-Solomon's coded FSK as a function of normalized laser linewidth  $\Delta\nu T$  for modulation index  $h = 1.0$

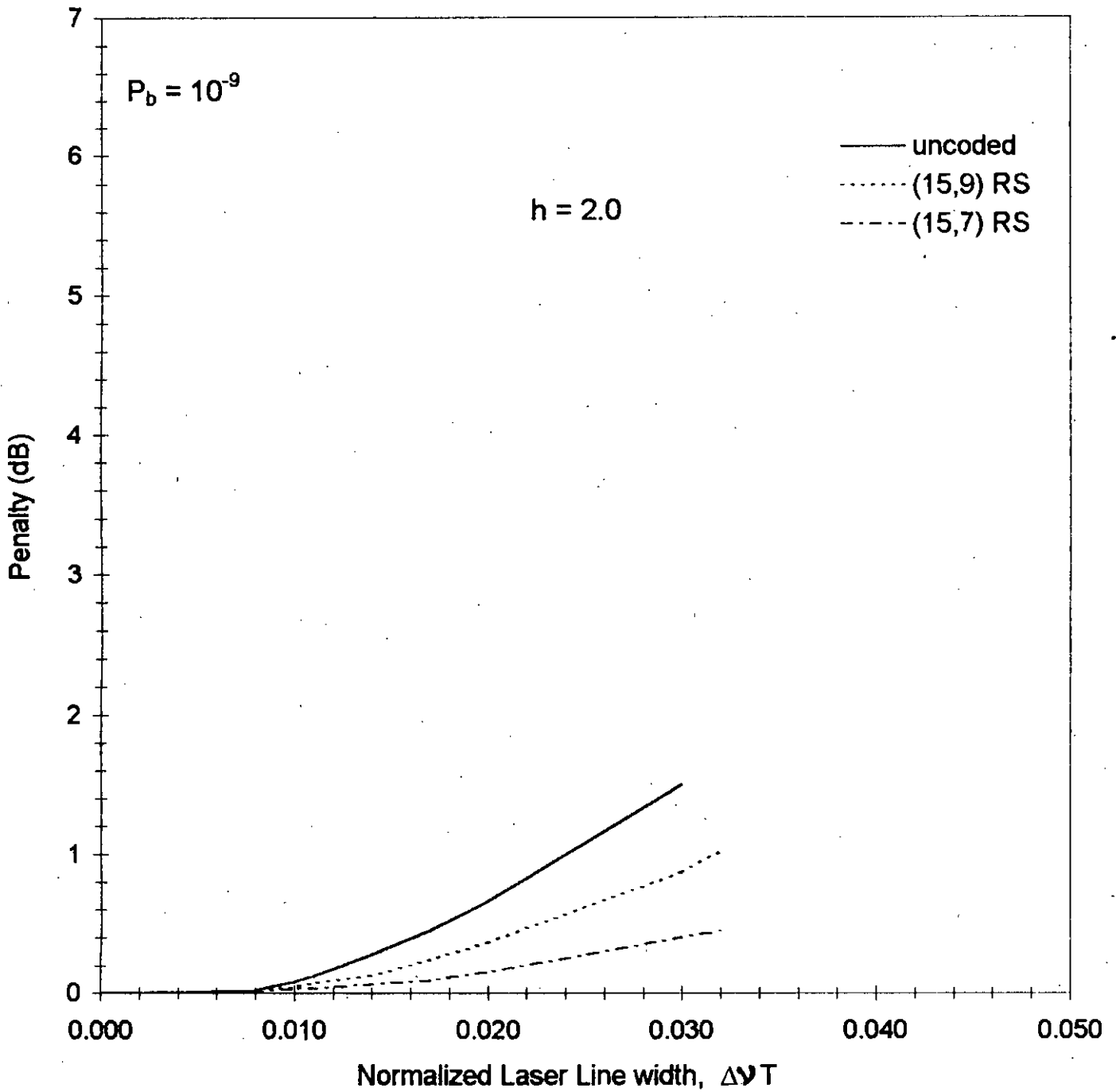


Fig. 2.45 Plots of power penalty due to phase noise at  $P_b = 10^{-9}$  for uncoded and Reed-Solomon's coded FSK as a function of normalized laser linewidth  $\Delta\nu T$  for modulation index  $h = 2.0$



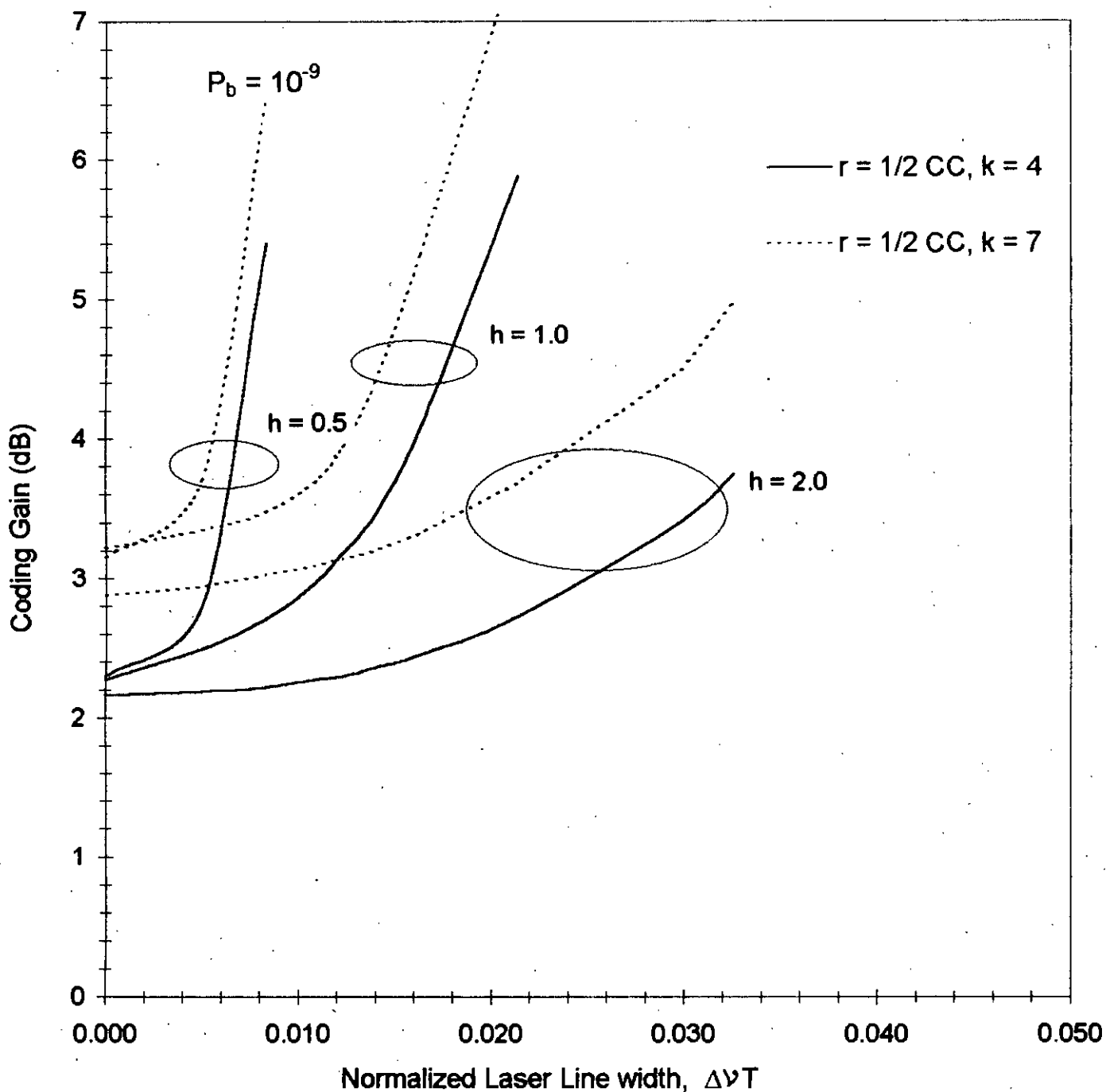


Fig. 2.46 Plots of coding gain at bit error rate  $P_b = 10^{-9}$  vs normalized laser linewidth  $\Delta\nu T$  for rate 1/2 convolutionally coded FSK with constraint length  $K = 4$  and  $K = 7$  for  $h = 0.5$ ,  $h = 1.0$  and  $h = 2.0$

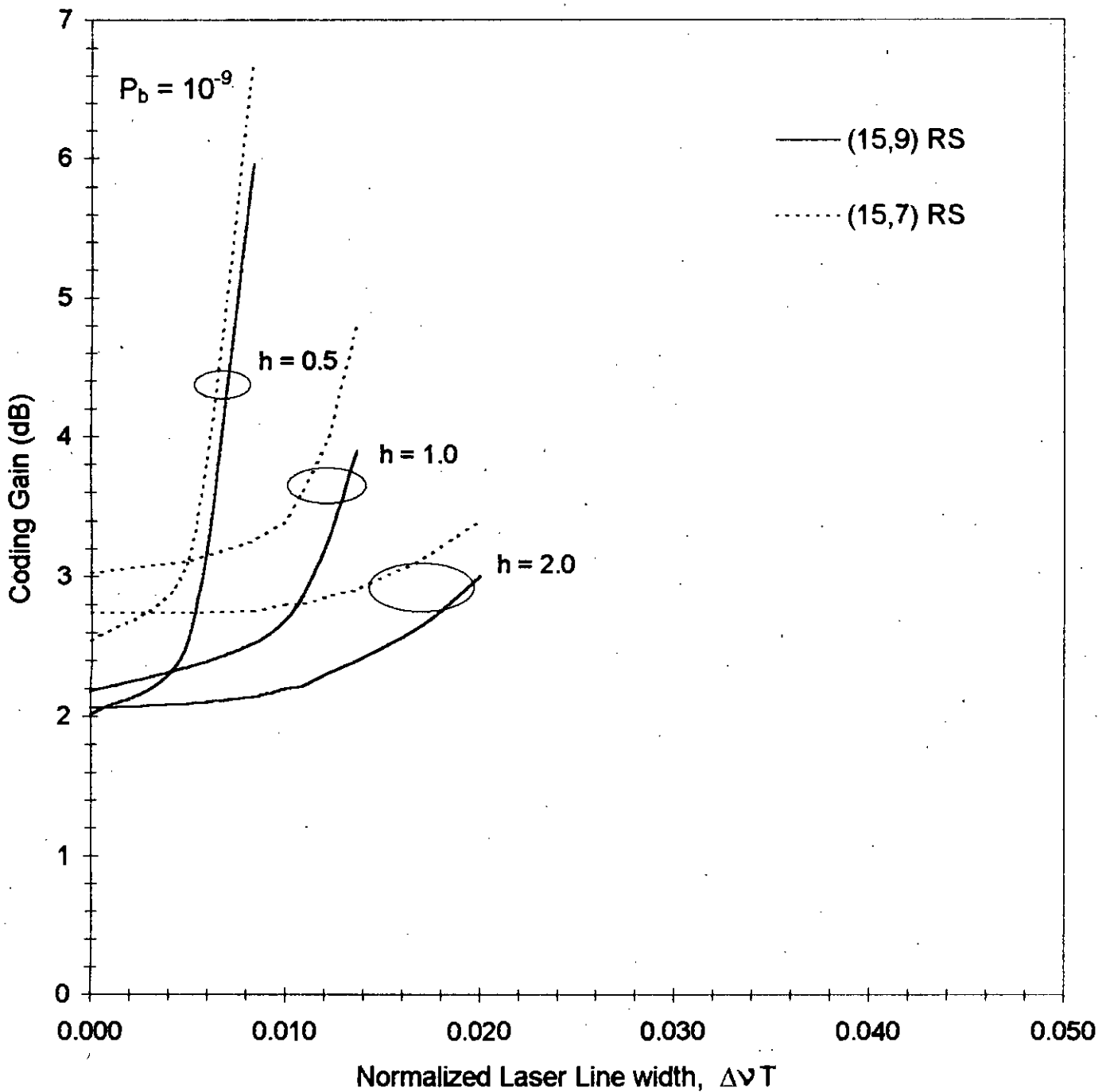


Fig. 2.47 Plots of coding gain at bit error rate  $P_b = 10^{-9}$  vs normalized laser linewidth  $\Delta\nu T$ , Reed-Solomon's coded (15,9) and (15,7) for FSK  $h = 0.5$ ,  $h = 1.0$  and  $h = 2.0$

respectively. The figures reveal that there is considerable amount of coding gain that can be achieved in the absence/presence of laser phase noise. When the linewidth is zero, the amount of coding gain is around 2.2 dB for  $k = 4$  and 3.2 dB for  $k = 7$  when Convolutional coding is employed. For non-zero linewidth coding gain is higher and increases with increasing values of normalized linewidth  $\Delta\nu T$ . However, the coding gains are less at higher values of the modulation index  $h$ . This is due to the fact that effect of intersymbol interference due to phase noise is less at higher values of  $h$  and coding is more effective in the presence of noise.

# **CHAPTER 3**

## **OPTICALLY PREAMPLIFIED FSK WITH AND WITHOUT CODING**

Table of contents :

- 3.1 Prologue
- 3.2 Preamplifier basics
- 3.3 The combined receiver model
- 3.4 Theoretical analysis of preamplified FSK
- 3.5 Coded FSK with optical preamplifier
- 3.6 Results and discussion
- 3.7 Conclusions and suggestions for future work

### 3.1 Prologue :

In comparative study between direct detection and heterodyne detection it is evident that direct detection is about 10 - 20 dB less sensitive than heterodyne detections. But this limitation can be overcome by adding an preamplifier in the receiver front-end. Lately direct detection receivers for FSK signals employing erbium doped fibre amplifier (EDFA)[19] and Mach-Zehnder Interferometer (MZI) have gained prominence over heterodyne detection receivers. In addition to the low coupling loss associated with erbium amplifier there are other particular advantages too. The inherent polarization sensitivity and the life time associated with the process are such that the crosstalk in the presence of a number of wavelength is significantly reduced so the amplifier behaves almost like a true traveling wave device, which should eliminate the problems of backward propagating signals. The noise figure of EDFA is also lower than SLA, partly because of the intrinsic mechanisms, but mainly due to the reduced coupling loss at the input.

### 3.2 Preamplifier basics :

The basic principle behind the operation of any optical amplifier is to stimulate the electron hole pair recombination in phase with the received optical signal. The amplifier is biased with a suitable injection current and the amplifier gain is dependent upon the injection current and the length of the amplifier over which the incident electromagnetic field travels. Although the amplifier is used to improve the receiver sensitivity by providing gain to the received signal, it itself generates some noise due to amplifier spontaneous emission (ASE). This noise corrupts the amplified optical signal. The characteristics can be defined as zero mean and gaussian and its PSD can be expressed as [21]

$$S_n(f) = \begin{cases} \frac{N_0}{2} = \frac{1}{2} N_{sp} (G-1) h\nu & |f \pm f_c| \leq \frac{B_0}{2} \\ 0 & \text{otherwise} \end{cases} \quad (3.2.1)$$

where,  $N_{sp}$  is the amplifier's spontaneous emission factor,  $h$  is the Plank's constant,  $\nu$  is the optical frequency and  $B_o$  is the optical amplifier's noise equivalent bandwidth.

### 3.3 The combined receiver model :

In Fig. 3.1 a combined receiver model is shown in which an optical preamplifier precedes the MZI with a noise equivalent bandwidth(NEB) of  $B_o$  . The difference of the two photocurrents are applied to the amplifier which is followed by an equalizer. The equalizer is required to equalize the pulse shape distortion caused by the photodetector capacitance and due to the input resistance and capacitance of the amplifier. The reshaped pulses after passing through the baseband filter is detected at the decision circuit by comparing it with a threshold of zero value. Finally there is the decoder which performs the decoding of the transmitted code.

### 3.4 Theoretical analysis of preamplified FSK :

The received signal at the input of optical amplifier as shown in Fig. 3.1 can be expressed as [22]

$$x(t) = \sqrt{2P_{in}} \cos[2\pi f_c t + \phi_s(t) + \phi_n(t)] \quad (3.4.1)$$

where,  $P_{in}$  is the amplifier input power,  $f_c$  is the optical carrier frequency,  $\phi_s(t)$  is the phase due to angle modulation and  $\phi_n(t)$  is the instantaneous phase noise of the transmitting laser.

If the electric field due to the amplifier spontaneous emission can be expressed as a sum of cosine terms, then the signal at the output of the optical amplifier is [23]

$$E(t) = \sqrt{2GP_{in}\eta_{in}\eta_{out}} \cos[2\pi f_c t + \phi_s(t) + \phi_n(t)] \quad (3.4.2)$$

where,  $G$  is the amplifier gain,  $\eta_{in}$  and  $\eta_{out}$  are the input and output coupling efficiency of optical amplifier.

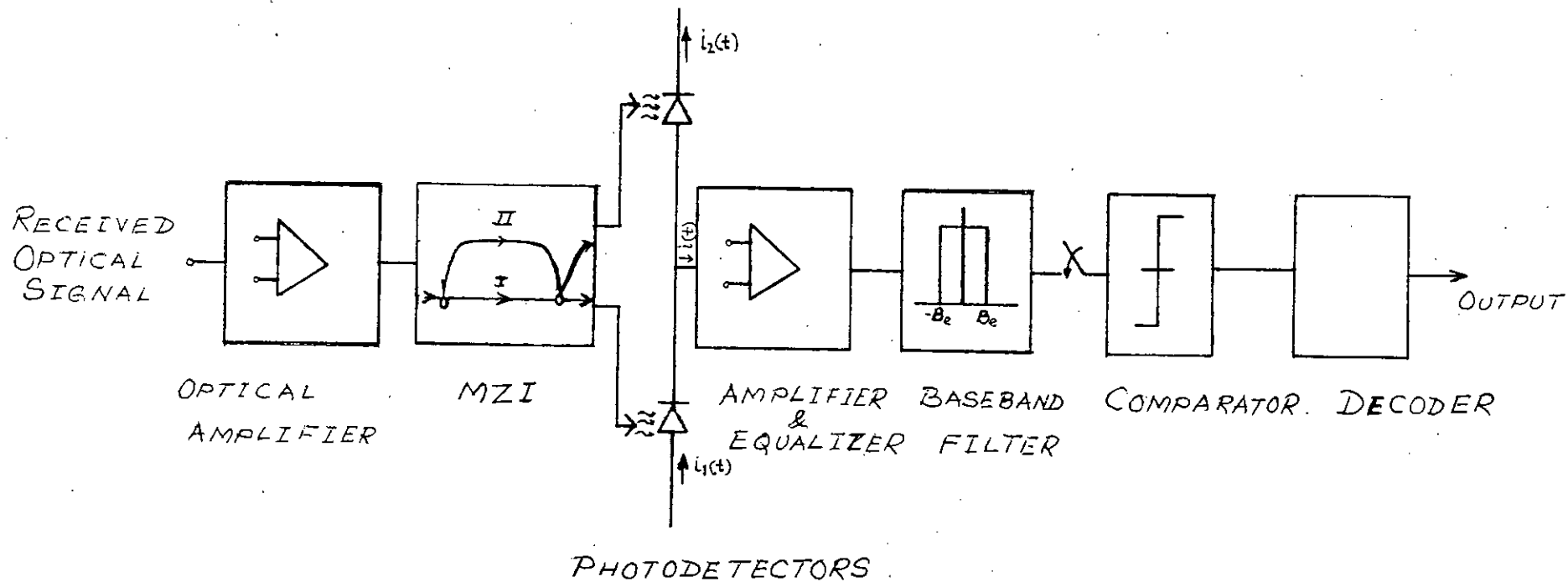


Fig. 3.1 Block diagram of a FSK direct detection receiver employing MZI with preamplifier and decoder

The frequency separation  $\delta\nu$  between the frequency components of the spectrum of ASE is an integer multiple of  $B_0$  such that,

$$M = \frac{B_0}{2\delta\nu}, \text{ an integer}$$

let us define  $P_s = P_{in} \eta_{in} \eta_{out}$ . Then

$$E(t) = \sqrt{2GP_s} \cos[2\pi f_c t + \phi_s(t) + \phi_n(t)] + \sum_{k=-M}^{k=M} \sqrt{2N_0 \delta\nu} \cos[2\pi(f_c + k\delta\nu)t + \Omega_k] \quad (3.4.3)$$

$$= s(t) + n(t) \quad (3.4.4)$$

The first and second terms of eq. 3.4.3 represent the signal and ASE noise components, respectively and  $\Omega_k$  is a random phase for each component of spontaneous emission.

The optical signal  $E(t)$  is passed through MZI and then fed to the photodetector. The output currents  $i_1(t)$  and  $i_2(t)$  of the upper and lower photodetectors, respectively can be expressed as

$$i_1(t) = R_d |E_1(t)|^2 \quad (3.4.5)$$

and 
$$i_2(t) = R_d |E_2(t)|^2 \quad (3.4.6)$$

where,  $R_d$  is the responsivity of the photodetector and  $E_1(t)$  and  $E_2(t)$  are the outputs of two arms of MZI. Following the same approach as in chapter 2, the signal component of balanced receiver current can be obtained as

$$i(t) = i_1(t) - i_2(t) \quad (3.4.7)$$

$$= GR_d P_s \cos[w_c \tau + \Delta\phi_s(t, \tau) + \Delta\phi_n(t, \tau) + \phi_0] \quad (3.4.8)$$

where,  $\tau$  is the delay due to path difference in MZI,  $\phi_0$  is the phase offset due to mismatch between  $f_c$  and MZI centre frequency,  $\Delta\phi_n(t, \tau) = \phi_n(t) - \phi_n(t - \tau)$  is the phase change due to the phase noise during the interval  $\tau$  and



$\Delta\phi_s(t, \tau) = \phi_s(t) - \phi_s(t - \tau)$ . For ideal conditions of demodulation then for a 'mark' ( $a_0 = +1$ ) transmission, the current  $i(t)$  can be expressed as

$$i_m(t) = GR_d P_s x(t) \quad (3.4.9)$$

where,

$$x(t) = \cos[\Delta\phi_n(t, \tau)] \quad (3.4.10)$$

Similarly for a 'space' transmission,

$$i_s(t) = -GR_d P_s x(t) \quad (3.4.11)$$

The total noise power can be expressed as

$$N = N_{shot} + N_{excess} + N_{S-SP} + N_{th} \quad (3.4.12)$$

where,  $N_{S-SP}$  is the power due to signal spontaneous beat noise power and the expressions of  $N_{shot}$ ,  $N_{excess}$ ,  $N_{th}$  are as given in chapter 2 section 2.3.

Then the bit error rate can be expressed as

$$BER = \frac{1}{2} \int_{-\infty}^{\infty} \text{erfc} \left[ \frac{2GR_d P_s \cos \Delta\phi_n}{\sqrt{2N}} \right] p(\Delta\phi_n) d(\Delta\phi_n) \quad (3.4.13)$$

### 3.5 Coded FSK with optical preamplifier :

Following the similar approach in chapter 2 the performance of coded FSK employing Convolutional coding and Reed-Solomon's coding for the present case can be evaluated.

### 3.6 Results and Discussion :

The performance results for optically preamplified FSK system with and without forward error correction coding are evaluated at a bit rate of 2.5 Gb/s following the theoretical analysis presented in section 3.4. The probability of bit error  $P_b$  is computed for uncoded and coded system for different sets of values of the normalized laser linewidth  $\Delta\nu T$  and modulation index  $h$ .

Figure 3.2 provides the bit error rate  $P_b$  versus transmitted signal power  $P_s$  (dB<sub>m</sub>) for  $h = 1.0$  when the laser linewidth is zero and amplifier gain is 30 dB. For non-zero linewidth, the BER plots are given in Fig. 3.3 through Fig. 3.5. Comparison of the results with those of FSK system without optical amplifier presented in chapter 2, it becomes evident that due to use of an optical preamplifier there is an improvement in the receiver sensitivity. However, for uncoded case, there occurs error rate floors depending on the value of  $\Delta\nu T$ .

When the optical amplifier's gain is increased to 40 dB, there is further improvement in the receiver sensitivity as depicted in Fig. 3.6 through Fig. 3.9.

Similar results for RS coded FSK with optical preamplifier are also provided in Fig. 3.10 through Fig. 3.13 for  $G = 30$  dB and Fig. 3.14 through Fig. 3.17 for  $G = 40$  dB.

The coding gain obtained at  $P_b = 10^{-9}$  for rate 1/2 Convolutional coding with  $k = 4, 7$  over uncoded system are plotted in Fig. 3.18 and Fig. 3.19 for  $G = 30$  dB and 40 dB respectively. It is observed that coding gain is higher at higher  $\Delta\nu T$ . Similar plots of coding gains for RS coded system are given in Fig. 3.20 and Fig. 3.21 for  $G = 30$  dB and 40 dB respectively. Comparing these curves with Fig. 3.18 and Fig. 3.19 we observe that coding gain is higher for RS coded case and increases with  $\Delta\nu T$ . Further, it is also clear that coding gain is higher at higher amplifier gain.

The power penalty due to laser phase noise at  $P_b = 10^{-9}$  for preamplified FSK system with and without coding is plotted in Fig. 3.22 and Fig. 3.23 for rate 1/2 CC and in Fig. 3.24 and Fig. 3.25 for (15,9) and (15,7) RS coding when  $G = 30$  dB and 40 dB respectively and  $h = 1.0$ . Comparing Fig. 3.22 with Fig. 3.24 we see that penalty is relatively small for RS coding than for Convolutional coding. Similar observations are also found when the amplifier gain is 40 dB as shown in Fig. 3.23 and Fig. 3.25 and there is further reduction in the power penalty due to increase of amplifier gain.

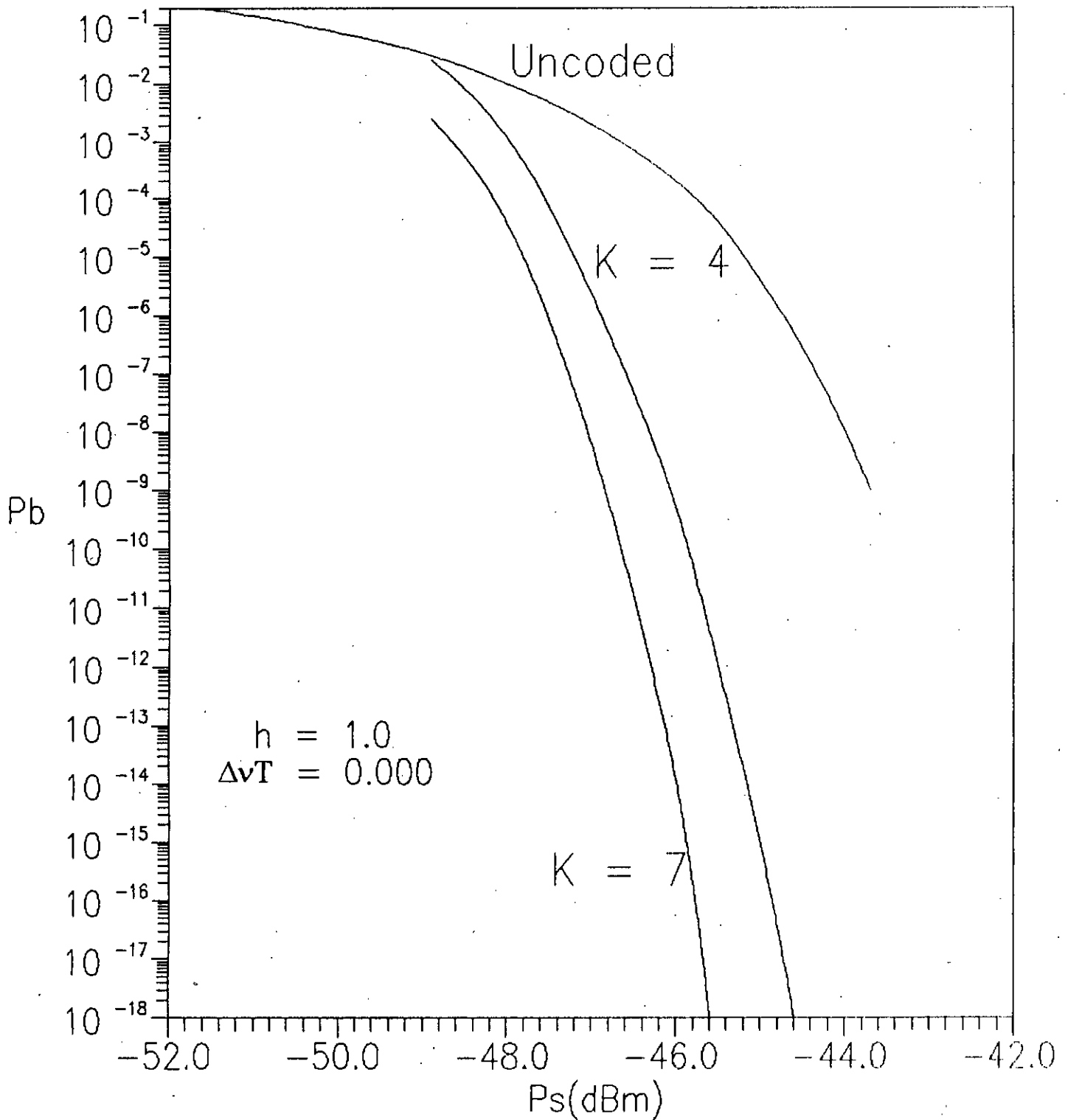
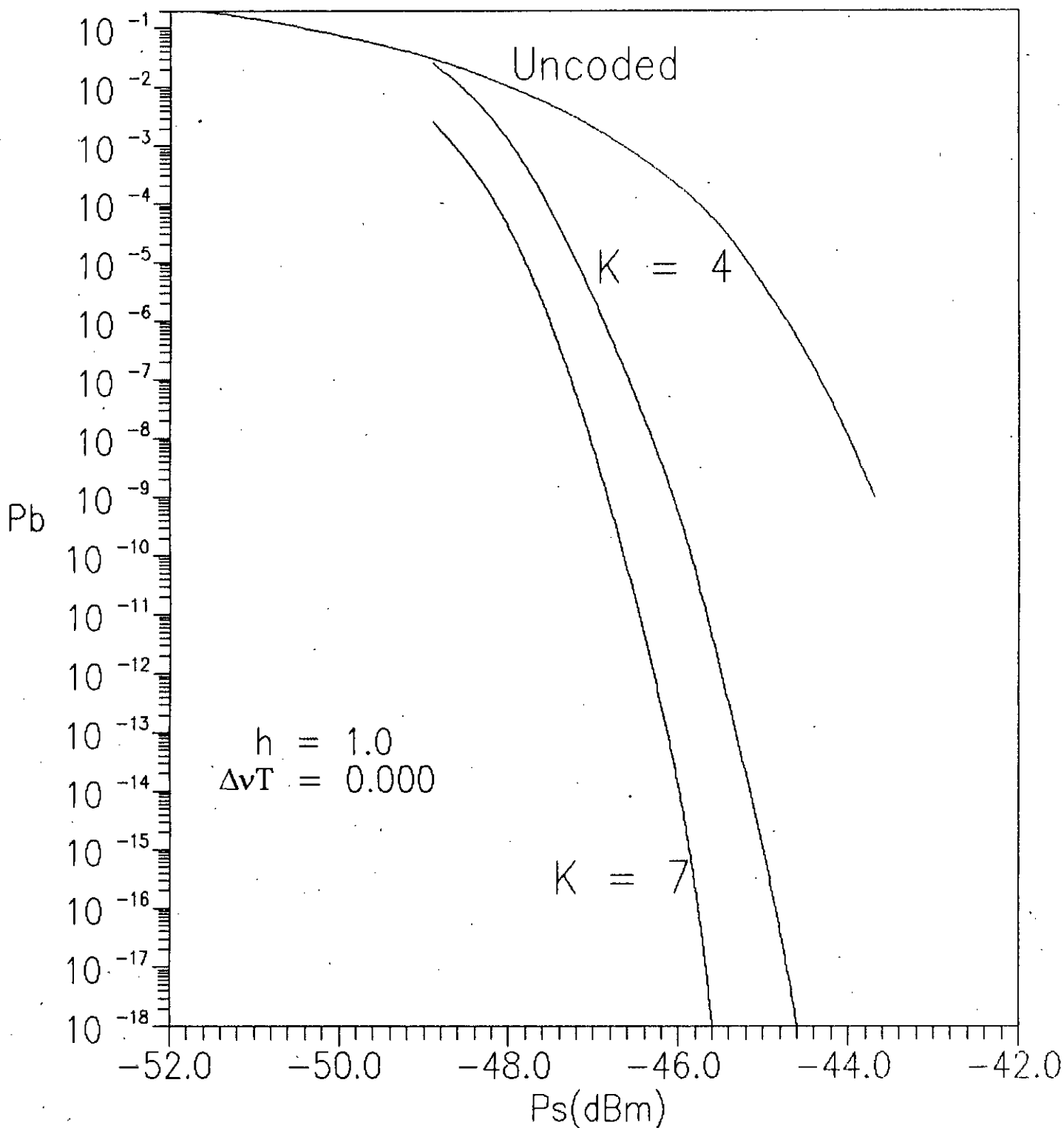
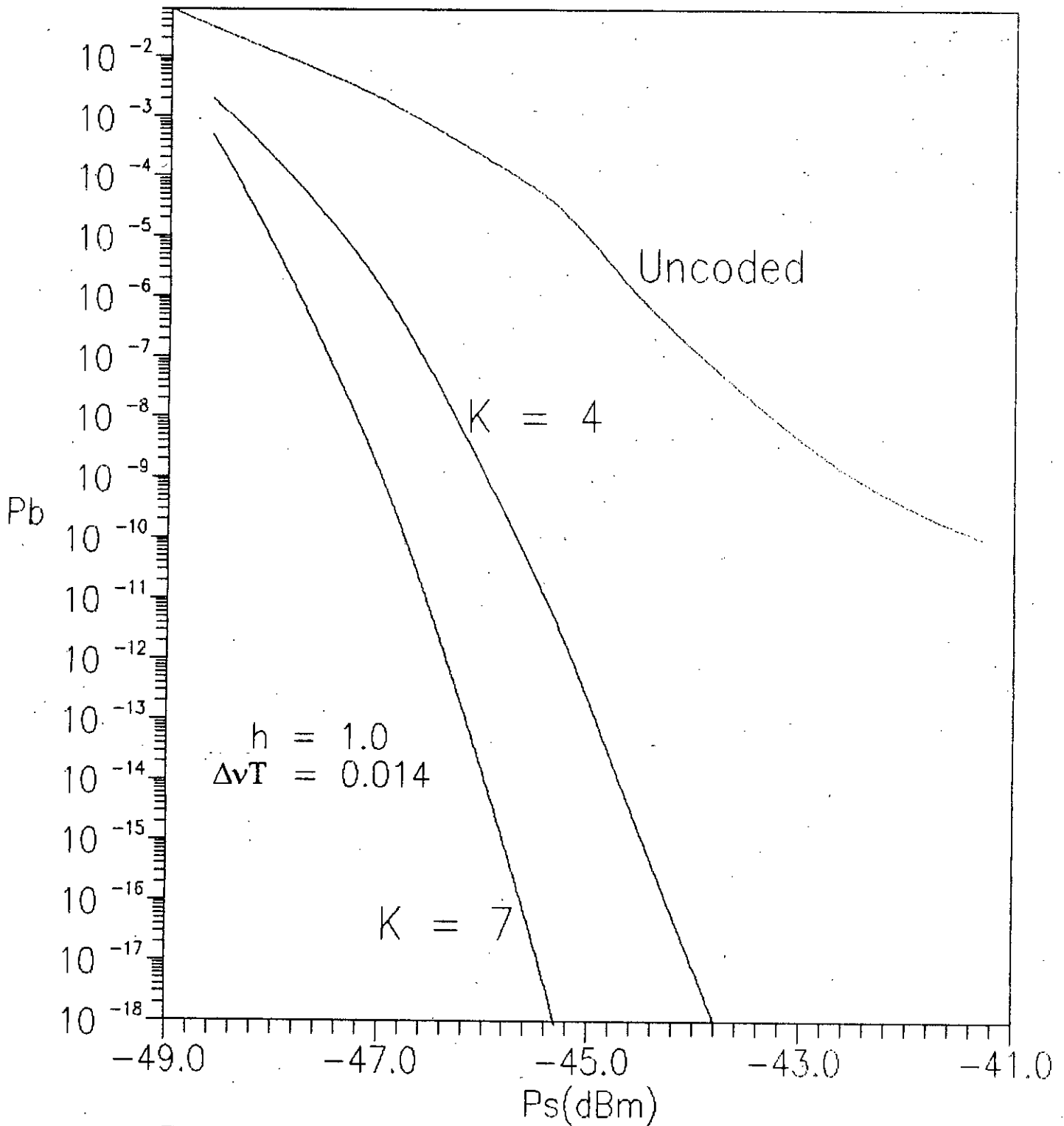


Fig. 3.2 Plots of bit error probability  $P_b$  vs transmitted signal power  $P_s(\text{dBm})$  for uncoded and rate 1/2 convolutionally coded (K = 4, 7) optically preamplified FSK ( $G = 30\text{dB}$ ) with modulation index  $h = 1.0$  and laser linewidth  $\Delta\nu T = 0.000$



**Fig. 3.2** Plots of bit error probability  $P_b$  vs transmitted signal power  $P_s(\text{dBm})$  for uncoded and rate 1/2 convolutionally coded ( $K = 4, 7$ ) optically preamplified FSK ( $G = 30\text{dB}$ ) with modulation index  $h = 1.0$  and laser linewidth  $\Delta\nu T = 0.000$



**Fig. 3.4** Plots of bit error probability  $P_b$  vs transmitted signal power  $P_s$ (dB<sub>m</sub>) for uncoded and rate 1/2 convolutionally coded ( $K = 4, 7$ ) optically preamplified FSK ( $G = 30$ dB) with modulation index  $h = 1.0$  and laser linewidth  $\Delta\nu T = 0.014$

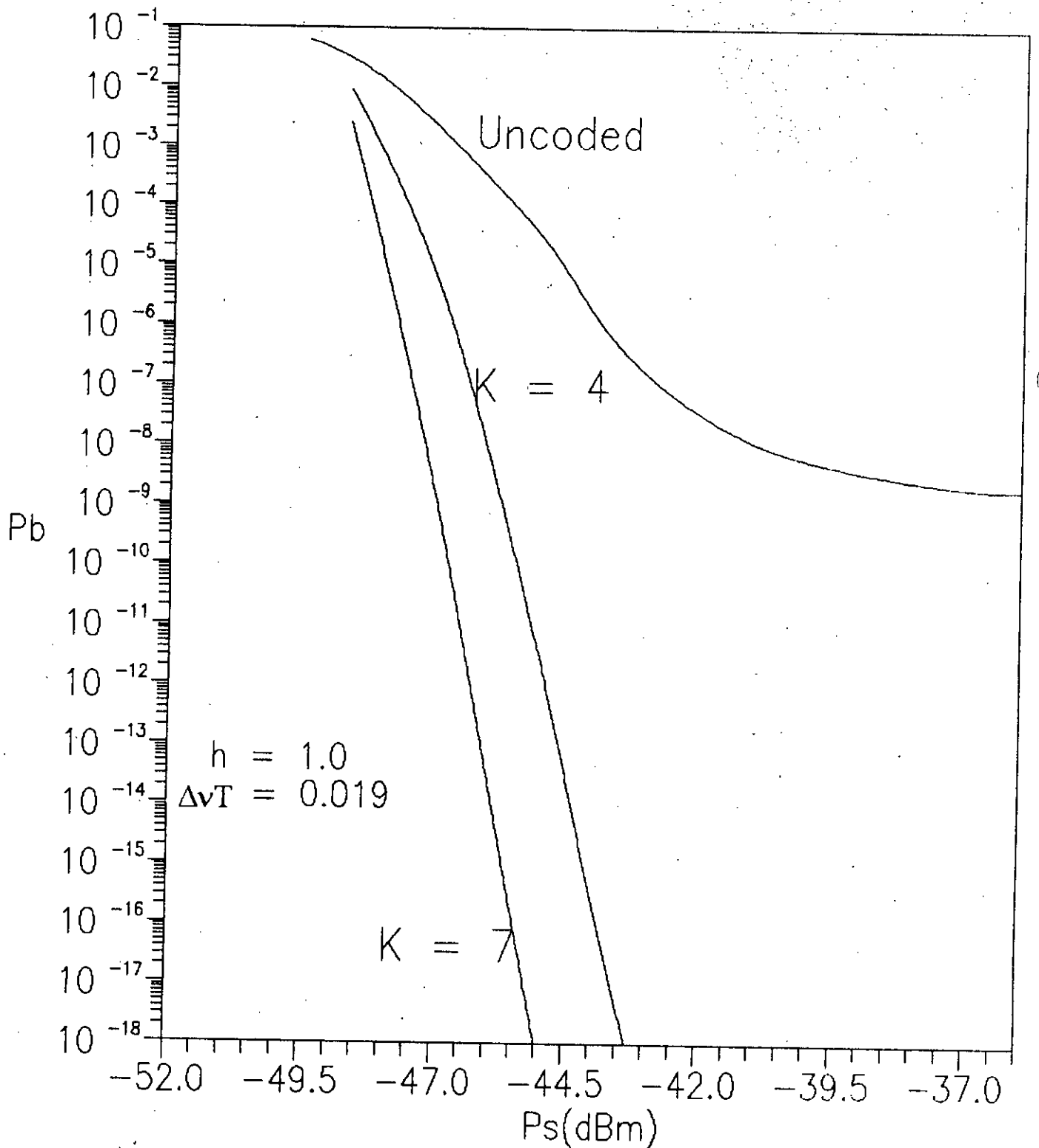
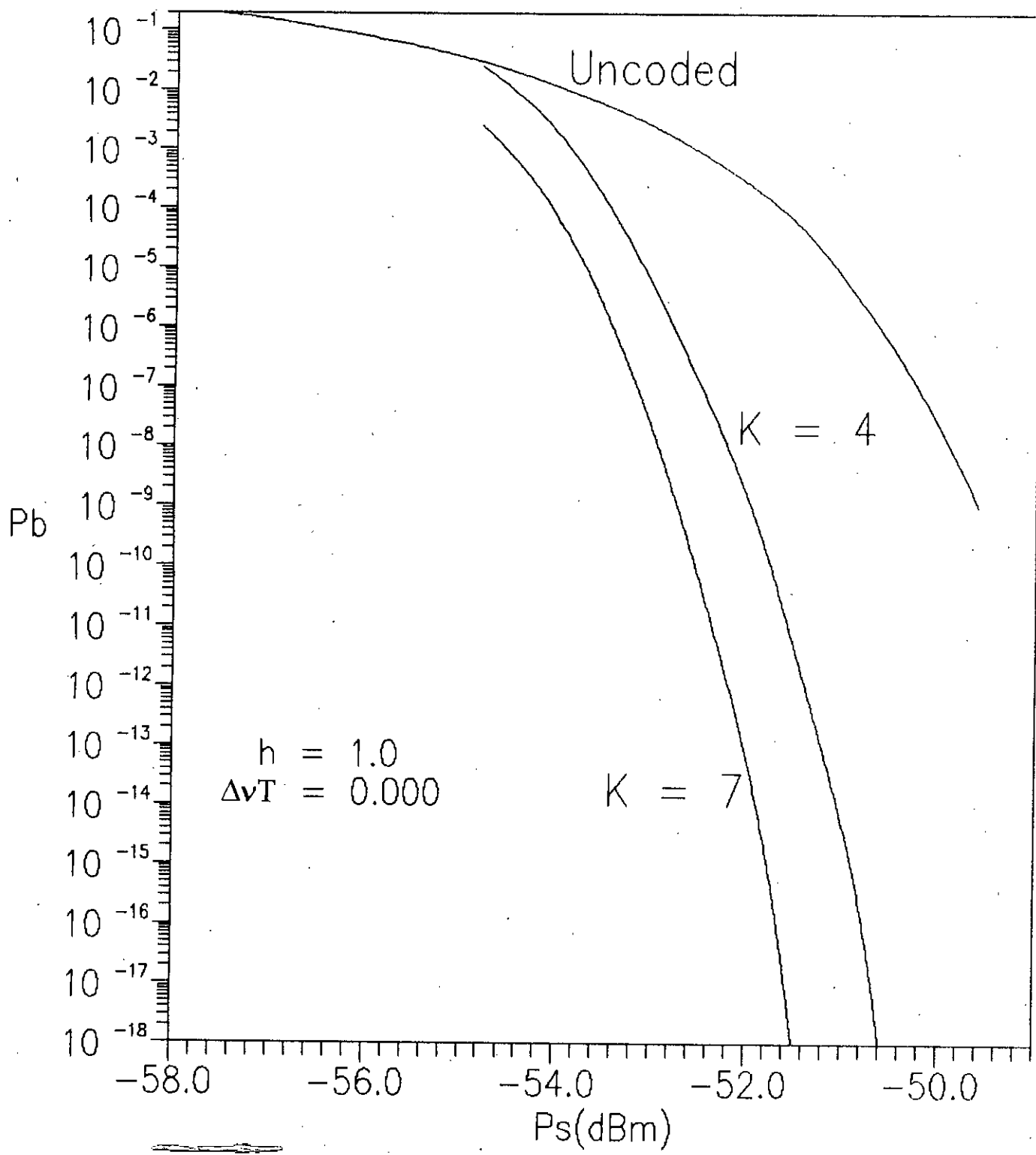
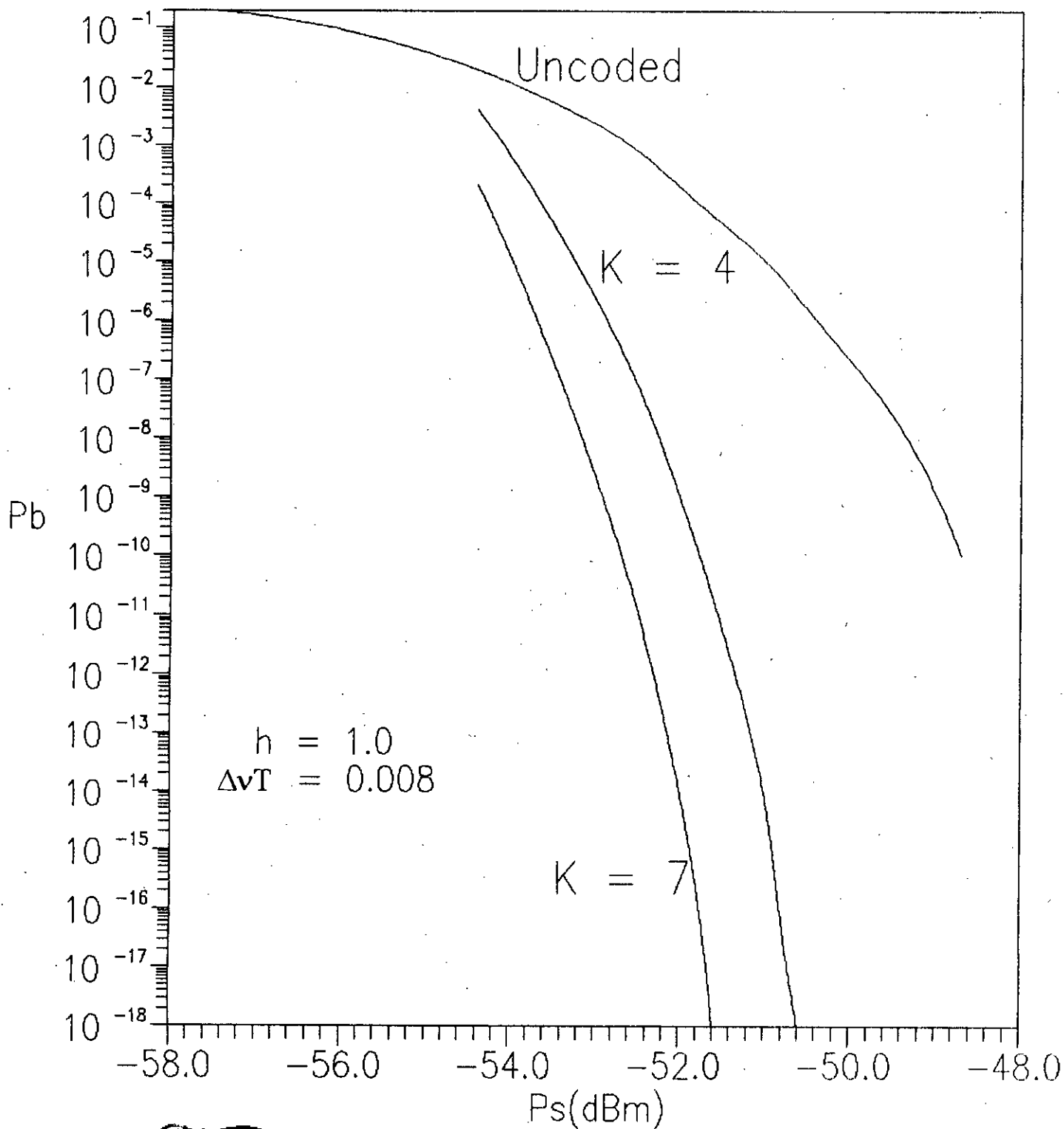


Fig. 3.5 Plots of bit error probability  $P_b$  vs transmitted signal power  $P_s$ (dB<sub>m</sub>) for uncoded and rate 1/2 convolutionally coded ( $K = 4, 7$ ) optically preamplified FSK ( $G = 30$ dB) with modulation index  $h = 1.0$  and laser linewidth  $\Delta\nu T = 0.019$



**Fig. 3.6** Plots of bit error probability  $P_b$  vs transmitted signal power  $P_s(\text{dB}_m)$  for uncoded and rate 1/2 convolutionally coded ( $K = 4, 7$ ) optically preamplified FSK ( $G = 40\text{dB}$ ) with modulation index  $h = 1.0$  and laser linewidth  $\Delta\nu T = 0.000$



**Fig. 3.7** Plots of bit error probability  $P_b$  vs transmitted signal power  $P_s$ (dB<sub>m</sub>) for uncoded and rate 1/2 convolutionally coded ( $K = 4, 7$ ) optically preamplified FSK ( $G = 40$ dB) with modulation index  $h = 1.0$  and laser linewidth  $\Delta\nu T = 0.008$



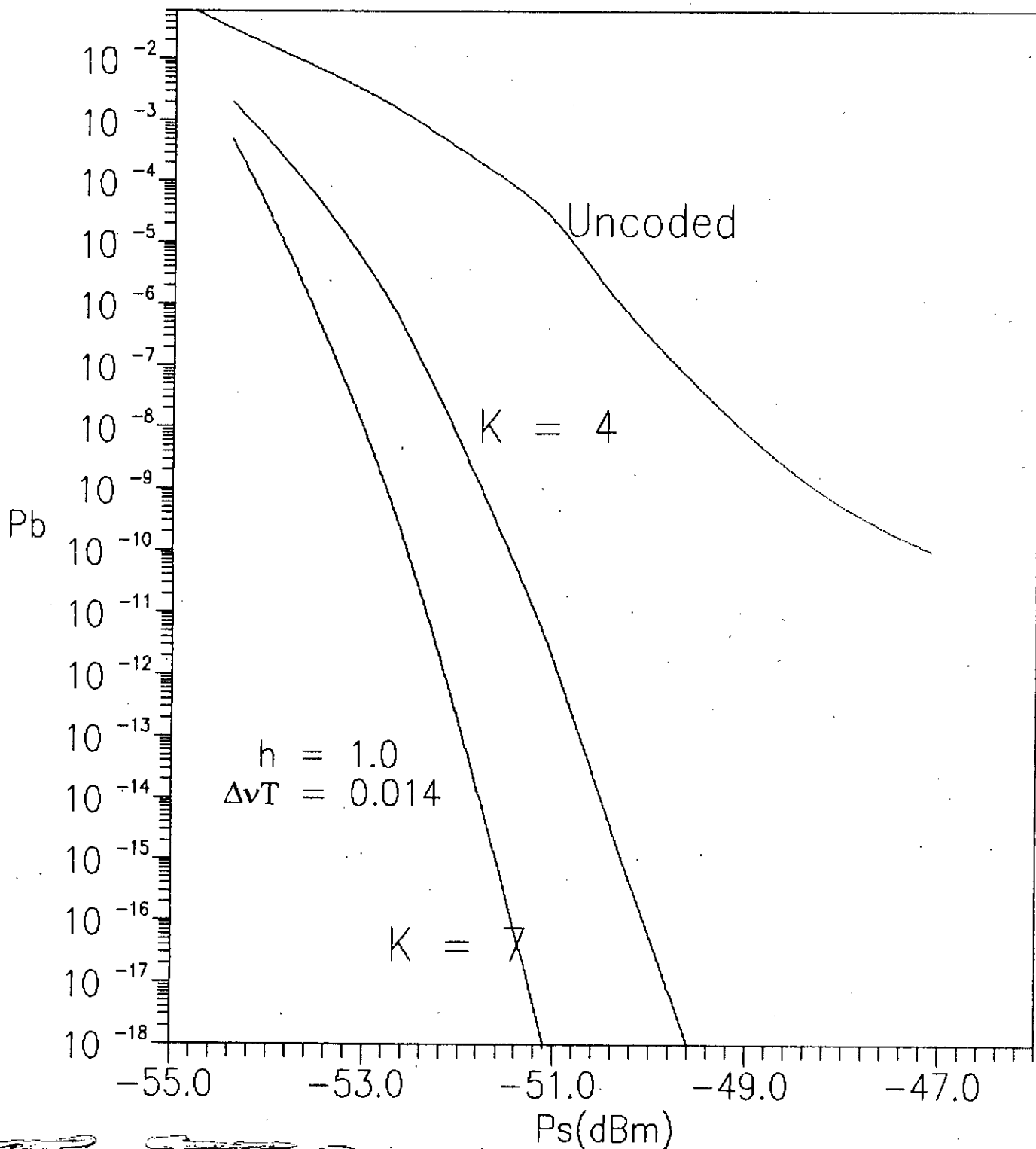


Fig. 3.8 Plots of bit error probability  $P_b$  vs transmitted signal power  $P_s$ (dB<sub>m</sub>) for uncoded and rate 1/2 convolutionally coded ( $K = 4, 7$ ) optically preamplified FSK ( $G = 40$ dB) with modulation index  $h = 1.0$  and laser linewidth  $\Delta\nu T = 0.014$

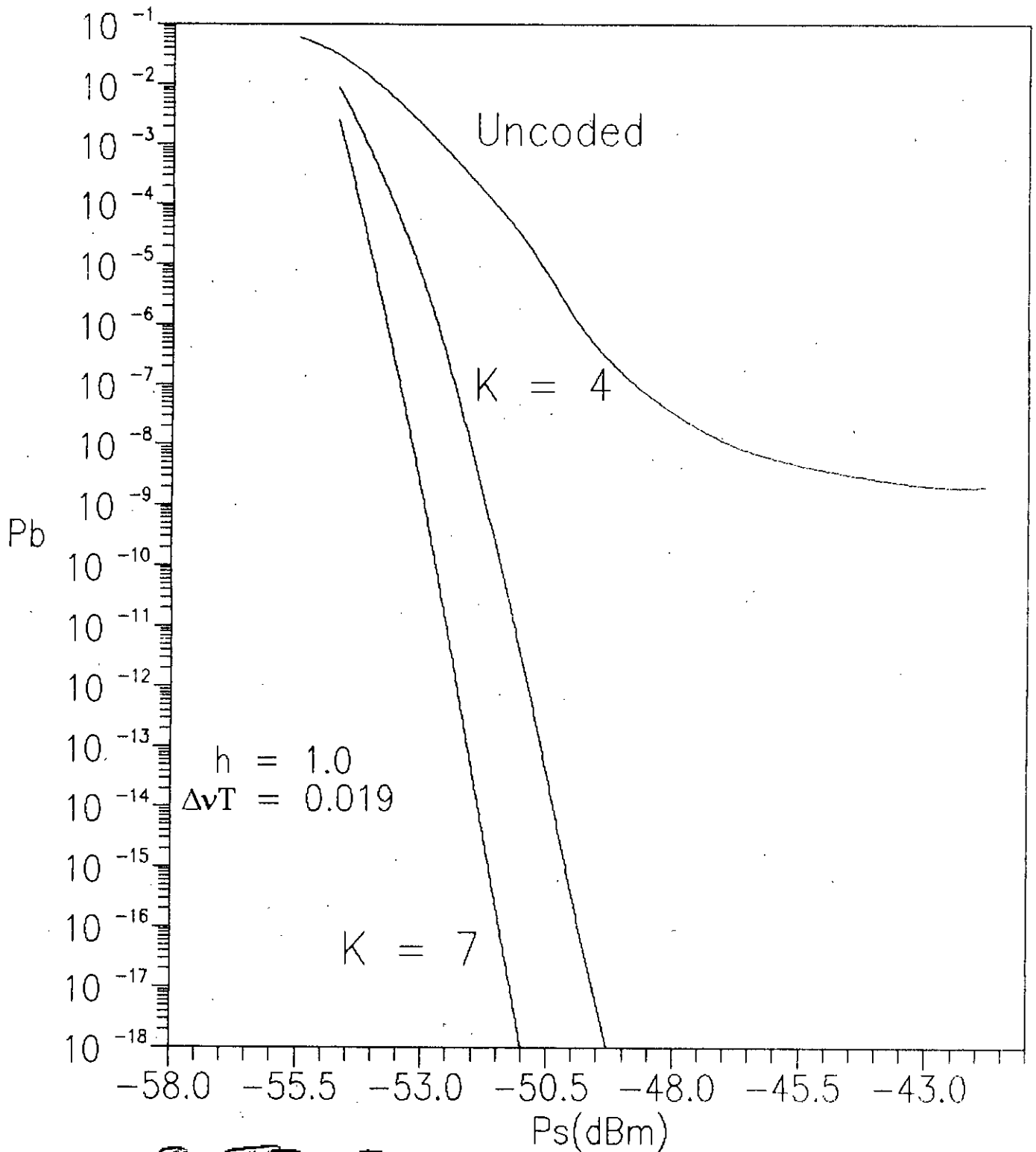
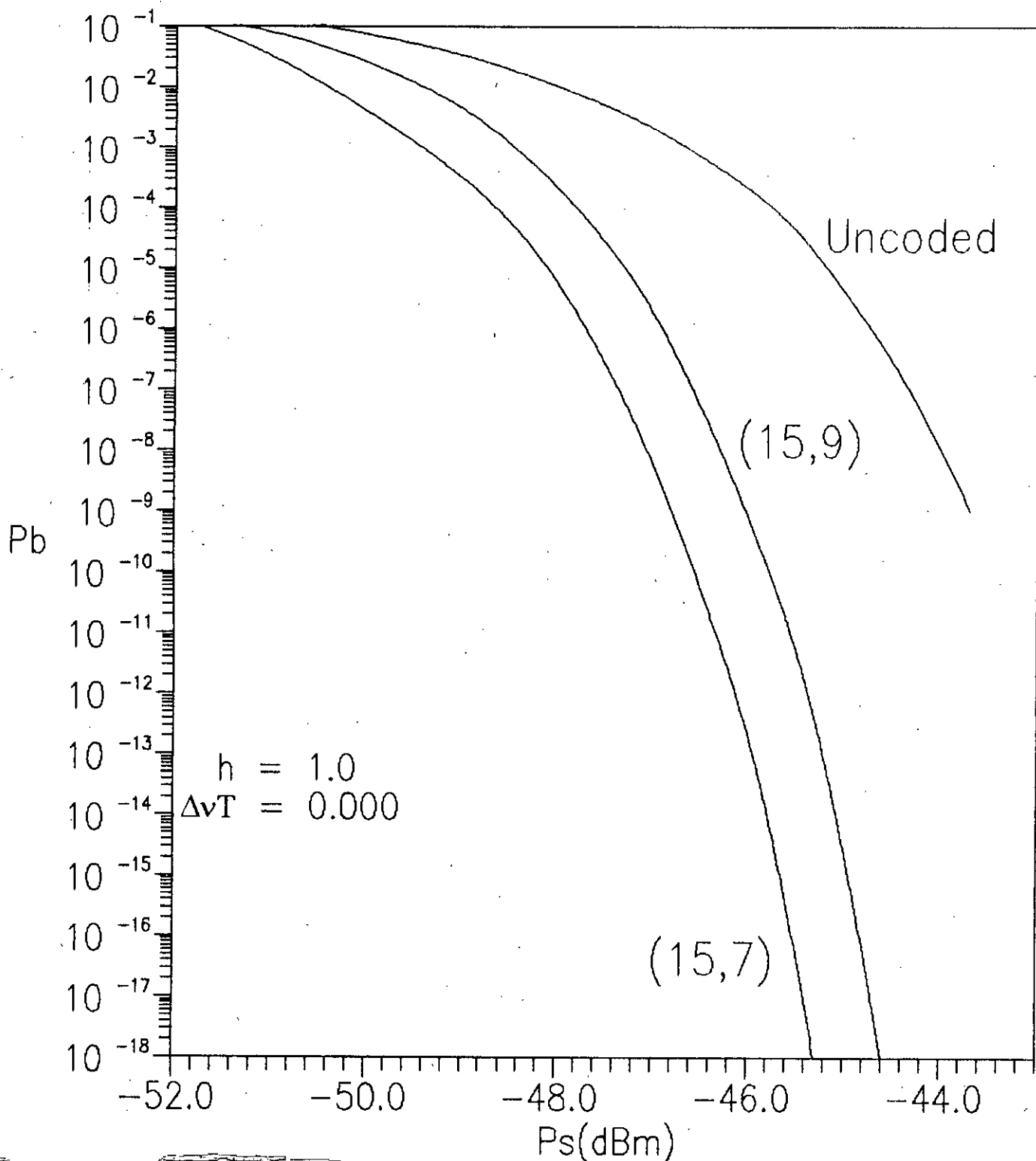
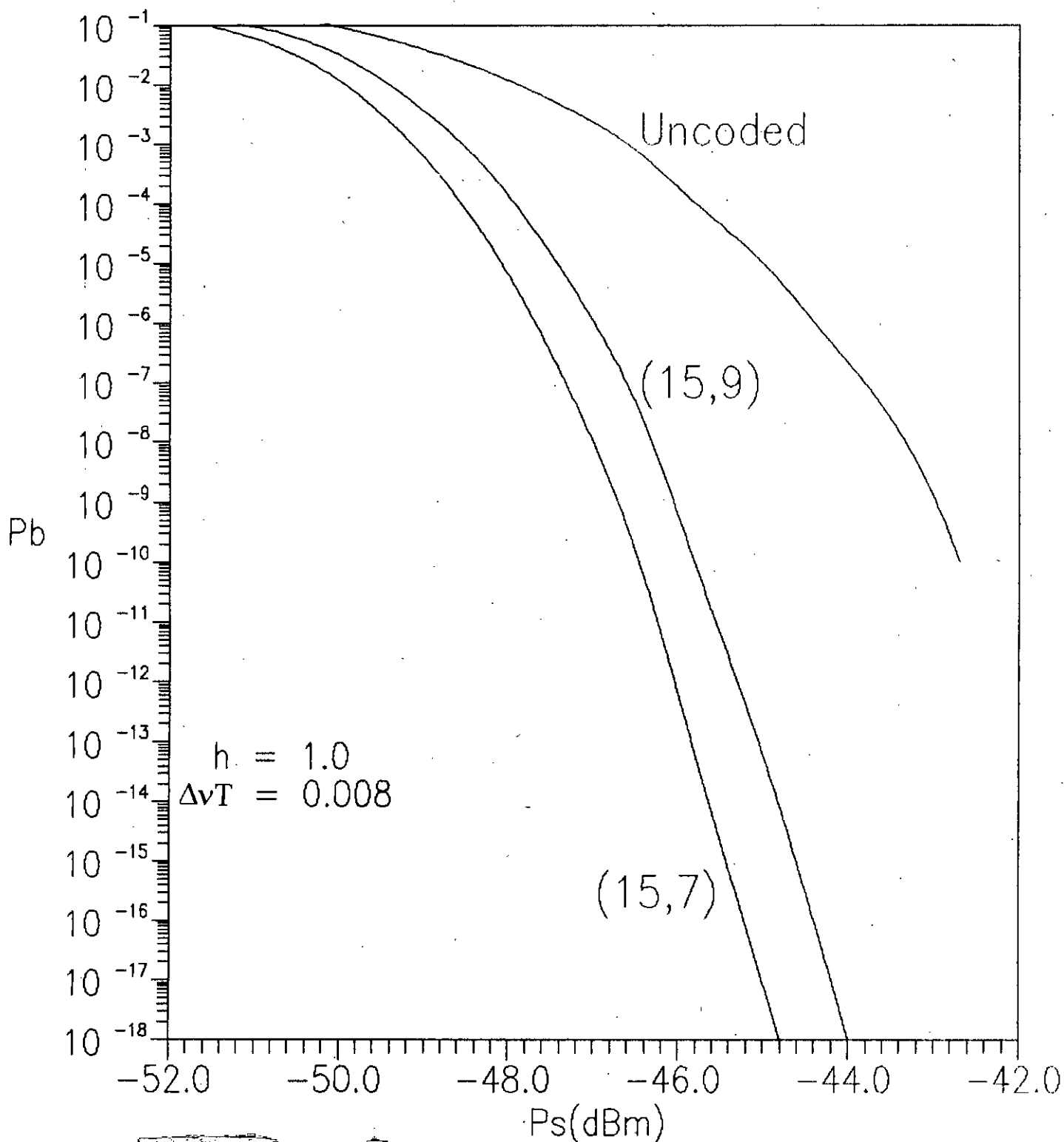


Fig. 3.9 Plots of bit error probability  $P_b$  vs transmitted signal power  $P_s$ (dB<sub>m</sub>) for uncoded and rate 1/2 convolutionally coded ( $K = 4, 7$ ) optically preamplified FSK ( $G = 40$ dB) with modulation index  $h = 1.0$  and laser linewidth  $\Delta\nu T = 0.019$



**Fig. 3.10** Plots of bit error probability  $P_b$  vs transmitted signal power  $P_s(\text{dBm})$  for uncoded and Reed-Solomon's coded optically preamplified FSK ( $G = 30\text{dB}$ ) with modulation index  $h = 1.0$  and laser linewidth  $\Delta\nu T = 0.000$



**Fig. 3.11** Plots of bit error probability  $P_b$  vs transmitted signal power  $P_s(\text{dB}_m)$  for uncoded and Reed-Solomon's coded optically preamplified FSK ( $G = 30\text{dB}$ ) with modulation index  $h = 1.0$  and laser linewidth  $\Delta\nu T = 0.008$

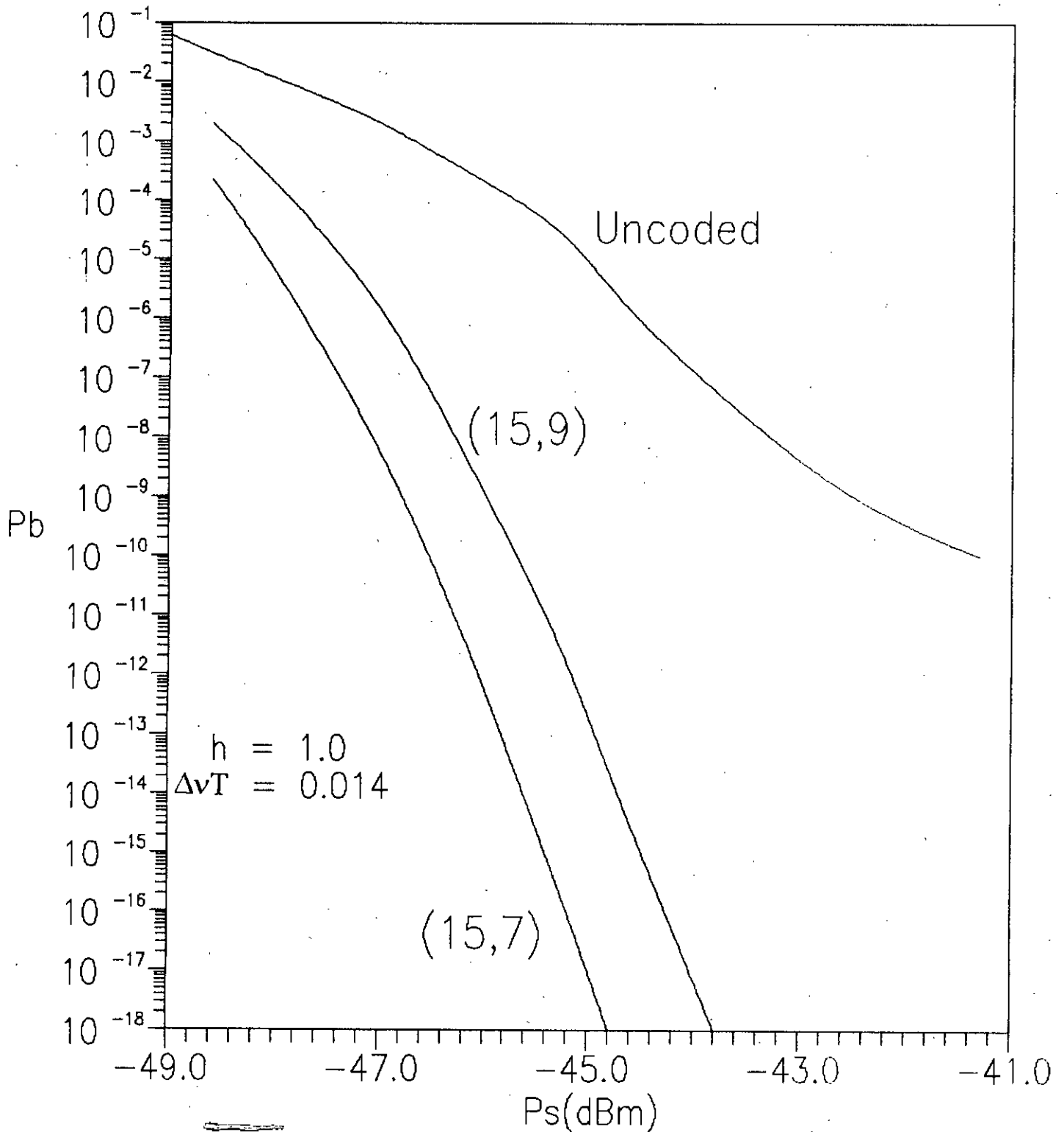
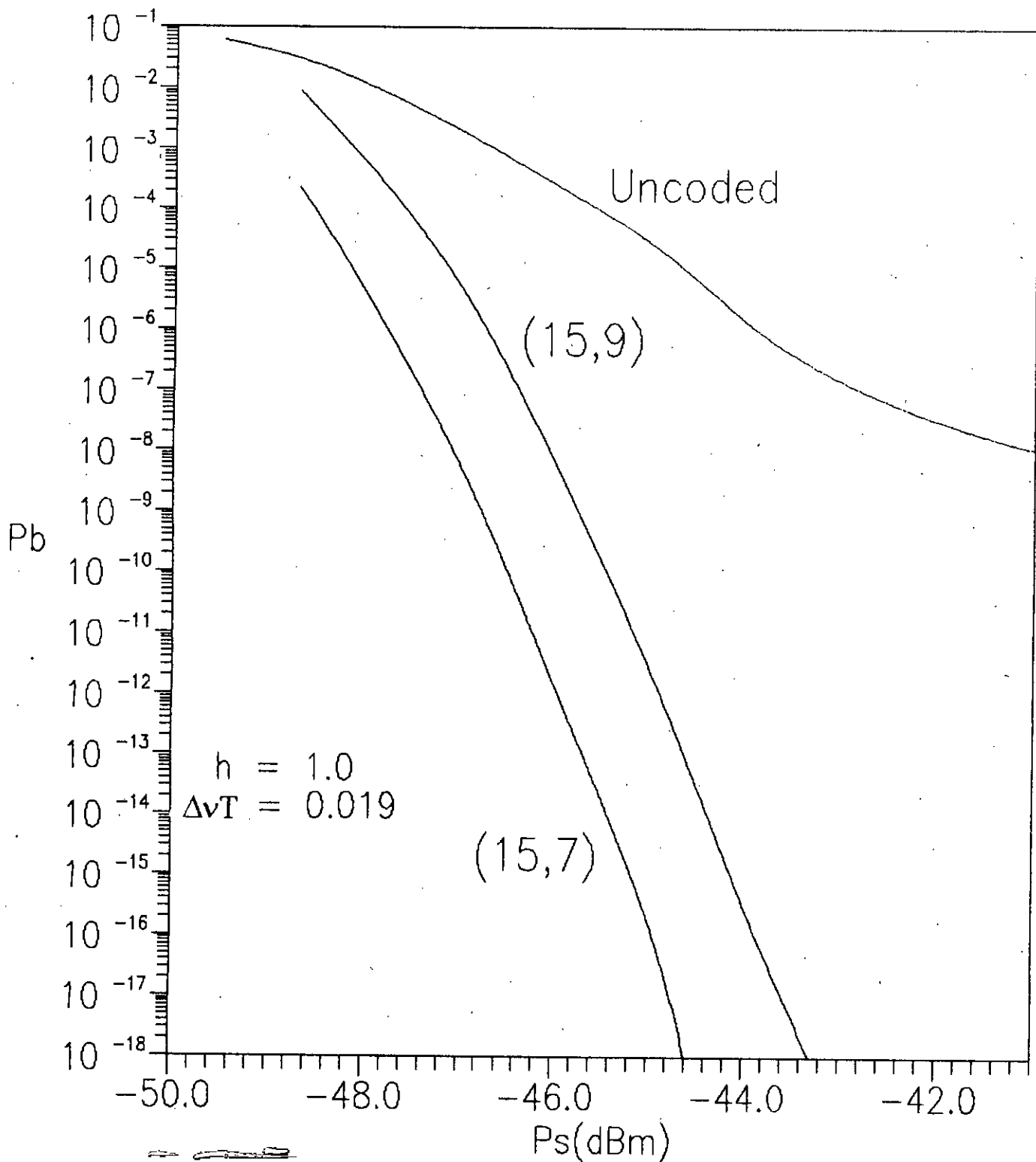
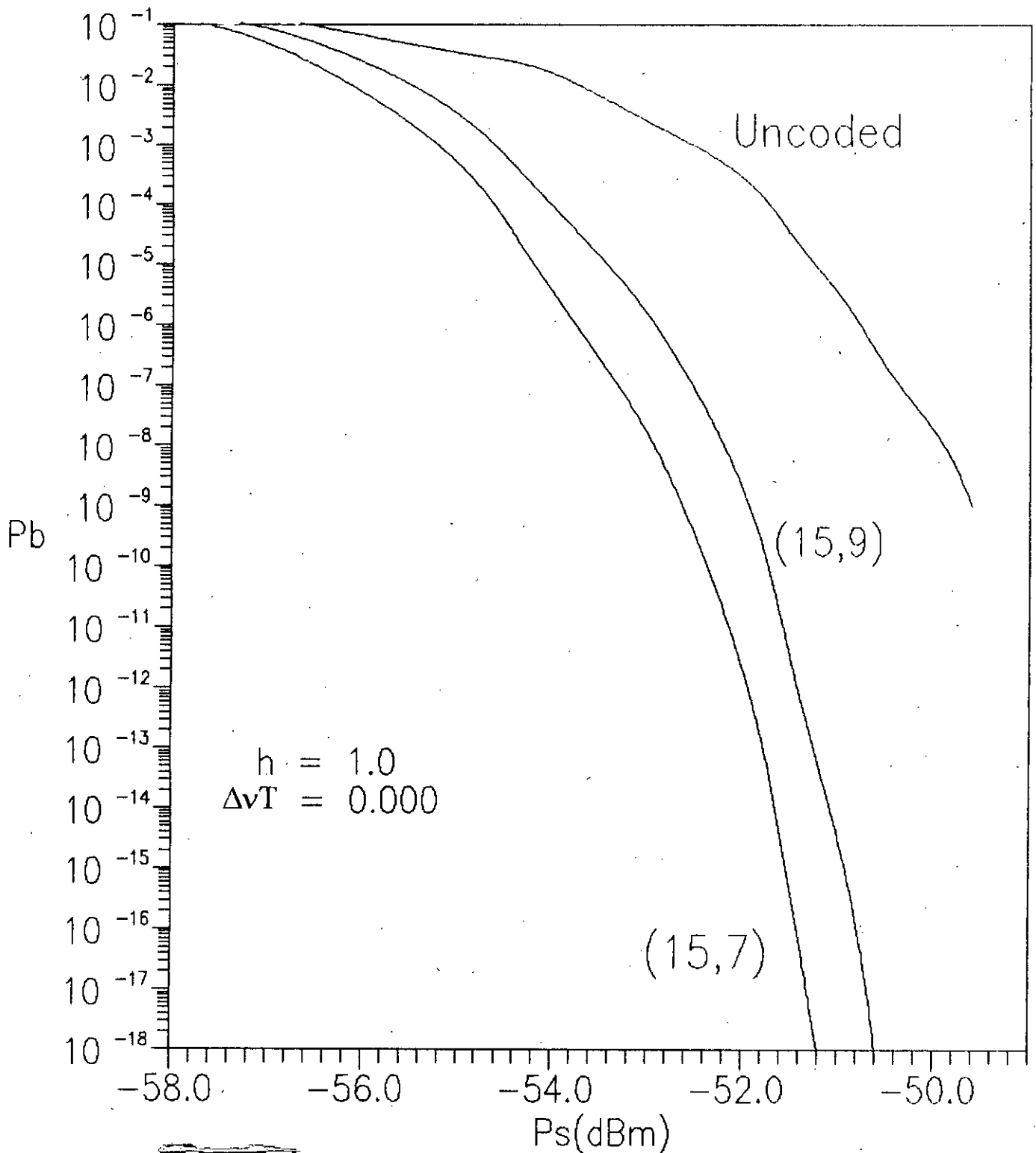


Fig. 3.12 Plots of bit error probability  $P_b$  vs transmitted signal power  $P_s(\text{dB}_m)$  for uncoded and Reed-Solomon's coded optically preamplified FSK ( $G = 30\text{dB}$ ) with modulation index  $h = 1.0$  and laser linewidth  $\Delta\nu T = 0.014$



**Fig. 3.13** Plots of bit error probability  $P_b$  vs transmitted signal power  $P_s$ (dB<sub>m</sub>) for uncoded and Reed-Solomon's coded optically preamplified FSK ( $G = 30$ dB) with modulation index  $h = 1.0$  and laser linewidth  $\Delta\nu T = 0.019$



**Fig. 3.14** Plots of bit error probability  $P_b$  vs transmitted signal power  $P_s(\text{dB}_m)$  for uncoded and Reed-Solomon's coded optically preamplified FSK ( $G = 40\text{dB}$ ) with modulation index  $h = 1.0$  and laser linewidth  $\Delta\nu T = 0.000$

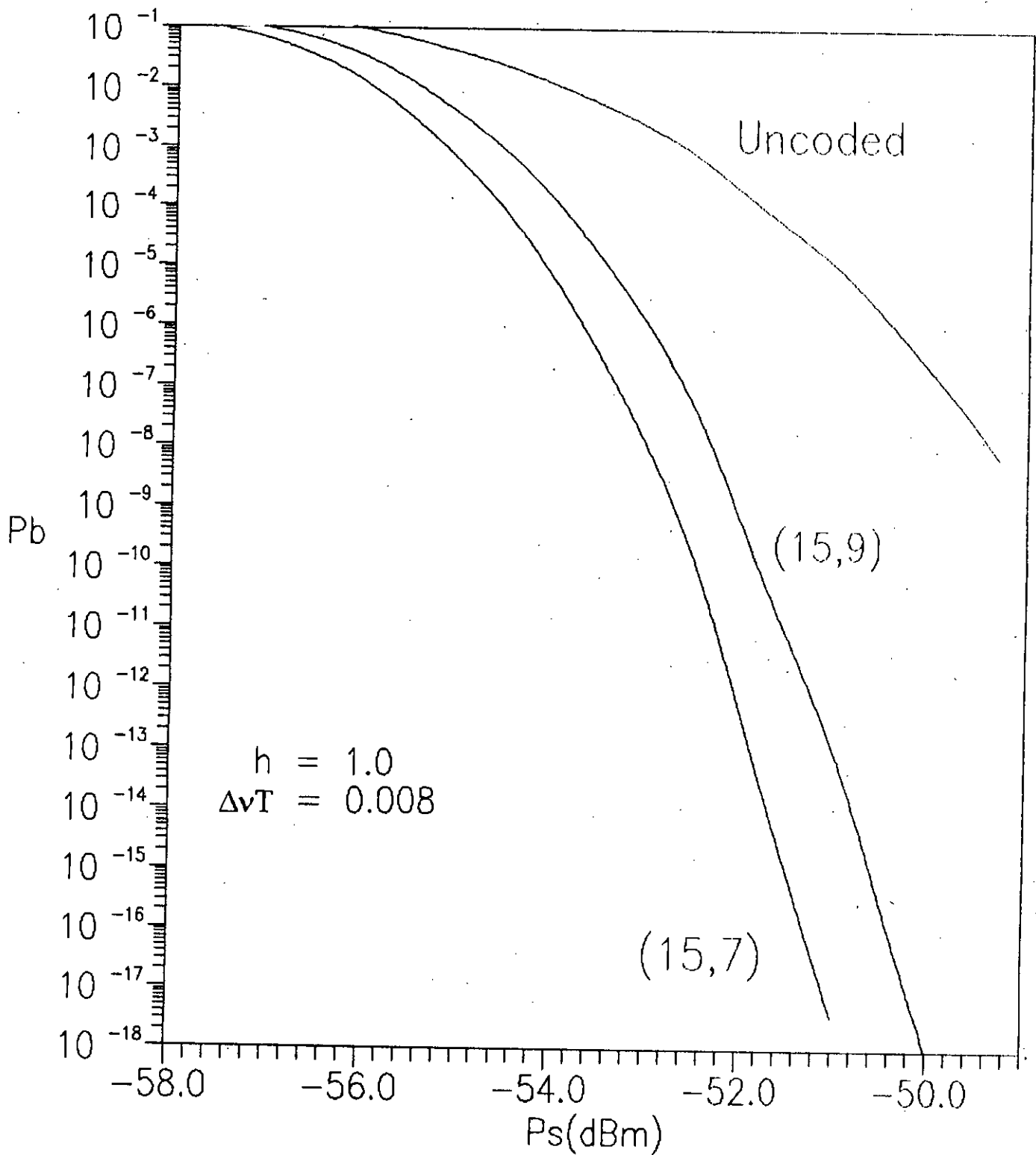


**Fig. 3.15** Plots of bit error probability  $P_b$  vs transmitted signal power  $P_s$ (dB<sub>m</sub>) for uncoded and Reed-Solomon's coded optically preamplified FSK ( $G = 40$ dB) with modulation index  $h = 1.0$  and laser linewidth  $\Delta\nu T = 0.008$



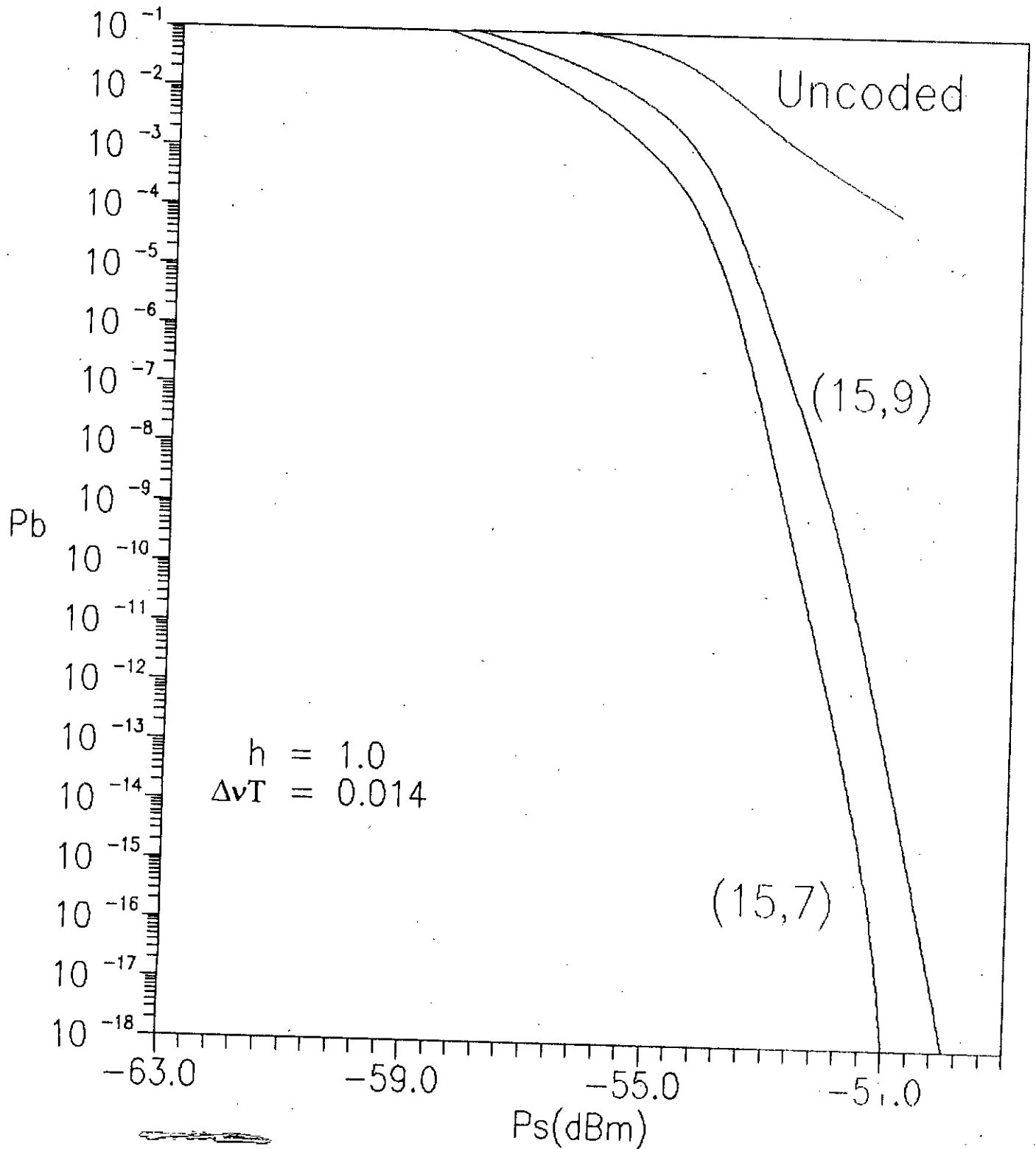


**Fig. 3.16** Plots of bit error probability  $P_b$  vs transmitted signal power  $P_s$ (dB<sub>m</sub>) for uncoded and Reed-Solomon's coded optically preamplified FSK ( $G = 40$ dB) with modulation index  $h = 1.0$  and laser linewidth  $\Delta\nu T = 0.014$

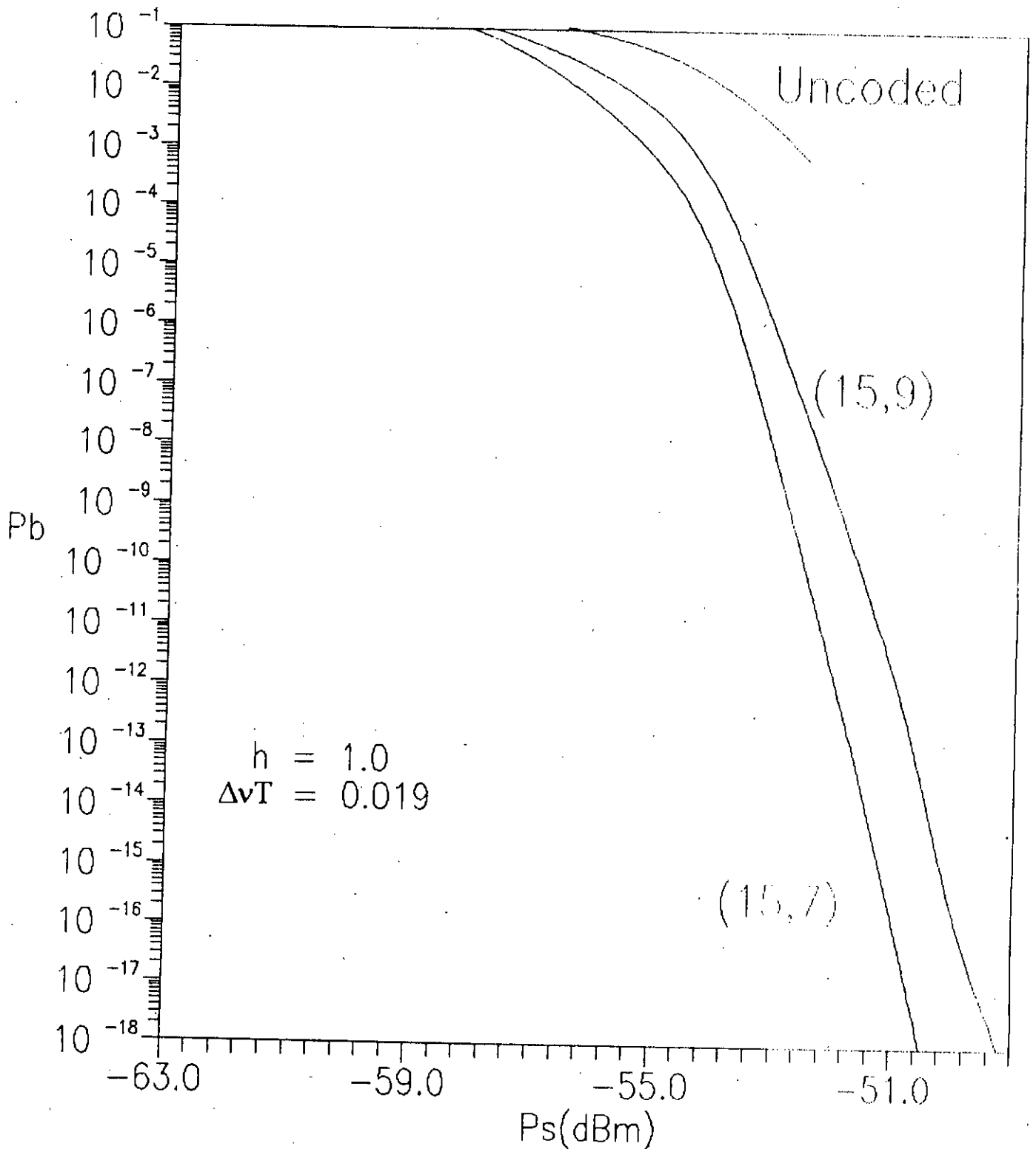


**Fig. 3.17** Plots of bit error probability  $P_b$  vs transmitted signal power  $P_s$ (dB<sub>m</sub>) for uncoded and Reed-Solomon's coded optically preamplified FSK ( $G = 40$ dB) with modulation index  $h = 1.0$  and laser linewidth  $\Delta\nu T = 0.019$

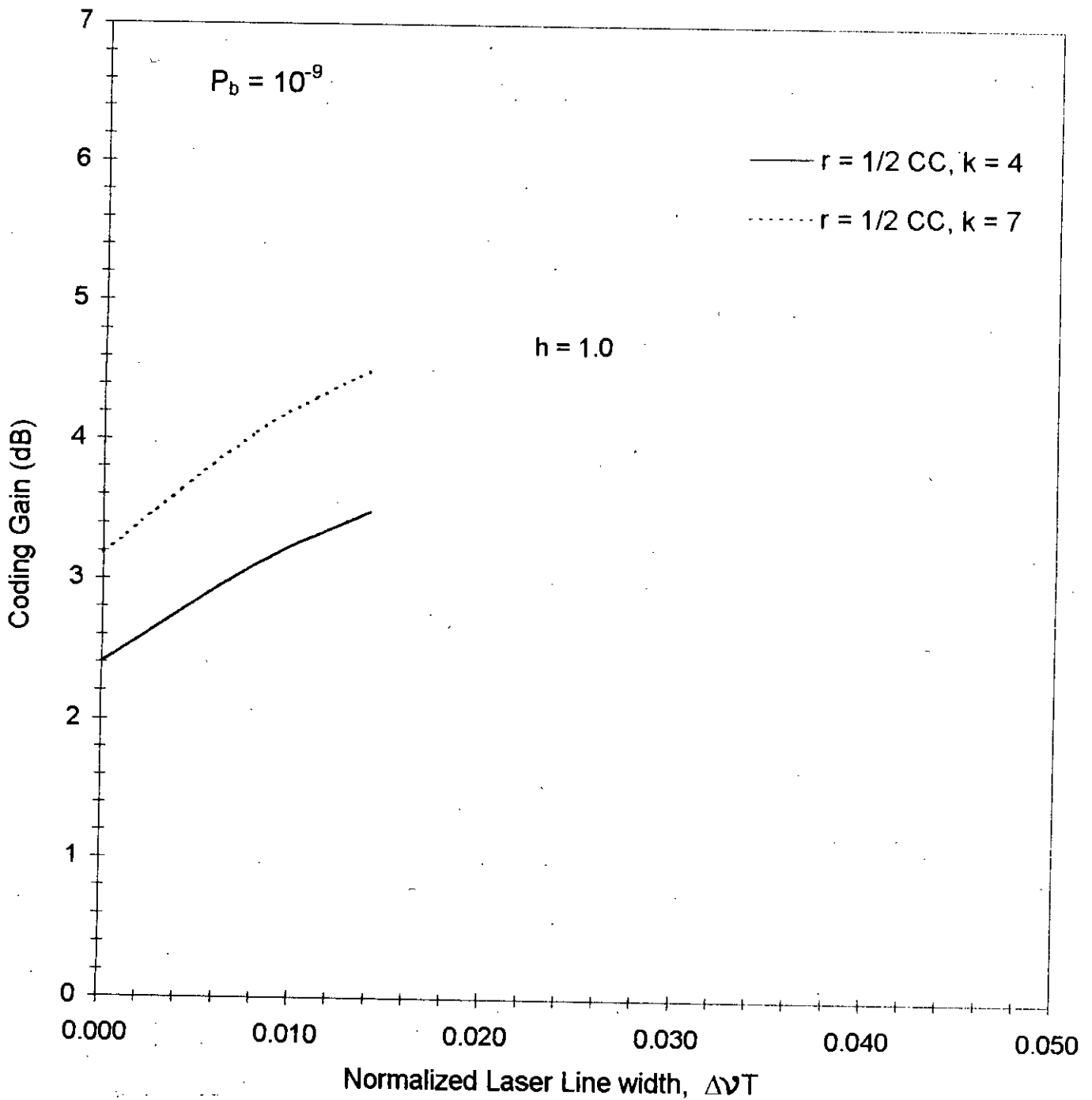


**Fig. 3.18** Plots of coding gain at bit error rate  $P_b = 10^{-9}$  vs normalized laser linewidth  $\Delta\nu T$  for rate 1/2 convolutionally coded optically preamplified FSK ( $G = 30\text{dB}$ ) with constraint length  $K = 4$  and  $K = 7$  for  $h = 1.0$

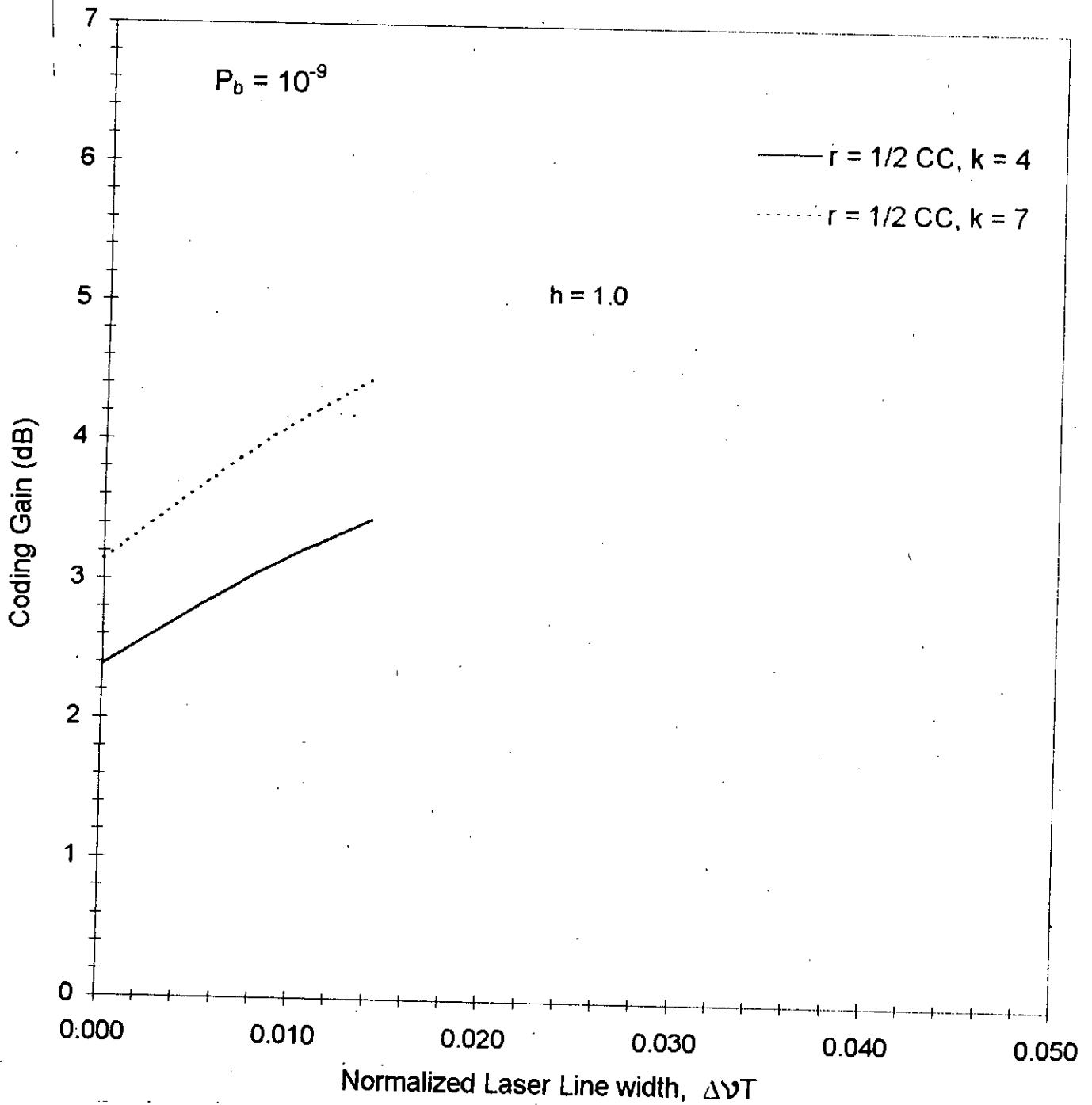


Fig. 3.19 Plots of coding gain at bit error rate  $P_b = 10^{-9}$  vs normalized laser linewidth  $\Delta\nu T$  for rate 1/2 convolutionally coded optically preamplified FSK ( $G = 40\text{dB}$ ) with constraint length  $K = 4$  and  $K = 7$  for  $h = 1.0$

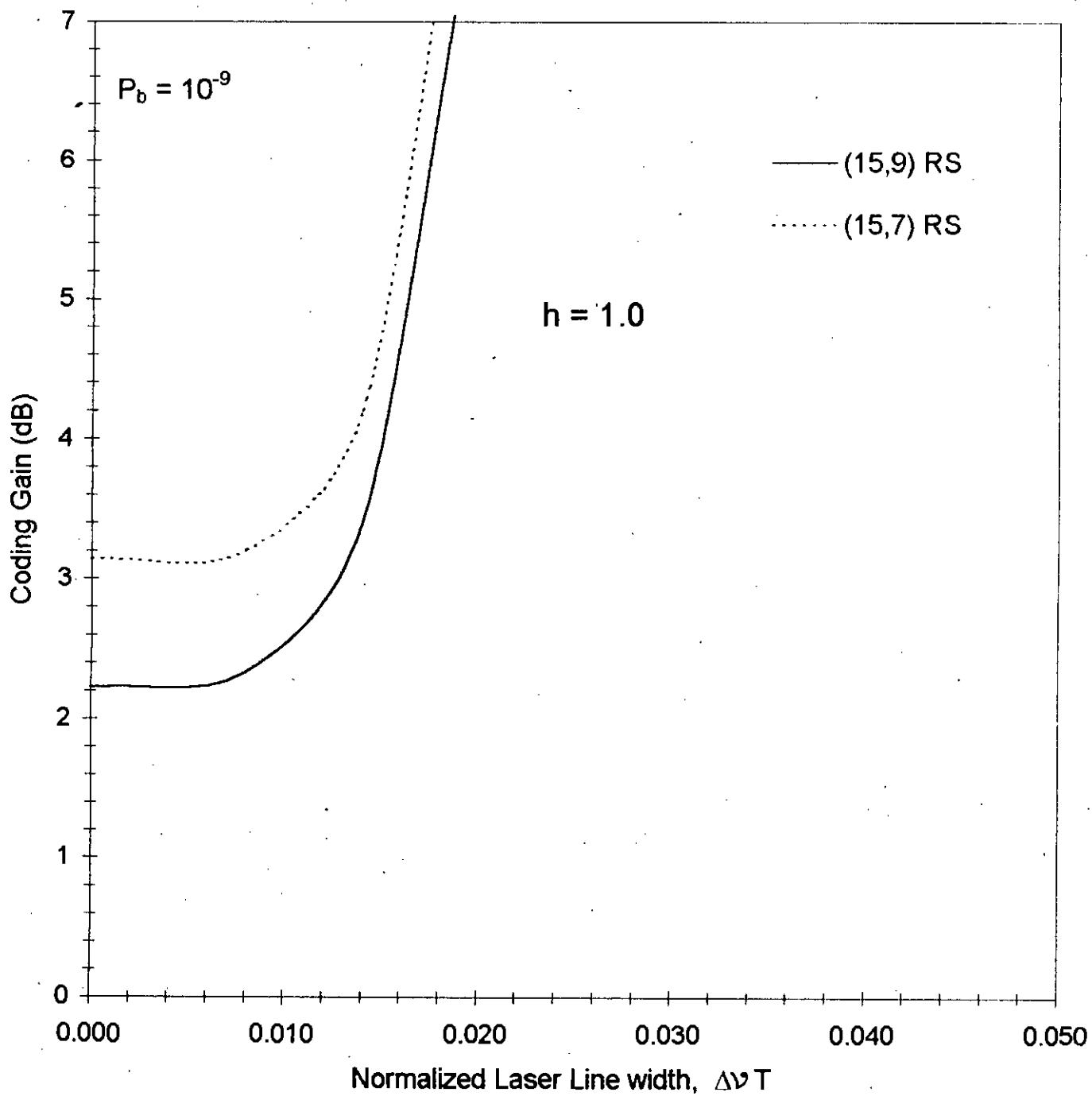


Fig. 3.20 Plots of coding gain at bit error rate  $P_b = 10^{-9}$  vs normalized laser linewidth  $\Delta\nu T$ , Reed-Solomon's (15,9) and (15,7) coded optically preamplified FSK ( $G = 30\text{dB}$ ) for  $h = 1.0$

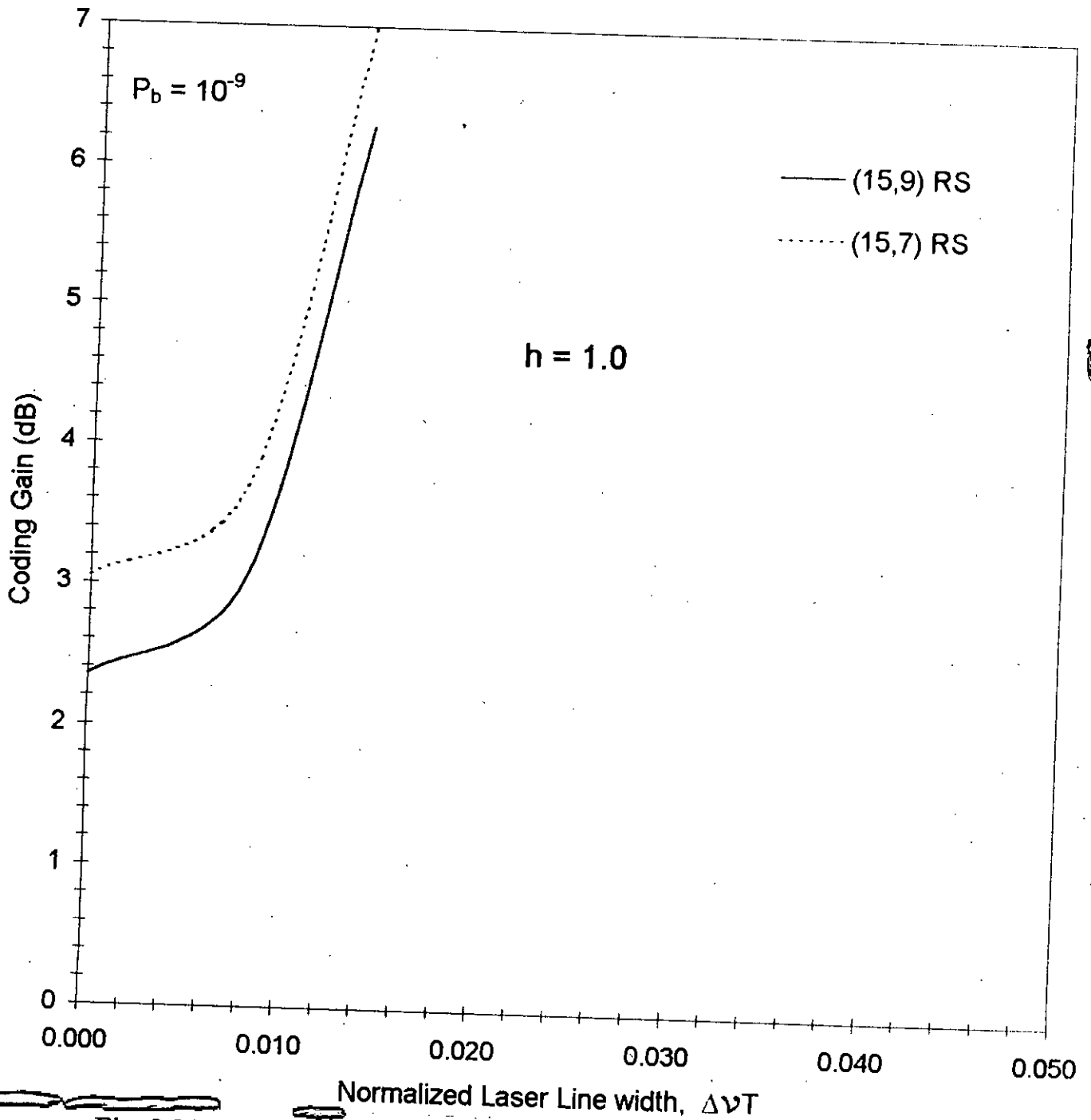


Fig. 3.21 Plots of coding gain at bit error rate  $P_b = 10^{-9}$  vs normalized laser linewidth  $\Delta\nu T$ , Reed-Solomon's (15,9) and (15,7) coded optically preamplified FSK ( $G = 40\text{dB}$ ) for  $h = 1.0$

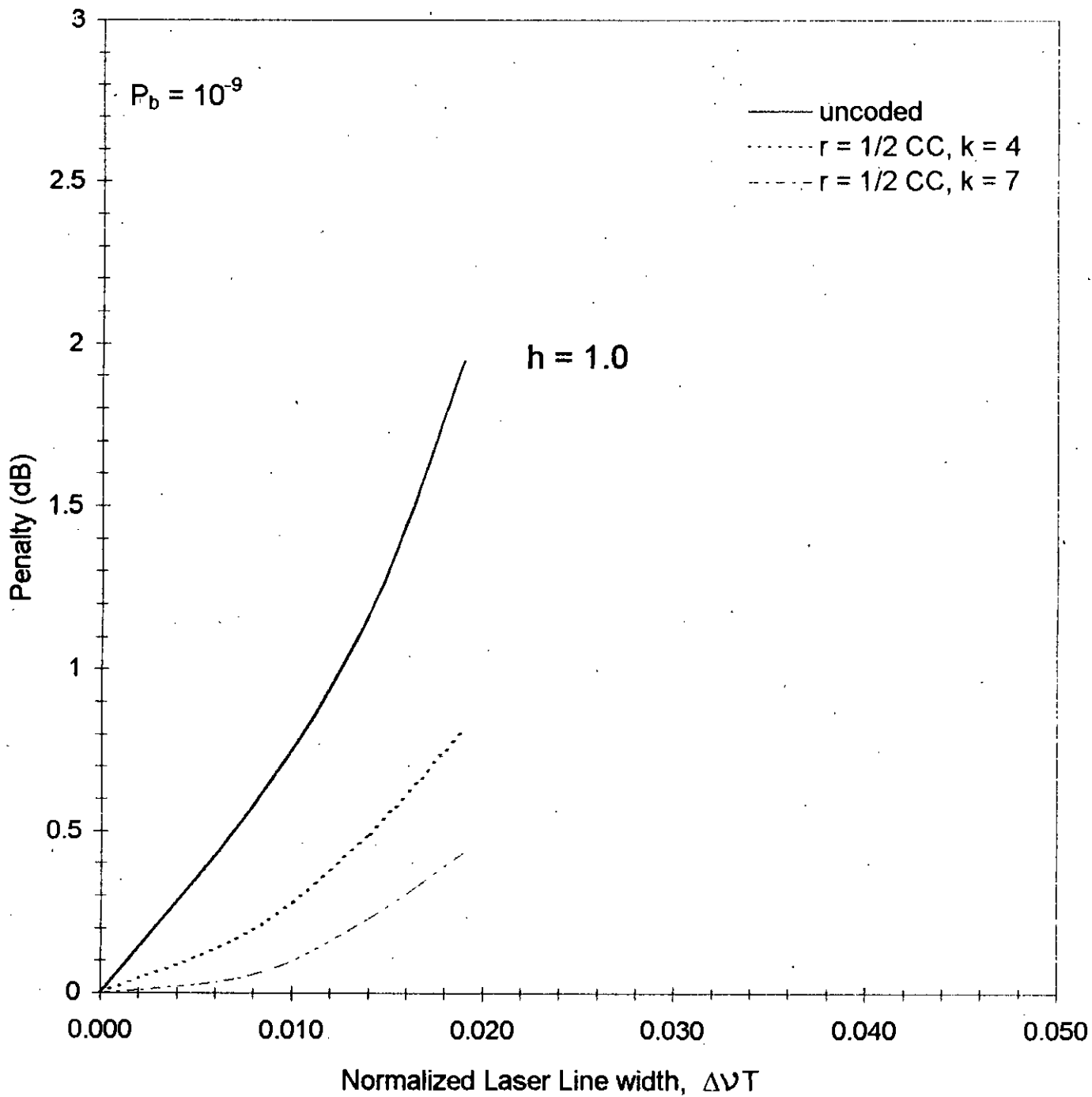


Fig. 3.22 Plots of power penalty due to phase noise at  $P_b = 10^{-9}$  for uncoded and rate 1/2 convolutionally coded optically preamplified FSK ( $G = 30\text{dB}$ ) as a function of normalized laser linewidth  $\Delta\nu T$  for modulation index  $h = 1.0$

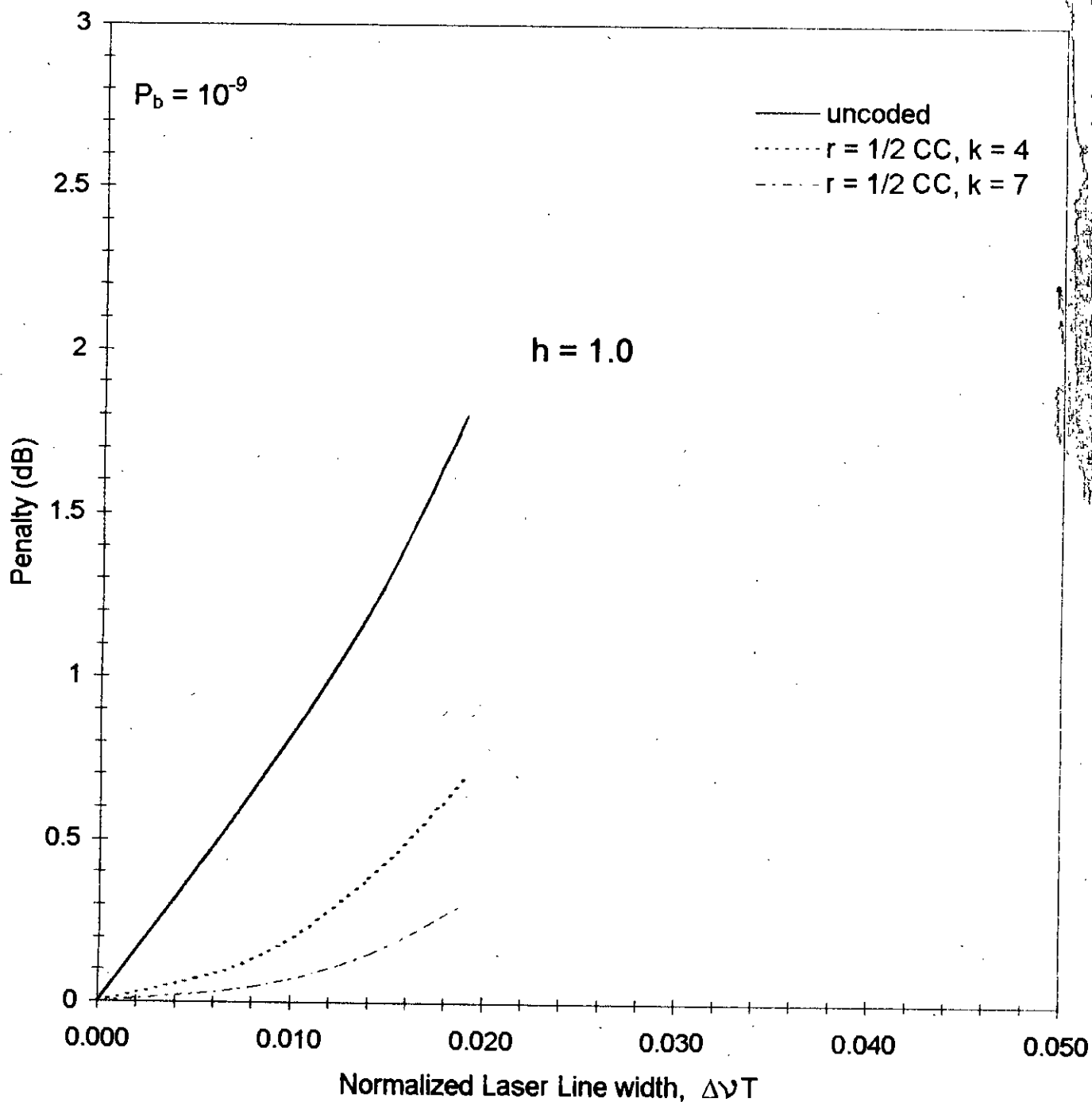


Fig. 3.23 Plots of power penalty due to phase noise at  $P_b = 10^{-9}$  for uncoded and rate 1/2 convolutionally coded optically preamplified FSK ( $G = 40\text{dB}$ ) as a function of normalized laser linewidth  $\Delta\nu T$  for modulation index  $h = 1.0$



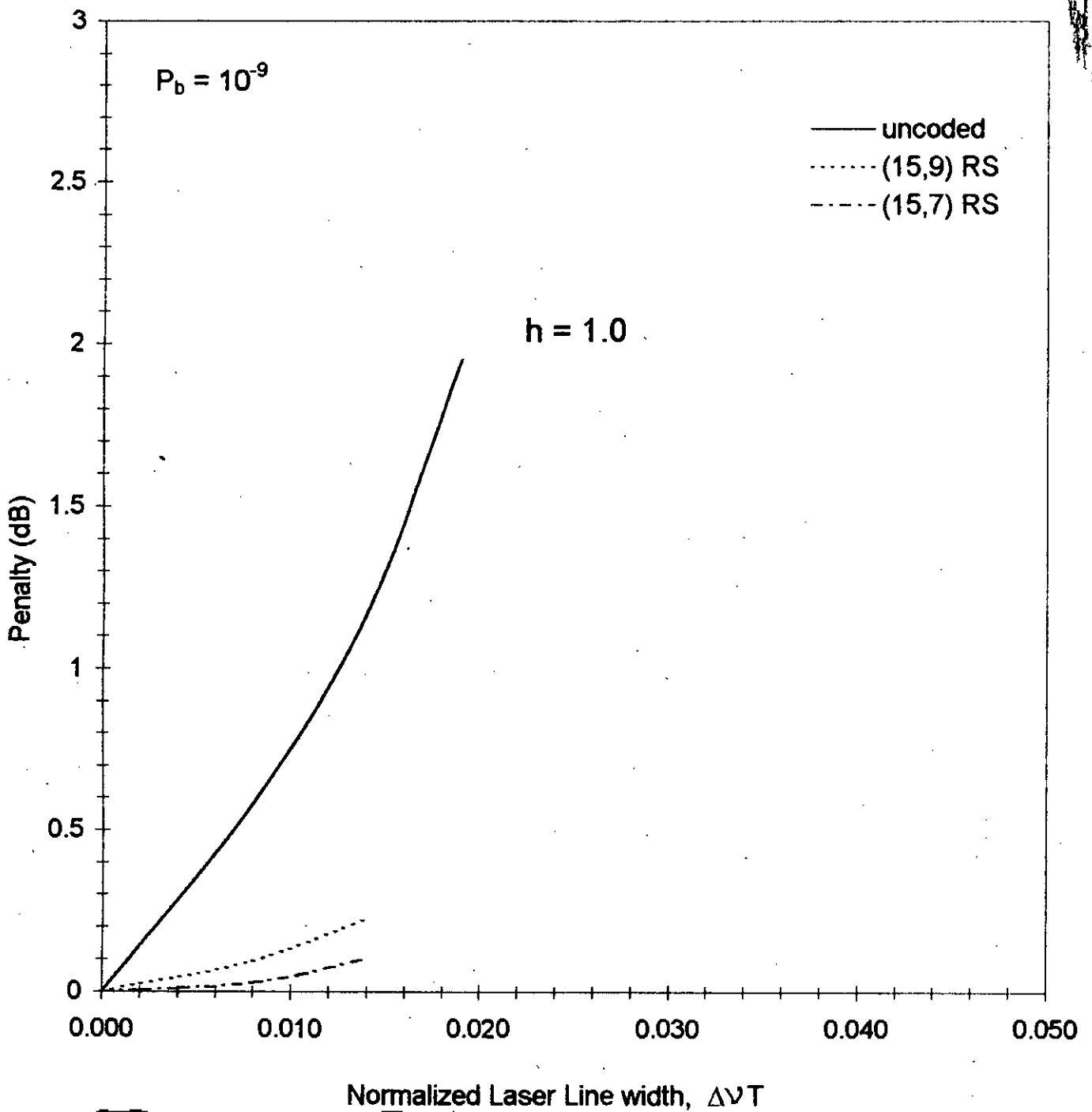
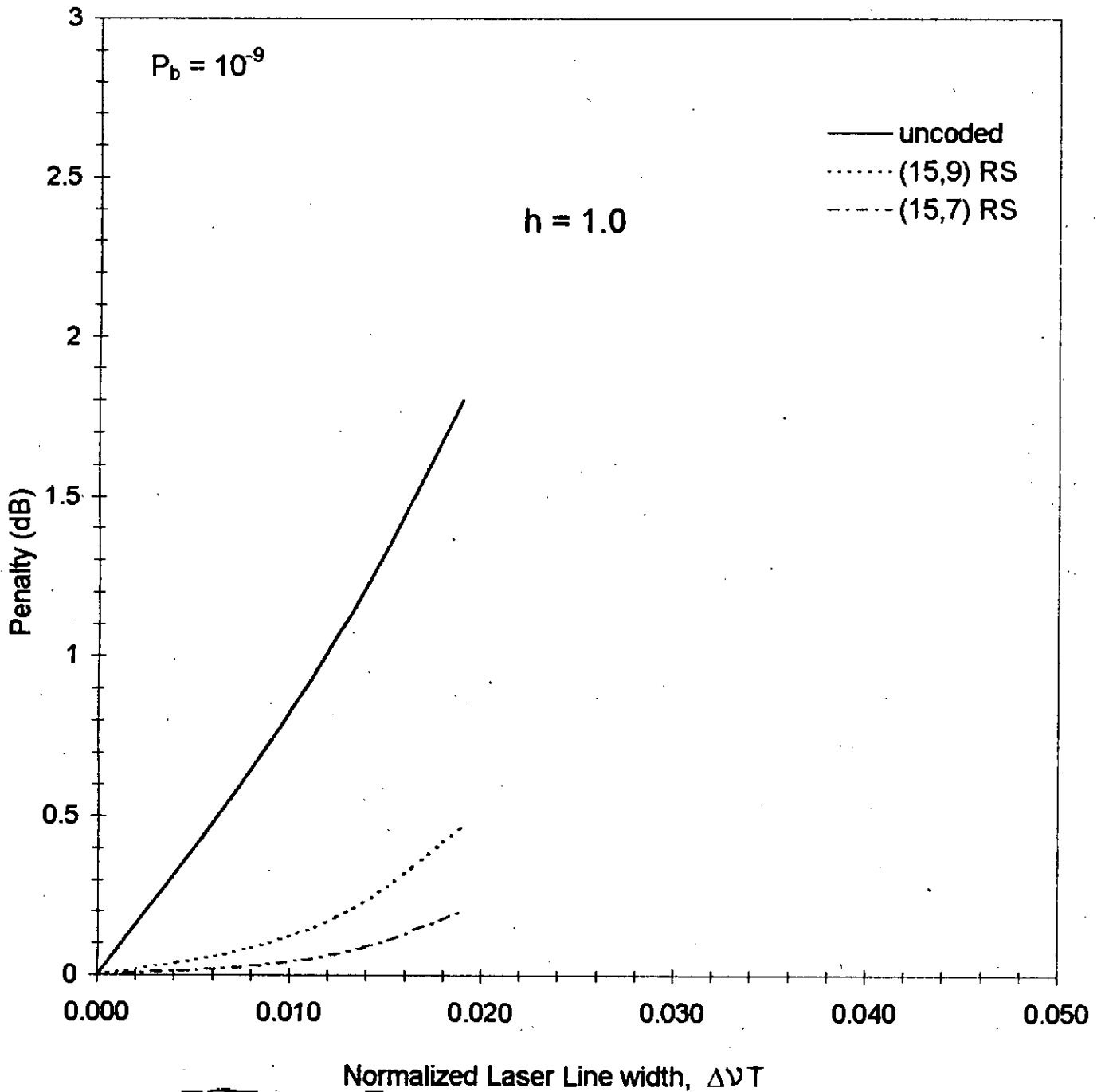


Fig. 3.24 Plots of power penalty due to phase noise at  $P_b = 10^{-9}$  for uncoded and Reed-Solomon's coded optically preamplified FSK ( $G = 30\text{dB}$ ) as a function of normalized laser linewidth  $\Delta\nu T$  for modulation index  $h = 1.0$



**Fig. 3.25** Plots of power penalty due to phase noise at  $P_b = 10^{-9}$  for uncoded and Reed-Solomon's coded optically preamplified FSK ( $G = 40\text{dB}$ ) as a function of normalized laser linewidth  $\Delta\nu T$  for modulation index  $h = 1.0$

### 3.7 Conclusions and suggestions for future work :

A theoretical analysis is presented to evaluate the performance of optical direct detection FSK system with and without forward error correction coding. A Mach-Zehnder Interferometer (MZI) is used in the receiver to act as an optical frequency discriminator (OFD). Two FEC coding techniques, viz. CC and RS coding are employed to investigate the efficacy of forward error correction coding in reducing the effect of laser phase noise, relaxing laser linewidth and in reducing the required transmitted signal power to achieve a reliable system performance.

In chapter 2, following the theoretical formulation, the performance of uncoded and coded optical FSK systems are evaluated at a data rate of 2.5 Gb/s for different sets of values of the normalized laser linewidth  $\Delta\nu T$  and the modulation index  $h$ . Performance results show that the uncoded system suffers bit error rate (BER) floor due to the adverse effect of laser phase noise. When coding is applied, the BER floor disappears for  $\Delta\nu T \leq 0.01$  and are significantly lowered by two/three orders of magnitude for higher values of  $\Delta\nu T$ . Thus, coding offers a considerable reduction in the required signal power to achieve  $P_b = 10^{-9}$  compared to the uncoded case.

Further, the uncoded system suffers penalty in signal power due to phase noise which is higher at higher linewidth. When coding is employed, the penalty is drastically reduced within the limit of 0.5-1.2 dB when  $\Delta\nu T \leq 0.01$   $h = 0.5$  which is 3.2 dB for the uncoded case. The penalty can be further reduced by increasing the modulation index.

It is also found that when rate 1/2 CC is employed for  $h = 0.5$ , the coding gain at  $P_b = 10^{-9}$ , is about 2.2 dB for  $k = 4$  and 3.2 dB for  $k = 7$ . Though almost similar coding gain is observed for (15,9) and (15,7) RS code, but in the preamplified case it is evident that RS code responds better in comparison to CC code. This implies that RS code offers higher coding gain. Further it can be noticed that coding gain is higher at high values of modulation index  $h$ .

In the present work, the performance of a single channel, FSK direct detection optical system employing MZI as an optical filter in the receiver is studied. The complete potential of MZI can be utilized when a multiplexer/demultiplexer or frequency selection switch for a multichannel WDM/FDM system is fabricated using the periodicity of transmittance versus frequency characteristics of an MZI[19]. The present analysis can be extended for multichannel OFDM systems employing MZI. The BER expression of eq. 2.3.38 can be used but an additional term due to crosstalk[21] should be included in the expression of total noise eq. 2.3.33. With a long haul multichannel system the applications of optical in-line amplifier can be investigated to determine the ultimate number of amplifier stages that can be cascaded while maintaining reasonable system performance. The effects of ISI terms can be reduced considerably by employing some form of cascaded combination of CC and RS coding which is termed as concatenated coding featuring an inner an outer coding scheme.

In this work the soft decision decoding is not exercised, which is expected to contribute a further coding gain of about 2 dB for CC and 2.5 dB for RS coding. Also the penalty variation with modulation index with soft decision decoding should reflect the same trend of improvement. This work can be executed in future.

In chapter 2, it is found that the degradation of performance due to increasing LW can be well compensated by increasing the modulation index  $h$ . But with increasing value of  $h$ , the transmission bandwidth will also increase resulting in an increase of loss due to chromatic dispersion, the effect of which is not considered in the present work. The fibre which is now in wide use are generally dispersion optimized at 1310 nm whereas the minimum loss occurs at wavelength of around 1550 nm. It is generally preferred to use the wavelength of minimum loss, so that with a relatively small source of power a substantial distance can be covered. Also, at this operating range the chromatic dispersion effect is non-trivial and particularly at high bit rate the penalty due to the above mentioned phenomena is quite large and may severely restrict the maximum achievable transmission distance. So, a thorough study on the chromatic dispersion effect of optical fibre is essential for an efficient system design.

• **REFERENCES :**

- [ 1 ] Y.T. Koh and F. Davidson, " Interleaved Concatenated Coding for the Turbulent Atmospheric Direct Detection Optical Communication Channel ". IEEE Transactions on Communications. vol. 37, no. 6, pp. 648-651, June 1989.
- [ 2 ] L.J. Cimini, JR. and G.J. Foschini, " Coding of Optical On-Off Keying Signals Impaired by Phase Noise ". IEEE Transactions on Communications. vol. 38, no. 9, pp. 1301-1307, Sept. 1990.
- [ 3 ] Bixio Rimoldi, " Design of Coded CPFSK Modulation Systems for Bandwidth and Energy Efficiency ". IEEE Transactions on Communications. vol. 37, no. 9, pp. 897-905, Sept. 1989.
- [ 4 ] R. J. McEliece, " Practical Codes for Photon Communication ", IEEE Trans. Inform. Theory, vol. IT-27, pp. 393-397, July 1981.
- [ 5 ] J. L. Massey, " Capacity, cut-off rate and coding for direct detection optical channel ", IEEE Trans. Commun., vol. Com-29, pp. 1615-1621, Nov. 1981.
- [ 6 ] D. Divsalar, R.M. Gagliardi and J. H. Yuen, " PPM performance for Reed-Solomon's decoding over an Optical-RF relay link ", IEEE Trans. Commun., vol. Com-32, pp. 302-305, March 1984.
- [ 7 ] V. W. S. Chan, " Coding for the atmospheric optical channel ", IEEE Trans. Commun., vol. Com-30, pp. 269-274, Jan. 1982.
- [ 8 ] E. Forestieri, R. Gangopadhyay and G. Prati, " Performance of convolutional codes in a direct detection optical PPM channel ", IEEE Trans. Commun., vol. Com-37, no. 12, pp. 1303-1317, Dec. 1989.
- [ 9 ] G. E. Atkin and K. S. Fung, " Performance analysis of coded optical PPM system using direct and coherent detection ", IEEE Proc. I, vol. 137.

- [ 10 ] G. C. Clark, Jr., and J. B. Cain, " Error Correction Coding for Digital Communications ". New York : Plenum, 1981.
- [ 11 ] A. M. Michelson and A. H. Levesque, " Error Control Techniques for Digital Communications ". New York : Wiley, 1985.
- [ 12 ] S. Lin and D.J. Costello, Jr., *Error Control Coding : Fundamentals and Applications*. Englewood Cliffs, N.J. : Prentice-Hall, 1983.
- [ 13 ] A. J. Viterbi and J.K. Omura, *Principals of Digital Communication and Coding*. New York : McGraw-Hill, 1979.
- [ 14 ] K. Iwashita and T. Matsumoto, " Modulation and detection characteristics of optical continuous phase FSK transmission system ", *J. Lightwave Technol.*, vol. LT-5, April 1987, pp. 452-460.
- [ 15 ] R. S. Vodhanel, J. L. Gimlet, N. K. Cheung and Tsuji, " FSK heterodyne transmission experiments at 560 Mbit/s and 1 G bit/s ", *J. Lightwave Technol.*, vol. LT-5, April 1987, pp. 461-468.
- [ 16 ] K. Emura, " Over 300 km transmission experiment on an optical FSK heterodyne dual filter detection system ", *Electron. Lett.*, vol. 22, October 1986, pp. 1096-1097.
- [ 17 ] R. Schweikert and A. J. Vinck, " A Convolutional Single-Parity-Check Concatenated Coding Scheme for High-Data-Rate Applications ". *IEEE Transactions on Communications*. vol. 39, no. 1, pp. 4-7, Jan. 1991.
- [ 18 ] H. Toba, K. Oda and K. Nosu, " Design and performance of FSK-direct detection scheme for optical FDM systems, " *J. Lightwave Technol.*, vol. 9, no. 10, Nov. 1991, pp. 1335-1343.

- [ 19 ] N. Takato, T. Kominato, A. Sugita, K. Jinguji, H. Toba and M. Kawachi, " Silica based integrated optic Mach-Zehnder multi/demultiplexer with channel spacing of 0.01-250 nm ", IEEE journal on selected areas in comm., vol. 8, no. 6, August 1990, pp. 1120-1127.
- [ 20 ] I. Garrett and J. Jacobsen, " Phase noise in weekly coherent systems ", IEEE Proceedings J. Optoelectronics, vol. 136, 1989 pp. 2179-2180.
- [ 21 ] R. Ramaswami and P. A. Humblet, " Amplifier induced crosstalk in multichannel optical networks " , J. Lightwave Technol., vol. 8, no. 12, December 1990, pp. 1882-1896.
- [ 22 ] L. G. Kazovosky and G. Jacobsen, " Multichannel CPFSK coherent optical communication systems " , J. Lightwave Technol., vol. 7, no. 6, June 1989, pp. 972-982.
- [ 23 ] N. A. Olsson, " Lightwave systems with optical amplifier " , J. Lightwave Technol., vol. 7, no. 6, July 1989, pp. 1071-1082.
- [ 24 ] M. J. O'Mahony, " Progress in optical amplifiers " Proc. of fourth Tirenna International workshop on Digital Comm., Tirenna, Italy, September 19-23, 1989.

## APPENDIX A

```
DOUBLE PRECISION W(10),P2K(10),PB(10),SNR(10),P(10),S,SUM,A
OPEN (10,FILE =C:\OUTp11.DAT)
OPEN (20,FILE =C:\WEIGHT2.DAT)
OPEN (30,FILE =C:\NP1.DAT)
C N= NO OF CONSTRAINT LENGTH
N=1
C M= NO OF WEIGHTS FOR A GIVEN CONSTRAINT LENGTH
M=6
C NP= NO SNR/BER POINTS
NP=10
DO 1 I=1,NP
READ (30,*) SNR(I), P(I)
C READ (*,*) SNR(I), P(I)
WRITE (*,*) SNR(I), P(I)
1 CONTINUE
DO 3 J=1,M
WRITE(*,*) 'GIVE WEIGHTS'
C READ(*,*) W(J)
READ(20,*) W(J)
C WRITE(20,*) W(J)
3 CONTINUE
READ(*,*) CL,DF
WRITE(*,*) CL
DO 10 I=1,NP
ADF=DF
S=0.0
A=ABS(4*P(I)*(1-P(I)))
WRITE(*,*)A=,A,' P=',P(I),' DF=',DF
SUM=0.D0
WRITE(*,*)S=,S,' SUM=',SUM
DO 11 J=1,M
PWR=ADF/2.0
P2K(J)=(A)**PWR
SUM=W(J)*P2K(J)
S=S+SUM
ADF=ADF+2.0
WRITE(*,*) 'S=',S, 'SUM=',SUM
11 CONTINUE
PB(I)=S
WRITE(*,*)PB=,PB(I)
WRITE(10,15) SNGL(SNR(I)),SNGL(PB(I))
15 FORMAT('SNR =',E18.4,' ',PB =',E18.4)
PAUSE
10 CONTINUE
STOP
END
```



## APPENDIX B

```

C PROGRAM TO FIND BER FOR DIFFERENT VALUE OF PS-DBM DUE TO NON-UNIFORM FM
C RESPONSE IMPLICIT DOUBLE PRECISION (A-H,J-M,O-Z)
REAL NU
COMMON M(10), XMEAN
OPEN(11,FILE='A:MOMENT2.DAT')
OPEN(10,FILE='BERB.DAT')
C DIMENSION M(10)
C VARIABLE DEFINITION: RD=RESPONSIVITY=1.0, FE= NOISE FIGURE= 3DB
C MOD. INDEX,H=(2*DELF/RB), LINEWIDTH=NU(NORMALIZED)=DT=(DELFNEW*T)
C TAO=(T/2*H), VARIANCE=VAR=2*PI*(NU/T)*TAO=2*PI*DT1
C BW=(280.0)*(10.0)**(6.0)
C BIT RATE IS CHANGED TO THE THESIS VALUE FOR CHECK=2.5GB
C BW=(2.5)*(10.0)**(9.0)
C CHOOSE BIT RATE, RB, TAKE BW=2*RB
RB=(2.5)*(10.0)**(9.0)
BW=(2.0*RB)
T=(1.0/RB)
C CHOOSE THE VALUE OF MOD.INDEX, H
READ(11,*)(M(I),I=1,10)
H=1.0
WRITE(10,*) 'H=',H
WRITE(*,*) 'H=',H
TAO=T/(2.0*H)
C CHOOSE THETA0BAR=XMEAN, FOR A PARTICULAR H
C WHERE XMEAN=(-PI/2)+(PI/2)*Q(TS)
XMEAN=-0.3
WRITE(*,*)XMEAN=XMEAN
C CHOOSE THE VALUE OF NU
GO TO 74
GO TO 174
NU=0.0
DT=NU
DT1=(NU/T)*TAO
WRITE(10,*)DT1=,DT1
C SET THE VALUE OF PS_DBM
PS_DBM=-34.0
WRITE(10,*)DT1=,DT1
WRITE(*,*)DT1=,DT1
WRITE(10,*)DT=,DT
WRITE(*,*)DT=,DT
DO 21 I=1,12
PSIG=.001*(10.0)**(PS_DBM/10.0)
CALL SNRT(PSIG,SNR,BW,DT1)
JITA=SQRT(SNR/2.0)
C WRITE(*,*)PS=,PSIG,JITA=,JITA
X=0.0
C FOR X=0.0, PDF=PDFN=1.0 AS, PDFN=PDF[1+...*HE(X)], AND HE.N(0) IS ALWAYS ZERO FOR ANY
VALUE OF N
CALL ERFC(X,ERFCZ,JITA)
BER=0.5*ERFCZ
C WRITE(10,*)PS_DBM,BER
C WRITE(*,*)PS-DBM=,PS_DBM,'BER=',BER,'PSIG=',PSIG
WRITE(10,*)PS_DBM,BER
PS_DBM=PS_DBM+2.0
21 CONTINUE
C CHOOSE THE VALUE OF LINEWIDTH(NORMALIZED)= NU
C PAUSE

```

```

C ILLUSTRATIVE VALUE:DT=.001,.005,.01,.03.....0.19SAY.H=.5,1,1.5,..3SAY.
74 JUMP=1.0
C CHANGE NEEDED IN DT, OR IN INTEGRATION LIMIT
DO 1 NU=.004,.007,.002
DT=NU
DT1=(NU/T)*TAO
CALL CDF1(DT1,CDF)
WRITE(10,*)DT1=,DT1,'CDF=',CDF
WRITE(*,*)DT1=,DT1,'CDF=',CDF
WRITE(10,*)DT=,DT
WRITE(*,*)DT=,DT
PS_DBM=-34.0
C WRITE(*,*)DT1=,DT1
C WRITE(10,*)DT=,DT
C WRITE(*,*)DT=,DT
DO 2 IU=1,15
PSIG=.001*(10.0)**(PS_DBM/10.0)
CALL SNRT(PSIG,SNR,BW,DT1)
JITA=SQRT(SNR/2.0)
C WRITE(*,*)PS=,PSIG,'JITA=',JITA
C C=XMEAN-AA, WHERE AA--3.5 BE CHOSEN EARLIER BY USING PRODUCT.FOR
C=(XMEAN-2.0)
D=(XMEAN+2.0)
CALL SMPSPNY(C,D,DT1,JITA,SY,CDF)
BER=(0.5*SY)
C WRITE(*,*)PS_DBM=,PS_DBM,'BER=',BER
WRITE(10,*)PS_DBM,BER
PS_DBM=PS_DBM+2.0
2 CONTINUE
1 CONTINUE
GO TO 100
174 JUMP=2.0
C CHANGE NEEDED N DT
DO 3 NU=0.001,.007,0.002
DT=NU
DT1=(NU/T)*TAO
CALL CDF1(DT1,CDF)
WRITE(10,*)DT1=,DT1,'CDF=',CDF
WRITE(*,*)DT1=,DT1,'CDF=',CDF
WRITE(10,*)DT=,DT
WRITE(*,*)DT=,DT
PS_DBM=-34.0
C WRITE(*,*)DT1=,DT1
C WRITE(10,*)DT=,DT
C WRITE(*,*)DT=,DT
DO 4 LU=1,15
PSIG=.001*(10.0)**(PS_DBM/10.0)
CALL SNRT(PSIG,SNR,BW,DT1)
JITA=SQRT(SNR/2.0)
C WRITE(*,*)PS=,PSIG,'JITA=',JITA
C C=XMEAN-AA, WHERE AA BE CHOSEN EARLIER BY USING PRODUCT.FOR
C=(XMEAN-2.0)
D=(XMEAN+2.0)
CALL SMPSPNY(C,D,DT1,JITA,SY,CDF)
BER=(0.5*SY)
C WRITE(*,*)PS_DBM=,PS_DBM,'BER=',BER
WRITE(10,*)PS_DBM,BER
PS_DBM=PS_DBM+2.0
4 CONTINUE
3 CONTINUE
100 STOP
END

```

```

*****
SUBROUTINE SMPSNY(C,D,DT1,JITA,SY,CDF)
IMPLICIT DOUBLE PRECISION (A-H,J-M,O-Z)
C COMMON XMEAN
C SET THE ACCURACY LIMIT YOU DESIRE FROM THE INTEGRATION
DELY=0.01
C SET THE MAXIMUM ITERATION YOU DESIRE,IMAX
IMAX=10
S11Y=0.00
SY=0.0
DC=D-C
IF(DC)20,19,20
19 WRITE(*,*) 'ERROR IN BOUNDARY VALUE'
RETURN
20 IF(DELY)22,22,23
22 WRITE(*,*) 'ERROR: CHOOSE +VE VALUE FOR DELY'
RETURN
23 IF(IMAX-1)24,24,25
24 WRITE(*,*) 'ERROR: CHOOSE +VE VALUE FOR MAXIMUM ITERATION DESIRED'
RETURN
25 HY=DC/2.0+C
NHALFY=1
XMEAN=-0.3
X=HY
XX=X-XMEAN
WRITE(*,*) 'XMEANSUB=',XMEAN
CALL PDFN(XX,PDF1,DT1,CDF)
C WRITE(*,*) 'X=',X, 'PDF1=',PDF1
CALL ERFC(X,ERFCZ,JITA)
C GET THE VALUE OF F(X)=PDF1*ERFCZ
FUNHY=PDF1*ERFCZ
C WRITE(*,*) 'IT IS WORKING'
C WRITE(*,*) 'HY=',HY, 'FUNHY=',FUNHY
SUMKY=FUNHY*DC*2.0/3.0
C XMEAN=-0.3
X=C
XX=X-XMEAN
CALL PDFN(XX,PDF1,DT1,CDF)
C WRITE(*,*) 'X=',X, 'PDF1=',PDF1
CALL ERFC(X,ERFCZ,JITA)
C GET THE VALUE OF F(X)=PDF1*ERFCZ
FUNC=PDF1*ERFCZ
C WRITE(*,*) 'C=',C, 'FUNC=',FUNC
X=D
XX=X-XMEAN
CALL PDFN(XX,PDF1,DT1,CDF)
C WRITE(*,*) 'X=',X, 'PDF1=',PDF1, 'CHECK D=',D
CALL ERFC(X,ERFCZ,JITA)
C GET THE VALUE OF F(X)=PDF1*ERFCZ
FUND=PDF1*ERFCZ
C WRITE(*,*) 'D=',D, 'FUND=',FUND
C BER OBTAINED FROM THE FIRST ITERATION IN SIMPSON.BER=SY
SY=SUMKY+(FUNC+FUND)*DC/6.0
C WRITE(*,*) 'SY=',SY, 'SUMKY=',SUMKY
C WRITE(*,*) 'IMAX=',IMAX
DO 28 IY=2,IMAX
S11Y=SY
C FOR 2ND ITERATION KEEP THE CONTRIBUTION OF F(X) AT C,D & HY IN SY
SY=(SY-(SUMKY/2.0))/2.0
NHALFY=NHALFY*2.0
ANHLFY=NHALFY

```

```

FRSTY=C+(DC/ANHLFY)/2.0
X=FRSTY
XX=X-XMEAN
C PRINT*,FRSTY
CALL PDFN(XX,PDF1,DT1,CDF)
C WRITE(*,*)X=,X,PDF1=,PDF1
CALL ERFC(X,ERFCZ,JITA)
C GET THE VALUE OF F(X)=PDF1*ERFCZ
FUNFTY=PDF1*ERFCZ
SUMKY=FUNFTY
YK=FRSTY
C WRITE(*,*)FRSTY=,FRSTY,SUMKY=FUNFTY=,FUNFTY
KLASTY=NHALFY-1
FENCY=DC/ANHLFY
DO 26 KY=1,KLASTY
YK=YK+FENCY
X=YK
XX=X-XMEAN
CALL PDFN(XX,PDF1,DT1,CDF)
C WRITE(*,*)X=,X,PDF1=,PDF1
CALL ERFC(X,ERFCZ,JITA)
C GET THE VALUE OF F(X)=PDF1*ERFCZ
FUNYK=PDF1*ERFCZ
SUMKY=SUMKY+FUNYK
C WRITE(*,*)FUNYK=,FUNYK,FENCY=,FENCY,YK=,YK
26 CONTINUE
SUMKY=(SUMKY*2.0*DC)/(3.0*ANHLFY)
C WRITE(*,*)SUMKY=,SUMKY,SY=,SY
SY=SY+SUMKY
C WRITE(*,*)SY=,SY,S11Y=,S11Y
27 IF(ABS(SY-S11Y)-ABS(DELY*SY)) 29,28,28
28 CONTINUE
C WRITE(*,*)INTE=,INTE
C WRITE(*,*)DESIRED ACCURACY FROM THE INTEGRATION IS NOT FOUND.
29 AINTE=SY
C WRITE(*,*)AINTE=,AINTE
RETURN
END

```

\*\*\*\*\*

```

C SUBROUTINE TO OBTAIN PROBABILITY DENSITY FUNCTION

```

```

SUBROUTINE PDF(X,PDFX,DT1)
IMPLICIT DOUBLE PRECISION (A-Z)
C CONSTANT IDENTIFICATION
PI=22.0/7.0
XAVG=0.0
VAR=(2.0*PI*DT1)
EXPO=((X-XAVG)**2)/(2.0*VAR)
ANUMER=EXP(-1.0*EXPO)
DENO=SQRT(2.0*PI*VAR)
PDFX=ANUMER/DENO
C WRITE(*,*)X=,X,PDFX=,PDFX
RETURN
END

```

\*\*\*\*\*

```

C PROGRAM TO FIND ERFC(Z)
SUBROUTINE ERFC(X,ERFCZ,JITA)
IMPLICIT DOUBLE PRECISION (A-H,J-M,O-Z)
C CONSTANT IDENTIFICATION

```

```

C OPEN(8,FILE='A.ERF.DAT')
C PRINT*, 'JUST ENTERED THE SUBROUTINE ERFC.....'
Z=JITA*COS(X)
C DOUBLE PRECISION Z,Y,P,PP,Q1,Q2,A1,A2,A3,A4,A5,PI,ZZ
PI=22.0/7.0
ZZ=ABS(Z)
SIGN=Z/ZZ
A1=0.2548295920
A2=-0.284496736
A3=1.4214137410
A4=-1.453152027
A5=1.0614054290
C ERROR=1.5E-7
P=0.3275911
PP=1.0/(1.0+P*ZZ)
Q1=EXP(-(ZZ**2.))
Q2=A1*PP+A2*(PP**2.)+A3*(PP**3.)+A4*(PP**4.)+A5*(PP**5.)
Y=(1.0-Q1*Q2)*SIGN
Y=1.0-Y
C WRITE(*,*)ERFC_',Z,',Y
ERFCZ=Y
RETURN
END

```

C\*\*\*\*\*

```

C PROGRAM TO FIND SIGNAL TO NOISE RATIO
SUBROUTINE SNRT(PSIG, SNR, BW, DT1)
IMPLICIT DOUBLE PRECISION(A-Z)
C CONSTANT IDENTIFICATION
E=1.6E-19
PI=(22.0/7.0)
RD=1.0
CUR=(RD*PSIG)
C WRITE(*,*)CUR=,CUR
XAVG=1.0
C VARIANCE= PROD= 2*PI*DT1, RES=LOAD RESISTANCE, FE=NOISE FIGURE
K=1.38E-23
TEMP=300.0
RES=50.0
FE_DBM=3.0
FE=(10.0)**(FE_DBM/10.0)
VAR=2.0*PI*DT1
NSHOT=2.0*E*BW*CUR*(1.0+XAVG)
NEXCSS=0.5*(CUR**2.0)*VAR
NTHRM=(4.0*K*TEMP*FE*BW)/RES
NTOT=NSHOT+NEXCSS+NTHRM
C WRITE(*,*)NSHOT=,NSHOT,NEX=,NEXCSS,NTH=,NTHRM
AMP=2.0*RD*PSIG
C SNR=(AMP**2)/(TOTAL NOISE, NTOT)
SNR=(AMP**2.0)/NTOT
C WRITE(*,*)SNR=,SNR,DT1=,DT1
RETURN
END

```

C\*\*\*\*\*

```

* PROGRAM TO FIND PDF I(X), PDF THAT INCLUDES NON-UNIFORM
* RESPONSE IN ADDITION TO NON ZERO LW EFFECT
SUBROUTINE PDFN(X,PDF1,DT1,CDF)
IMPLICIT DOUBLE PRECISION(A-H,J-M,O-Z)
INTEGER R,N
COMMON M(10)
* PROGRAM TO FIND PDF FOR A PARTICULAR 'PHI'=X

```

```

C WRITE(*,*)CORRECT
C READ(11,*)(M(I),I=1,10)
C WRITE(*,*) M(1),M(2)
C WRITE(*,*)(M(I),I=1,10)
PI=22.0/7.0
SUM=0.0
C VARIANCE, VAR=(SIGMA)**2=2*PI*DELNEW*T=2*PI*DT1
VAR=2.0*PI*DT1
STD=SQRT(VAR)
C WRITE(*,*)STD=,STD
* SET N=0,2,4,...30 ETC. I.E R=R=0,1,2.....15 ETC.
DO 5 R=1,10
N=2*R
* GET X1=(DELPHI/SIGMA)=X/STD
X1=X/STD
* HMITEN=HN(X)=HMITEK
CALL HRMITE(X1,N,HMITEK)
ANUME=M(R)*HMITEK
CALL FACTO(N,IFAC)
FACTOK=IFAC
DENO=FACTOK*(STD**N)
C WRITE(*,*)DENO=,DENO
A1=ANUME/DENO
SUM=SUM+A1
5 CONTINUE
C WRITE(*,*)SUM=,SUM
* GET PDF DUE TO NON ZERO LW ALONE
CALL PDF(X,PDFX,DT1)
* GET N(DELPHI)=ETA=PDFX
ETA=PDFX
PDF1B=ABS((ETA)*(1.0+2.0*SUM))
C PDFK, ITS NAME HAS NO SIGNIFICANCE. ACTUALLY PDFK REPLACES
C PDFN, TO AVOID AMBIGUITY WITH SUBROUTINE NAME PDFN
PDFK=(PDF1B/(2.0*CDF))
PDF1=PDFK
C PDF1 IS THE NORMILIZED VALUE OFPDF1, PDF WITH NON UNIFORM FM
C WRITE(*,*)PDF1('X,')=,PDF1
C WRITE(10,*)PDF1('X,')=,PDF1
RETURN
END

```

\*\*\*\*\*

```

* PROGRAM TO FIND HERMITE POLYNOMIAL
SUBROUTINE HRMITE(X,N,HMITEN)
IMPLICIT DOUBLE PRECISION(A-Z)
INTEGER M,I1,IFAC,N
1 IF(X.EQ.0.0) GO TO 22
SUM=0.0
DO 6 M=0,(N/2),1
ANUMER=(-1)**(M)*(X**(N-2*M))
CALL FACTO(M,IFAC)
FACTOM=IFAC
I1=(N-2*M)
CALL FACTO(I1,IFAC)
FACTOD=IFAC
DENO=(FACTOM)*(2**M)*(FACTOD)
FRAC=ANUMER/DENO
SUM=SUM+FRAC
6 CONTINUE
C WRITE(*,*)SUM
C HMITEN=HN(X). IN OUR CASE N=2R=K AND X=(DELPHI/STD. DEV)
CALL FACTO(N,IFAC)

```

```

FACTON=IFAC
*****
HMITEN=IFAC*SUM
C WRITE(*,*)HMITE,N,'(,X,)',',',HMITEN
GO TO 23
22 HMITEN=0.0
23 RETURN
END
*****
C PROGRAM TO FIND FACTORIAL VALUE
SUBROUTINE FACTO(N, IFAC)
IFAC=1
DO 8 I=1,N
IFAC=IFAC*I
8 CONTINUE
RETURN
END

*****
C PROGRAM TO DETERMINE CUMULATIVE PDF=2.0*CDF=AREA UNDER PDF CURVE
C SUBROUTINE SMPSNY(C,D,DT1,JITA,SY)
SUBROUTINE CDF1(DT1,CDF)
IMPLICIT DOUBLE PRECISION (A-H,J-M,O-Z)
C SET THE ACCURACY LIMIT YOU DESIRE FROM THE INTEGRATION
C SET THE MAXIMUM ITERATION YOU DESIRE.IMAX
C MODIFICATION ON BER TO GET CDF, CUMULATIVE PDF
COMMON M(10)
C OPEN(11,FILE='A:MOMENT1.DAT')
C OPEN(10,FILE='CDF.DAT')
DELY=0.01
C=0.0
D=4.0
JITA=1.0
ERFCZ=1.0
IMAX=10
S11Y=0.00
SY=0.0
C READ(11,*)(M(I),I=1,10)
C WRITE(*,*)M(1),M(2)
DC=D-C
C IF(DC)20,19,20
C 19 WRITE(*,*) 'ERROR IN BOUNDARY VALUE'
C RETURN
C 20 IF(DELY)22,22,23
C 22 WRITE(*,*)'ERROR: CHOOSE +VE VALUE FOR DELY'
C RETURN
23 IF(IMAX-1)24,24,25
24 WRITE(*,*)'ERROR:CHOOSE+VE VALUE FOR MAXIMUM ITERATION DESIRED'
C RETURN
C READ(11,*)(M(I),I=1,10)
C WRITE(*,*)M(1),M(2)
25 HY=DC/2.0+C
NHALFY=1
X=HY
CALL PDFAB(X,PDF1,DT1)
C WRITE(*,*)X=',X,PDF1=',PDF1
C CALL ERFC(X,ERFCZ,JITA)
C GET THE VALUE OF F(X)=PDF1*ERFCZ
FUNHY=PDF1*ERFCZ
C WRITE(*,*)'IT IS WORKING'
C WRITE(*,*) HY=',HY,FUNHY=',FUNHY

```

```

SUMKY=FUNHY*DC*2.0/3.0
X=C
CALL PDFAB(X,PDF1,DT1)
C WRITE(*,*)X=,X,PDF1=,PDF1
C CALL ERFC(X,ERFCZ,JITA)
C GET THE VALUE OF F(X)=PDF1*ERFCZ
FUNC=PDF1*ERFCZ
C WRITE(*,*)'C=,C,FUNC=,FUNC
X=D
CALL PDFAB(X,PDF1,DT1)
C WRITE(*,*)X=,X,PDF1=,PDF1,'CHECK D=,D
C CALL ERFC(X,ERFCZ,JITA)
C GET THE VALUE OF F(X)=PDF1*ERFCZ
FUND=PDF1*ERFCZ
C WRITE(*,*)'D=,D,FUND=,FUND
C BER OBTAINED FROM THE FIRST ITERATION IN SIMPSON,BER=SY
SY=SUMKY+(FUNC+FUND)*DC/6.0
C WRITE(*,*)'SY=,SY,SUMKY=,SUMKY
C WRITE(*,*)'IMAX=,IMAX
DO 28 IY=2,IMAX
S11Y=SY
C FOR 2ND ITERATION KEEP THE CONTRIBUTION OF F(X) AT C,D & HY IN SY
SY=(SY-(SUMKY/2.0))/2.0
NHALFY=NHALFY*2.0
ANHLFY=NHALFY
FRSTY=C+(DC/ANHLFY)/2.0
X=FRSTY
C PRINT*,FRSTY
CALL PDFAB(X,PDF1,DT1)
C WRITE(*,*)X=,X,PDF1=,PDF1
C CALL ERFC(X,ERFCZ,JITA)
C GET THE VALUE OF F(X)=PDF1*ERFCZ
FUNFTY=PDF1*ERFCZ
SUMKY=FUNFTY
YK=FRSTY
C WRITE(*,*)'FRSTY=,FRSTY,'SUMKY=FUNFTY=,FUNFTY
KLASTY=NHALFY-1
FINCY=DC/ANHLFY
DO 26 KY=1,KLASTY
YK=YK+FINCY
X=YK
CALL PDFAB(X,PDF1,DT1)
C WRITE(*,*)X=,X,PDF1=,PDF1
C CALL ERFC(X,ERFCZ,JITA)
C GET THE VALUE OF F(X)=PDF1*ERFCZ
FUNYK=PDF1*ERFCZ
SUMKY=SUMKY+FUNYK
C WRITE(*,*)'FUNYK=,FUNYK,'FINCY=,FINCY,'YK=,YK
26 CONTINUE
SUMKY=(SUMKY*2.0*DC)/(3.0*ANHLFY)
C WRITE(*,*)'SUMKY=,SUMKY,'SY=,SY
SY=SY+SUMKY
CDF=SY
C WRITE(10,*)'CDF=,CDF
27 IF(ABS(SY-S11Y)-ABS(DELY*SY)) 29,28,28
28 CONTINUE
C WRITE(*,*)'INTE=,INTE
C WRITE(*,*)'DESIRED ACCURACY FROM THE INTEGRATION IS NOT FOUND.'
29 AINTE=SY
C WRITE(*,*)'AINTE=,AINTE
RETURN
WRITE(10,*)'DT1=,DT1,'CDF=,CDF

```



C STOP  
END

```
*****  
* PROGRAM TO FIND PDF1(X), PDF THAT INCLUDES NON-UNIFORM  
* RESPONSE IN ADDITION TO NON ZERO LW EFFECT  
SUBROUTINE PDFAB(X,PDFA1,DT1)  
IMPLICIT DOUBLE PRECISION(A-H,J-M,O-Z)  
C THIS PROGRAM IS SPECIFICALLY USED TO FIND CDF, I.E FOR SUBROUTINE  
C CDF. PDFAB= ABOLUTE VALUE, PDFN= NORMALIZED VALUE OF.PDF  
INTEGER R,N  
COMMON M(10)  
* PROGRAM TO FIND PDF FOR A PARTICULAR 'PHI'=X  
C WRITE(*,*)'CORRECT'  
C READ(11,*)(M(I),I=1,10)  
C WRITE(*,*) M(1),M(2)  
C WRITE(*,*)(M(I),I=1,10)  
PI=22.0/7.0  
SUM=0.0  
C VARIANCE, VAR=(SIGMA)**2=2*PI*DELNEW*T=2*PI*DT1  
VAR=2.0*PI*DT1  
STD=SQRT(VAR)  
C WRITE(*,*)'STD=',STD  
* SET N=0,2,4,...30 ETC. I.E R=R=0,1,2.....15 ETC.  
DO 5 R=1,10  
N=2*R  
* GET X1=(DELPHI/SIGMA)=X/STD  
X1=X/STD  
* HMITEN=HN(X)=HMITEK  
CALL HRMITE(X1,N,HMITEK)  
ANUME=M(R)*HMITEK  
CALL FACTO(N,IFAC)  
FACTOK=IFAC  
DENO=FACTOK*(STD**N)  
C WRITE(*,*)'DENO=',DENO  
A1=ANUME/DENO  
SUM=SUM+A1  
5 CONTINUE  
C WRITE (*,*)'SUM=',SUM  
* GET PDF DUE TO NON ZERO LW ALONE  
CALL PDF(X,PDFX,DT1)  
* GET N(DELPHI)=ETA=PDFX  
ETA=PDFX  
PDFA1=ABS((ETA)*(1.0+2.0*SUM))  
C PDFK, ITS NAME HAS NO SIGNIFICANCE. ACTUALLY PDFK REPLACES  
C PDFN. TO AVOID AMBIGUITY WITH SUBROUTINE NAME PDFN  
C PDFA1= ABSOLUTE VALUE OF PDF1, NEEDED FOR CDF1  
C WRITE(*,*)'PDFA1('X,')=',PDFA1  
C WRITE(10,*)'PDFA1('X,')=',PDFA1  
RETURN  
END  
*****
```

## APPENDIX C

```
C PROGRAM FOR BER CALCULATION OF RS CODE
DOUBLE PRECISION P(10),PB(10),SNR(10),S,SUM,A,FACN,FACJ,FACNMJ
INTEGER NML
OPEN(10,FILE='C:\OUTR1.DAT')
OPEN(20,FILE='C:\INP1.DAT')
C NP= NO OF BER/SNR PTS.
NP=10
READ (*,*) N,K
L=(N-K)/2
C B=(N-1)/(2*N)
DO 1 I=1, NP
READ (20,*) SNR(I), P(I)
S=0.0
DO 4 J=L, N
CALL FRP(N,FacN)
CALL FRP(J,FacJ)
NMJ=N-J
CALL FRP(NMJ,FacNMJ)
T=FLOAT(L)
A=(P(I)**J)*((1-P(I))**NMJ)
SUM=(T*FACN*A)/(N*FACJ*FACNMJ)
S=S+SUM
PB(I)=S
4 CONTINUE
WRITE(10,3) SNGL(SNR(I)),SNGL(PB(I))
3 FORMAT('SNR =',E18.4,' ','PB =',E18.4)
1 CONTINUE
STOP
END
```

C\*\*\*\*\*

```
SUBROUTINE FRP(Ind,FactA)
DOUBLE PRECISION FactA
FactA=1.0
IF(Ind .eq. 0) go to 2
DO 1 K=Ind,1,-1
Facta=Facta*Float(K)
1 CONTINUE
RETURN
2 Facta=1.0
RETURN
END
```

